OZDEMIR, ABDULLAH

ELECTRON TRANSPORT USING THE DISCRETE ORDINATES METHOD

The University of Oklahoma PH.D. 1981

THE UNIVERSITY OF OKLAHOMA

GRADUATE COLLEGE

ELECTRON TRANSPORT USING THE DISCRETE ORDINATES METHOD

A DISSERTATION

SUBMITTED TO THE GRADUATE FACULTY

in partial fulfillment of the requirements for the degree of

DOCTOR OF PHILOSOPHY

BY

ABDULLAH ÖZDEMİR

Norman, Oklahoma

1981

ELECTRON TRANSPORT

USING THE DISCRETE ORDINATES METHOD

A DISSERTATION

APPROVED FOR THE SCHOOL OF AEROSPACE, MECHANICAL

AND NUCLEAR ENGINEERING

APPROVED BY

Duane Lindstrom

Charles W. Tewell

Dain M. Eglo

Luther W. White

David N. Anderson

DISSERTATION COMMITTEE

ABSTRACT

The purpose of this study is to develop an electron transport model which can be used with the standard ANISN computer code. The basis for the development of this model is the cross-section format used in ANISN calculations. The cross-section data which have been generated with the electron transport model can be used in several nuclear engineering computer codes. Previous electron transport work has always required special-purpose codes. Two major developments in this study may be outlined as: (i) the application of the condensed random walk concept of the ETRAN family of computer codes into the discrete ordinates (ANISN) format; (ii) and the formulation of inelastic cross-sections by the collisional average energy loss model. The inelastic cross-sections are employed in a continuous slowing down mode in the ANISN format, so the general model is referred to as ANISN-CSDM. The characteristics of ANISN-CSDM are: the application of an elastic multiple scattering approximation to replace detailed (single-scatter) small interval calculations. This approximation permits more efficient approximate calculations and makes the deep-penetration radiation transport analysis possible within

reasonable computer storage and time limitations. A single-inelastic scatter and an elastic scatter are allowed per energy step by defining a model energy loss and equating this to an energy group width, thereby specifying a mechanism for continuous slowing down of the primary particle. The average energy loss of the primary particle does not include small energy transfer collisions whose magnitude is less than a chosen η value. Their energy deposition is included in the overall inelastic cross-sections. The ANISN-CSDM model of electron transport effectively includes a deflection operator for these small energy transfer collisions, because their energy loss is represented by the model energy transfer collision in each energy group which employs a Legendre expansion scattering representation. That is, the many small energy transfer collisions are replaced by a few large energy transfer collisions with their associated deflection. It has been observed that the ANISN-CSDM transport results do not strongly depend on the choice of η value.

The types of problems which have been solved are: The scalar flux solutions in thin aluminum slabs, energy/angle transmission through relatively thick aluminum, gold and water slabs; and energy deposition in thick aluminum and in water slabs whose thickness is greater than the range of the incident particle. The calculated results obtained

using ANISN-CSDM are compared with Monte Carlo results performed with an ETRAN code and with available experimental results.

ACKNOWLEDGMENTS

I wish to express my heartfelt gratitude to Dr. Duaine Lindstrom, my dissertation committee chairman, Associate Professor of nuclear engineering at the University of Oklahoma, for his constant advice and encouragement in the preparation of this dissertation. I also want to thank my committee members, Dr. David Anderson, Dr. Davis Egle, Dr. Charles Terrell and Dr. Luther White for their suggestions and assistance.

I deeply appreciate the financial assistance provided by my government. Special mention is due the International Atomic Energy Agency which provided me the opportunity to begin my graduate studies abroad.

TABLE OF CONTENTS

LIST OF TABLES

LIST OF FIGURES

FIGURE Page

NOMENCLATURE

η, or E_C	upper bound of small energy transfers
Z	atomic number of transport medium
M	atomic (molecular) weight of transport medium
ρ	density of transport medium (gm/cm^3)
$R_0(E_0)$	range of primary particle at energy E_0
N	number density of primary particle (#particles/cm^3)
$S(E_0)$	total stopping power at energy E_0
E_0	usually initial energy of primary particle
W, or E	final energy of scattered particle
A_o	Avagadro's number (0.602217×10^{24} atoms/mole)
E_0-W, or E_0-E	energy of secondary particle
$Q = E_0$-E	energy transfer to target electron
Ze	charge of primary particle (Z=1 for electron)
δ-ray	a secondary knock-on electron
I	mean ionization potential of transport medium
Σ_t	total reaction cross-section
$\Sigma_s(g \rightarrow g)$	total in-group (elastic) scattering cross-section
$\Sigma_s(g \rightarrow g+1)$	total energy transfer (inelastic) cross-section
$\phi(\vec{r},E,\vec{\Omega},t)$	angular particle flux
$\Phi(\vec{r},E,t)$	total (scalar) flux

$\mu = \cos\theta$	cosine of deflection angle θ
μ_j	discrete angular directions
W_j	corresponding angular quadrature weights of μ_j's
$P_\ell(\mu)$	Legendre polynomials
$\langle W(E_0)\rangle$	average energy of scattered particle at initial energy E_0
$\langle \Delta W(E_0)\rangle$, or $\langle \Delta E(E_0)\rangle$	average energy loss of primary particle due to inelastic collisions at initial energy E_0
$\Sigma_{>\eta}(E_0)$	total energy transfer cross-section for energy losses greater than η at energy E_0
ε_g	mean energy loss of a particle in energy group g
$\sigma(g \to g')$	group skipping cross-section
$\vec{\Omega}$	initial direction of primary particle
$\vec{\Omega}'$	final direction of primary particle

$\vec{\Omega} = \frac{\vec{v}}{|\vec{v}|}$ = unit vector

$\vec{\Omega} \cdot \vec{\Omega}' = |\vec{\Omega}||\vec{\Omega}'| \cos\theta = \cos\theta$

CSDM	Continuous slowing down model

CHAPTER I

INTRODUCTION

Methods for mathematical modeling of radiation transport of neutral particles, -neutrons and photons- have been well developed as part of the analysis and the shielding design of nuclear reactors. Therefore, there are many convenient computer codes to produce transport results for neutral particles, but the charged particle transport methods are not as yet well developed. There is one relatively reliable Monte Carlo computer code which is called ETRAN and was designed by Berger and Seltzer (1). It is very limited in its geometric applications and has difficulty producing physically acceptable results. Recently, Halbleib and Vandevender (2,3,4,5) used the ETRAN computer code to develop a new set of electron/photon rediation transport codes known as EZTRAN, CYLTRAN, SPHERE and ACCEPT. The method of solution in these computer codes is the condensed-history of particle approach introduced into ETRAN by Berger (1). These new codes are more flexible than ETRAN in simulating any desired geometry.

Most studies of electron transport concern radiation damage, biomedical, space shielding and plasma applications and depend upon approximate methods of solution. One may note that the approximate methods often exclude some useful information. Some developments have been done in electron and light ion transport theory using methods other than Monte Carlo schemes. Variations of one such technique, the discrete ordinates method, (DOM) have been reported by Bartine (6), Hoffman (7) and Morel (8), but none of them has yet been developed into a generally useful computer code. Recently, a good mathematical model to produce electron or ion transport results was suggested by Ligou (9). But again the associated discrete ordinates computer code is yet to be developed.

This work discusses the present state of the electron transport studies. It suggests a means for using a wide range of present neutral particle (neutron/photon) computer codes to perform electron transport analyses. The method which has been developed in this study can be used to produce reliable electron transport results, much as are done in neutral particle transport analyses.

A. Unsolved Problems in Electron Transport

A survey of unsolved problems in mathematical modeling of electron transport is given in the following

paragraphs. Most of them have been investigated recently, with some of them still under study. A mathematical model called the discrete ordinates method is used frequently in neutral particle transport analyses. One of several available computer codes which use this method is the code ANISN (12). The first attempt to apply the ANISN to electron transport problems was made by Bartine, et al. (6). Their results showed good agreement for low Z (the atomic number of transport medium) transport materials but poor agreement for high Z transport materials. It is pointed out by Ligou (9) that the continuous deflections result from continuous interactions. In Bartine's work he assumed no deflection at all for continuous slowing down collisions. One may note that the energy loss per cm is proportional to the magnitude of Z. Probably the angular deflections associated with continuous interactions should not be neglected for a high Z transport medium. Ligou also points out that if continuous interactions are considered correctly, then there will be a deflection operator in the transport equation to account for continuous interactions. This operator is called the Fokker-Planck operator (9).

The angular behavior of inelastic collisions is modeled approximately in the present study. Group transfer collisions result in energy degradation. There exists an angular deflection associated with the magnitude of the

energy loss. It seems appropriate to prescribe angular redistribution within each group as primary particle slows down to lower energy groups. As a particle moves to low energy groups, it becomes less and less forward peaked.

It was stated previously that no discrete ordinates electron transport production computer code is yet available (8). Although ANISN has been used by a few investigators (6,7) to perform electron and ion transport calculations, the modified form of the ANISN computer code used by Bartine (6), Hoffman (7) has not been released to the scientific community for its use. Morel (8) used the computer code DTF69, one which is very similar to ANISN, to produce one-group electron transport results. He reported a one-group calculation where inelastic collisions have not been taken into account. Therefore, more work should be done to formulate an approximate method for treating inelastic electron collisions and to include it in an electron transport model which considers both elastic and inelastic collisions. The Electron transport model presented in this study is intended to fill that gap.

A theoretical treatment of both elastic and inelastic scattering collisions with the associated angular deflections was made by Ligou (9). He states that if the continuous slowing down collisions were handled accurately, i.e., small energy transfer collisions, there should be an additional

term to take into account the angular deflections associated with small energy transfer collisions. Angular changes associated with large energy transfer collisions can be accounted for by the usual method of Legendre polynomial expansions. Even though Ligou's (9) work takes into account the angular deflections due to large energy and small energy transfer collisions, he does not give computational results. A discrete ordinates computer code needs to be designed based on the new mathematical model described above to test the accuracy of his suggestion.

Neutral particle transport codes, such as ANISN, are sufficiently general so that they might be used for electron and other charged-particle transport analyses. The successful use of such a general code, without modification for specific particle characteristics, would make possible improved analyses in a number of application areas.

B. Application Areas of Charged Particle Transport Calculations

The general mathematical methods of neutral particle transport analysis can, in general, be applied to electron transport in the manner discussed in this work. In addition, the methods can probably be applied to the transport of any charged particles.

The study of charged particle transport could be applied specifically in a number of areas depending on the

nature of problem investigated. These areas may be classified as follows:

1. Radiation Damage

When a solid is exposed to highly energetic particles, changes in the material properties become significant. An example of this is when the products of a fission reaction, which are primarily high Z (Z=atomic number) charged particles, irradiate ceramic fuel materials and structural materials of a nuclear reactor. Certain charged fission products continue to irradiate primarily reactor core region. Hence any observable change in the performance of material which is exposed to highly energetic charged particles can be called radiation effects of charged particles. The gross changes in the solid are called radiation damage.

The distribution of primary charged particles and secondary particles in transport medium constitute a problem of charged particle transport. The complexity of the problem (compared to that of neutral particle transport) comes in the fact that charged particles carry a certain amount of electronic charge which results in very frequent Coulomb interactions with the transport medium, which in turn require energy degradation of the incident particle.

One of the significant applications of charged particle transport analyses is the radiation damage to nuclear materials, where radiation itself is produced internally by

the system (10). A brief discussion of radiation damage to nuclear materials and reactor components follows. This discussion is included here because radiation damage has a direct effect on nuclear and mechanical design of nuclear reactor components. Radiation damage effects to nuclear materials may be classified as either radiation damage in nuclear fuels or in nuclear fuel cladding.

Radiation damage to nuclear fuels are the result of fission products whose kinetic energy is of the order of 100 Mev. As these products slow down in the nuclear fuel medium, their kinetic energy appears in the form of heat and gives rise to atomic displacement. The heat is removed from the system by cooling the fuel assembly, but radiation damage remains in the fuel or in the cladding. A certain fraction of fission products are inert gases, which are highly insoluble in solids. These gases form bubbles in the fuel. Part of these cause swelling; the remainder are released, resulting in a gas pressure build-up in the fuel rods. Mechanical deformation of the fuel rods is a current design problem. Fuel cladding materials are subject to high thermal loading and radiation. The irradiated cladding material at high temperatures suffers a loss of ductility over the reactor lifetime (about 20-30 years). Occasionally, this causes fuel rod fractures. In fast reactors, the most significant radiation damage is the formation of voids in cladding. These voids are created by fast neutrons at high doses.

The formation of voids in irradiated metals can produce significant percentage volume changes. Therefore, it becomes a problem of Fast Breeder Reactor design which is the second generation of fission reactors. In brief, interactions of radiation with materials always has been a design problem in the course of development of nuclear reactor families. It appears that the successful and economical applications of nuclear science very much depend on the development of material science at high temperatures with the consideration of interaction of radiation with the host medium.

There are some applications of charged radiation damage problems. All of these may not be included here. Some of the applications of highly energetic radiations will be briefly included in the following paragraphs.

In general, one may consider the erosion of first wall (7,11) of fusion reactor by the following processes. The first one is sputtering where the first wall material may be ejected due to successive collisions initiated by incident energetic plasma particles which fall on the first wall. The second one is evaporation where wall surface heats up to a sufficiently high temperature such that atoms of first wall could gain enough energy above the surface binding energy. This results in evaporation. The third one is the blistering which occurs due to explosion of gas bubbles which have formed close to the wall surface. The formation of gas bubbles is due to injection of plasma gas atoms which are not soluble in

first wall material (10).

Work has been carried out by Hoffman (7) to determine the sputtering yield, ion reflection coefficients and angular and energy distributions of sputtered particles using neutral particle transport code ANISN (12).

2. Plasma Heating by Charged Particles (13,14,15)

Here the energy of a highly energetic charged particle can be imparted to a plasma medium through collisions. One of the schemes is to pass highly energetic ions (heavy charged particles) through a neutralizer and then inject them into a plasma in such a way that they behave like a source of energetic particles and impart their energy to heat it up. Another method of heating plasma is by relativistic electrons. In these problems the plasma medium is treated as a transport medium for highly energetic charged particles. Energy transfer to plasma ions is again achieved by collisions of highly energetic imparted particles.

3. Application of High Energy Charged Particles in Medical Physics

The work in this area was initiated because of an interest in transport theory and its applications in space technology. Similar applications were considered in high energy electron-irradiation therapy. The object in these studies is to determine the electron flux $\phi(\vec{r},E,\vec{\Omega},t)$ (distribution of particles) due to primary and secondary particles.

A complete determination of electron flux requires consideration of all secondary particles produced by primary electrons. The detailed knowledge of primary praticle flux and secondary particle flux will help to determine the amount of energy absorbed per unit volume of transport medium. Energy absorption can be determined by a knowledge of electron flux and stopping power of transport medium, where macroscopic energy absorption cross section is treated as the energy loss per unit path length traveled. The formulation of energy absorption cross-section will be discussed in Chapter (IV).

4. Charged Particle Shielding in Space Technology

In this application of charged particle transport theory, it is necessary to protect man and space facilities against trapped charged particles of sufficient intensity to produce radiation damage. High energy electrons are observed to be the predominant means of energy absorption in systems that are subject to continuous electron flux. Total energy absorption will probably put a limit on the space systems. In order to minimize the total shield weight, more work may have to be done in optimizing laminated wall structures (16).

5. Nuclear Measurements (17,18,60,61,65)

The purpose of this subsection is to present very briefly where the results of charged particle transport

calculations would be applied in nuclear measurements. In a wide category of radiation detectors (ion chambers, proportional counters, Geiger tubes), the net result of the radiation interaction may be thought of as the appearance of electric charge within the active volume of a detector. Then, this charge may be collected by an application of an output signal. The negative and positive charges are created by the primary radiation flow in opposite directions in a detector after application of the electric field. For every charged particle, for example: beta or alpha particles, which deposit a significant amount of energy in the fill gas, produce a signal pulse. The counting efficiency of a detector depends upon the probability of the primary radiation which penetrates through window thickness. A primary particle may be absorbed or backscatted while it crosses the window thickness before it reaches the active volume of the detector. It is perhaps too early to mention that here the window thickness (a small fraction of the primary particle range) represents a slab geometry for radiation transport analysis in terms of the energy deposition and transmission studies of the primary particle.

In fast electron spectroscopy with scintillators, primary particles may make large angle scattering and result in bremsstrahlung photon production. They both reduce the energy of primary particles. These events depend on the scintillation material and its thickness. Electrons lose energy over the protective cover before they reach the

scintillator itself. Magnitude of energy loss increases with the atomic number of the scintillator material. Low atomic number scintillator material may be used for electron spectroscopy because it minimizes the energy loss of primary particles. Similarly, in semiconductor detectors a charged particle will lose some of its initial energy over the dead layer (or window) before it reaches the active region of the detector. The analyses of the magnitudes of energy losses and the effect of multiple scattering on the detector response may be made by the charged particle transport calculational models.

C. A Brief Outline of Developments in This Work

In full range deep penetration radiation transport problems a complete energy and particle absorption may be considered in the Continuous Slowing Down Model of electron transport (ANISN-CSDM). This is because the primary particle is assumed to have no kinetic energy at the thickness of material which is equal to the range of primary particle, $R_0(E_0)$, at its initial energy E_0. In general, the ANISN-CSDM, which will be discussed in depth in Chapter (II), may be visualized as a particle transport model that allows the primary particle at the mean energy of any energy group g to slow down to the mean energy of energy group g + 1 by an inelastic collision. In this model the primary particle is not permitted to skip adjacent energy groups following an

inelastic collision. Group skipping is permitted in the Group Skipping Model (GSM) of electron transport; however, it will not be covered in detail in this investigation. The GSM of electron transport is different from the ANISN-CSDM in the sense that the particle may skip one or more energy groups depending on the magnitude of energy loss that occurs in a particular inelastic collision. Following an inelastic collision, two particles should be considered: One of them is designated the primary particle and the other one is the secondary particle, each of which will be placed in an appropriate energy group as a function of its kinetic energy after inelastic collision. A more detailed description and some preliminary formulation of the GSM will be briefly introduced in Chapter (IV). Several individual inelastic collisions are treated separately in the GSM, but all inelastic collisions are approximated by one average energy loss collision in the ANISN-CSDM at the initial energy. In summary, the GSM depends on a range of different energy loss collisions and the ANISN-CSDM depends on grouping of collisions and representing their overall behavior by an average interaction at the mean values of an energy group structure.

The model which has been developed and tested in this work for electron transport is similar to Ligou's (9) mathematical model except that here the associated angular deflections due to elastic and inelastic collisions are treated approximately and consistently. The mathematical model of

the electron transport scheme is incorporated into the Cross-Section Processing Computer Code (CRXPC) which is designed for this particular electron transport model, ANISN-CSDM. Complete energy and particle conservation is achieved in the computations because all possible inelastic electron-electron collisions are included in the model. The basic theory of cross-section production will be discussed in Chapter (IV). In principle, cross-sections are produced based on total energy loss at the mean value of established energy group structure for multigroup calculations.

This study uses the standard ANISN computer code without modification. As a result, the radiation transport model developed here can be tested by other numerical computer codes employing the ANISN input format.

In Chapter (II) the theoretical development of electron transport methods is outlined. Chapter (III) discusses the discrete ordinates method formulation of the Boltzmann transport equation. Chapter (IV) presents the formulation of the cross-section theory of the ANISN-CSDM model of radiation transport. A brief discussion of extended transport corrected cross-section and the electron group-skipping model are also included. In this chapter a new scheme of electron transport cross-sections has been developed. This scheme includes an approximate treatment of angular distribution of scattered particles according to an average energy loss model.

The average energy loss is defined as the mean energy

loss of inelastic collisions which could occur at the electron's initial energy. In the average energy loss calculation the very small energy loss collisions are excluded, but cross-sections are corrected to provide complete energy conservation. The overall average energy loss has been calculated by using the Møller differential single scattering energy loss cross-section (21). This energy loss model will be called "The squashed electron transport model."

The angular distribution of inelastically scattered electrons is also derived from the Møller cross-sections, deriving Legendre coefficients consistent with the energy losses considered in the mean energy loss. Rutherford scattering cross-sections are used for the elastic scattering with the screening parameter as given by the theory of Moliere. Since multiple elastic scatters may occur between energy loss collisions, the Legendre coefficients which determine the elastic scatter angular distributions are corrected for multiple scattering.

In Chapter (V) the results produced by ANISN-CSDM will be given. The results will be compared with other selected results which have been reported elsewhere. The comparisons show that the results produced by ANISN-CSDM agree fairly well with the reported discrete ordinates results of Bartine (6), Morel (8) and the results generated by Monte Carlo calculational models (1). In addition, they compare well with

some experimental results of Derrickson and Rester (57) and Anderson (59). From the comparisons it can be seen that the ANISN-CSDM model of electron transport may be used as an alternative to other calculational models.

The discussion of the results and conclusions, and recommendations are given in Chapters (VI) and (VII) respectively.

CHAPTER II

SURVEY OF THE THEORETICAL BASIS FOR ELECTRON TRANSPORT CALCULATIONS

A. A Review of Electron Transport Theory

The charged particle transport theory includes more complexities than neutral particle transport theory, because interaction mechanisms are different for neutral and charged particles. Interactions of charged particles are governed by nuclear plus long-range Coulomb forces whereas neutral particle interactions are governed by short-range nuclear forces only. Magnitudes for the energy losses of primary charged particles and their distribution in a transport medium are typical quantities sought in a general charged particle transport problem. A review of basic electron and other charged particle interactions with transport medium will follow. Interactions of charged particles (fission fragments, light ions, electrons, etc.) at high energies include

(i) elastic nuclear scattering (Coulomb scattering)

(ii) inelastic scattering from atomic electrons (primary energy loss mechanism of electrons at

low energies)

(iii) bremsstrahlung scattering; i.e., secondary photon production (primary energy loss mechanism of electrons at very high energies)

(iv) nuclear reactions

The first of three of these reactions will be considered for electron transport problems because nuclear reactions are negligible in electron transport. Some charged particles, such as hydrogen, deuterium, tritium, helium, etc. ions can initiate a group of nuclear reactions which may be classified as basic fusion reactions of light ions (15).

Inelastic and bremsstrahlung scatterings are responsible for energy losses of electrons. Inelastic scattering produces secondary electrons and bremsstrahlung scattering produces secondary photons. For example, test calculations show that at 40.0 Mev electrons in water, energy loss by bremsstrahlung makes up about 30% of the total energy loss while this is about 8% for 10.0 Mev primary electrons. In the energy range from 100.0 Mev to 1000.0 Mev energy transport is dominated by photons and energy transport by electrons is relatively small (19). It can be seen from the practical figures given above that the energy transport is governed by photon production at high energies. Then one can define the "critical energy" of an electron where the "stopping power" of the transport medium due to the

bremsstrahlung photon production becomes equal to that due to inelastic collisions. This occurs approximately at

$$E_c \cong \frac{800}{Z+1.2} \text{ MeV} \quad (16,20,21) \tag{2.1}$$

and, the ratio of the radiative loss to collision loss given by Bethe and Heitler (21) is as follows:

$$\left.\frac{(dE/ds)_{rad}}{(dE/ds)_{cols}}\right|_{E=E_0} = \frac{E_0 Z}{1600\ mc^2} \tag{2.2}$$

if $E < E_c$, collisional energy loss dominates

if $E > E_c$, radiative energy loss dominates.

Now total stopping power may be introduced which is the sum of collisional energy loss due to inelastic collisions per unit path length and radiative energy loss due to photon production per unit path length. That is

$$S(E) = \left[\frac{dE}{dx}\right]_{tot} = \left[\frac{dE}{dx}\right]_{col} + \left[\frac{dE}{dx}\right]_{rad} \text{ MeV/cm.} \tag{2.3}$$

Total stopping power represents the total amount of energy loss by an energetic charged particle due to inelastic collisions and production of bremsstrahlung photons in a transport medium per unit path length traveled by a particle. It is noted that the collisional energy loss is proportional to Z

and increases logarithmically as a function of electron energy whereas energy loss to secondary photon production is proportional to Z^2 and increases linearly with electron energy. Radiative energy loss in high Z material at high electron energies becomes very significant. This could be important in fusion reactor design because a photon is uncharged and leaves a plasma medium without any further interaction. Therefore in a hot plasma confined by a magnetic field bremsstrahlung photon production results in nonrecoverable energy loss; i.e., photons leave the system. Depending on the computational model used and energy range, it may be important that the transport of secondary particles be taken into account in addition to the transport of primary particles. Therefore the complexity of electron transport problem arises from the cumulative effect of all probably interactions and coupling between them. Exact calculation of total electron flux requires the transport of secondary "knock-on" electrons as well as primaries to obtain exact spatial distribution of energy deposition.

In the slowing down process of energetic electrons, they lose a small amount of energy by elastic nuclear scattering which may be attributed to its small mass compared to nucleus, and this loss is negligible compared to the loss of energy in an electron-electron collision. The theoretical maximum energy loss in an electron-electron collision is

equal to half of its initial energy before collision (22). The probability of the largest energy loss interactions is not too high but rather electrons generally make small energy loss collisions. For example, in order to lose an appreciable fraction of its energy, an electron must go through about 10^4-10^5 collisions, whereas neutral particles, i.e., neutrans or photons, undergo less than 50 collisions for corresponding fractional energy losses (38). This is one of the very significant distinctions between electron transport and neutral particle transport problems. It affects Monte Carlo calculations in the sense that longer histories may be required in electron transport calculations compared to neutron or photon histories. Detailed collision histories for electrons are not possible in reasonable computing times. To solve electron transport problems by Monte Carlo techniques, integral collision information is used to approximate the result that would be obtained from detailed collision histories. The resulting complex electron transport relationships have been expressed, for instance, in terms of multiple scattering (23), production and transport of secondary particles and fluctuations in energy losses (24). Either multiple scattering or energy loss fluctuations have a very strong effect on the spatial distributions of electrons in transport medium. First treatment of energy loss of charged particles was done by Bohr (25) and then Bethe

(21,26,27,28), who extensively investigated the problem. Bethe's theory of electronic stopping power is based on a plane-wave Born approximation (21). The stopping power is defined as the average energy loss per centimeter of path-length being traveled which is represented in slightly different forms by different authors (26,27,28,29,30,31,32,33,34). In general, at initial energy E_0, it may be represented as -considering all possible energy losses-

$$-\frac{dE}{dx} = N \int_{E_0/2}^{E_0} (E_0 - E) \times \frac{d\sigma_{inel}(E_0,E)}{dE} \, dE \qquad (2.4)$$

where

N = electron number density = $\left(\frac{A_0\rho}{M}\right) \times Z$

A_0 = Avagadro's number, ρ = density of medium, M = atomic weight of medium, $E_0 - E$ = energy loss in electron-electron collision, Z = number of electrons per atom.

The energy loss equation given above states that the average energy loss per cm. of pathlength being traveled may be produced by integrating the product of "given energy loss" times the associated inelastic differential scattering cross-section over all probably energy losses (29), provided that a uniform particle density is assumed in transport medium. In electron transport problems it is common that - energy losses are classified as "small energy transfers" and "large energy

transfers." Total energy loss may be taken as a sum of these two losses in the two classifications.

The most significant quantity in neutral/charged particle collisions is the magnitude of energy losses and angular distribution of scattered particles after collision. The detailed theories of energy loss mechanisms for various types of charged particles are extensively discussed in literature (10,21,22,30,31,32,33,34). A review of the basis of energy transfer to electrons will be given in the following paragraphs. The distinction of possible energy losses to target electrons may be made by drawing a line between small energy transfer collisions and large energy transfer collisions. It is difficult to draw a clear line between small energy losses and large energy losses. Let us denote the cut-off energy of these two energy losses by E_c. Selection of E_c may be made based on the following specifications:

(i) E_c is large enough compared to binding energies of electrons, I, in transport medium

(ii) E_c should be small enough such that for energy transfers of the order of E_c or energy transfers smaller than E_c, the effective collision parameter is large with respect to atomic dimensions. This implies that the charged particle can be treated as a point particle. In practical applications E_c values are in between I - 100I (6).

For small energy transfer collisions to electrons, $Q < E_c$, the average energy loss has been derived by Bethe (21,30,35). The average energy loss is obtained by summing over all the excitation probabilities of the atom, which is given as, average energy loss per cm.,

$$-\frac{dE}{dx} = \frac{2\pi N(Ze^2)^2}{mc^2\beta^2}\left[\ell n\frac{2mc^2\beta^2E_c}{I^2(1-\beta^2)} - \beta^2\right] \text{ for } Q < E_c \quad (2.5)$$

where

E_c = upper bound of the small energy transfer collisions

mc^2 = 0.511 Mev = electron rest mass energy

Ze = charge of primary particle

Z = 1 if primary particle is an electron

β = v/c = relativistic velocity of electron/speed of light

I = mean ionization potential of transport medium.

This expression applies to all types of primary charged particles where primary electrons and positrons are also included.

If the energy transfer to target electron by any kind of charge particle is large, $Q > E_c$, then the average energy loss depends on the type of primary particle. In this case the target electron is treated as a free particle. The energy transfer cross-sections for heavy particles to target electron are given by different authors. Such cross-sections have been outlined by Uehling (30).

The differential energy transfer cross-section for electron-electron collisions was calculated by Møller and given as follows for the transfer of energy Q in dQ:

$$\frac{d\sigma}{dQ} = \frac{2\pi e^4}{m\beta^2 c^2} \frac{1}{Q^2} \left[1 + \left(\frac{Q}{E_0 - Q}\right)^2 + \left(\frac{\gamma - 1}{\gamma}\right)^2 \left(\frac{Q}{E_0}\right)^2 - \frac{2\gamma - 1}{\gamma^2} \times \left(\frac{Q}{E_0 - Q}\right) \right] \tag{2.6}$$

where

$E_0 = mc^2(\gamma - 1)$ = kinetic energy of electron and

$\gamma = (1 - \beta^2)^{-\frac{1}{2}}$.

The collisional energy loss may be calculated per cm. of path length being traveled as given below using eqn. (2.6):

$$-\frac{dE}{dx} = N \int_{E_c}^{E_0/2} Q \, d\sigma \, (E_0, Q) \quad \text{for } Q > E_c. \tag{2.7}$$

which gives

$$-\frac{dE}{dx} = \frac{2\pi e^4 N}{m\beta^2 c^2} \left[\ln \frac{E_0}{4E_c} + 1 - \frac{2\gamma - 1}{\gamma^2} \ln 2 + \frac{1}{8} \left(\frac{\gamma - 1}{\gamma}\right)^2 \right] \tag{2.8}$$

The defined relativistic energy transfer differential cross-section above may be given in terms of initial and final energies of scattered particle per electron as follows:

$$\frac{d\sigma_{inel}(E_0, W)}{dW} = \frac{2\pi e^4}{mc^2\beta^2} \times \frac{1}{E_0^2} \left[\frac{1}{\left(\frac{W}{E_0}\right)^2} - \frac{2K - 1}{K^2} \frac{1}{\frac{W}{E_0}\left(1 - \frac{W}{E_0}\right)} + \frac{1}{\left(1 - \frac{W}{E_0}\right)^2} + \left(\frac{K - 1}{K}\right)^2 \right] \quad \text{per electron.} \tag{2.9}$$

where, also defining T,

$$K = \frac{E_0+mc^2}{mc^2} = \frac{E_0}{mc^2} + 1 = T + 1 \qquad (2.10)$$

E_0 = initial kinetic energy of primary particle

W = kinetic energy of scattered particle (primary particle)

The coefficient term in front of the brackets can be simplified by using the relativistic equivalent of v^2/c^2 and $e^4 = (r_0 \times mc^2)^2$. After clearing the terms one can obtain the following which is also reported in the literature:

$$\frac{d\sigma(E_0,W)_{inel}}{dW} = 2\pi r_0^2 \times \frac{(T+1)^2}{T^2(T+2)} \left[\frac{1}{(\frac{W}{E_0})^2} - \frac{2K-1}{K^2} \times \frac{1}{\frac{W}{E_0}(1-\frac{W}{E_0})} + \right.$$

$$\left. + \frac{1}{(1-\frac{W}{E_0})^2} + \left(\frac{K-1}{K} \right)^2 \right] \qquad (2.11)$$

This is the equation of differential inelastic scattering cross-section which will be used in the basic property calculations. It should be multiplied by electron number density to produce macroscopic properties. The appropriate form of the differential energy transfer cross-section has been used by several authors in producing transport results. In general, the total average energy loss per cm. of path length being traveled can be determined by summing up the energy loss contributions due to soft collisions and large energy transfer collisions. For electrons, this is given as

$$\left(-\frac{dE}{dx}\right)_{col} = \frac{2\pi e^4 N}{m\beta^2 c^2}\left[\ln\frac{E_0^2(\gamma+1)}{2I^2} + (1-\beta^2) - \frac{2\gamma-1}{\gamma^2}\ln 2 + \frac{1}{8}\left(\frac{\gamma-1}{\gamma}\right)^2\right] \quad (2.12)$$

The energy transfer differential cross-section is, in general, given in terms of doubly differential form in energy and angle as represented below:

$$\frac{d^2\sigma(E_0,W,\vec{\Omega}_0\cdot\vec{\Omega})}{dW d\Omega} = \frac{d\sigma(E_0,W)}{dW} \times \frac{\delta(\vec{\Omega}_0\cdot\vec{\Omega}-f(E_0,W))}{2\pi} \quad (2.13)$$

where $d\sigma(E_0,W)/dW$ given by eqn. (2.11).

For a given energy loss one can calculate the corresponding angular deflection by the following expressions, where $f(E_0,W)$ is also defined as well.

$$f(E_0,W) = \cos\theta_h = \mu_h = \left[\frac{W(E_0+2mc^2)}{E_0(W+2mc^2)}\right]^{1/2} \quad \text{for } \frac{E_0}{2} \le W \quad (2.14)$$

$$f(E_0,W) = \cos\theta_\ell = \mu_\ell = \left[\frac{(E_0-W)\times(E_0+2mc^2)}{E_0\times(E_0-W+2mc^2)}\right]^{1/2} \quad \text{for } \frac{E_0}{2} > W \quad (2.15)$$

$$\text{Here } \cos\theta_h \ge \cos\theta_\ell \ge 0 \quad (2.16)$$

and θ_h represents the angular deflection of highly energetic particle after collision, and θ_ℓ represents the angular deflection of less energetic particle after collision. By using the eqn. (2.11) the average properties such as "average energy" and "average angular deflection" of primary particle after all

possible inelastic collisions will be covered in detail in Chapter (IV). These average properties are the fundamental parameters in constructing the squashed electron transport model (ANISN-CSDM).

Energy losses defined above are due to inelastic collisions which are governed by Møller cross-section. No energy loss is assumed in elastic collisions. Bethe's theory has been reformulated by Rohrlich and Carlson (29) so that it is applicable to numerical calculations.

B. Techniques to Solve Electron Transport Problems

The techniques to solve the electron transport problems may be classified as

1. Analytical Methods (28,36,37)
2. Numerical Deterministic Methods (35,38,39,40,41,42)
3. Monte Carlo Method (16,19,20,24,38,40,43)
4. Discrete Ordinates Methods (7,8,43,44,45,46)

A discussion of these methods follows. Of these, Monte Carlo and Discrete Ordinates Methods will be discussed in detail because the transport results are produced by the latter, which is the developed scheme in this study, and will be compared with the results of the Monte Carlo Methods.

1. Analytical Methods

Most of the early works of electron transport were based on the extension of Bethe's stopping power theory. Some

of them do not include energy losses in the calculation of spatial distributions and angular distributions of primary particles. Analytical methods were basically developed assuming infinite uniform media. Therefore one could face great difficulties when the results of uniform media are applied to nonuniform media, such as difficulties at different material boundaries. Some of the analytical works are as follows:

The basic parameters which are necessary to formulate electron transport problems were discussed by Rohrlich and Carlson (29). Energy losses by large energy transfer collisions are defined to obtain numerical results. The other parameters, such as energy straggling is attributed to the statistical nature of the collisional energy loss process, and the elastic scattering cross-section is given in terms of Mott formulation. One may note that elastic scattering and inelastic scattering result in multiple scattering. Both of these collisions play a very significant role to produce electron transport results.

A general treatment of multiple elastic scattering of electrons was given by Goudsmit and Saunderson (23). The distribution of elastically scattered electrons, i.e., scattering probability, is given as a sum of the Legendre polynomials. This sum would be put into a form such that it represents the multiple elastic scattering distribution of electrons. One can then sample the mean scattering angle of a multiply

scattered electron from the cumulative multiple scattering distribution. Spencer (36) has treated the electron transport by including combined effects of scattering and slowing down of electrons in the theory of electron penetration in an unbound uniform media. The electron flux can be obtained from the knowledge of spatial moments. Therefore, in Spencer's solution procedure of electron transport equation, electron flux and source are first expanded into the Legendre polynomials and then the resulting equation is transformed into a form where the spatial moment coefficients can be calculated by numerical integration. In addition, elastic scattering cross-section and deep penetration radiation transport problems are discussed as well.

The first theoretical study of obtaining the electron distribution function was made by Lewis (47). His treatment is based on the large angle multiple scattering in an infinite uniform medium. Energy losses are calculated by the continuous slowing down model. The electron distribution function is expanded into spherical harmonics whose expansion coefficients can be determined exactly. The spatial distribution and angular distribution of the electrons scattered are found using the expansion coefficients of the electron distribution function to calculate moments of spatial and angular distributions. A numerical procedure to calculate the moments is not given in his work.

In a short review of the state-of-the-art of the basis of electron transport theory, calculations and related experiments were given by Zerby and Keller (16). In this review an attempt has been made to reflect the natural development of the electron transport calculations from the basic data and the fundamental transport theories. Their effort includes the sophisticated simple-geometry calculations as well as realistic complex geometry calculations. The primary interactions which affect the transport of electrons and model used in electron transport theory are examined. Also the work includes the summaries of electron transport computer codes for complex geometrics where a brief description of their functions is given as well as the pitfalls associated with the solution procedures stated.

2. Numerical Deterministic Methods

The phase space time evolution method and segments model method may be included in numerical deterministic methods. They both use the continuous slowing down model for energy loss and the modified Goudsmit-Saunderson multiple scattering distribution to obtain angular redistribution of electrons. The characteristics of phase space time evolution method and segments model methods may be defined as follows:

a. Phase space time evolution method

In addition to the characteristics stated above it uses geometry and bookkeeping techniques similar to those

used in Monte Carlo methods to obtain transport results such as energy deposition. Calculational procedure includes step-by-step following of an expanding wave in phase space, recording all phase information in each time step. It is a deterministic method, i.e., calculational procedure does not include statistical variation. In includes time-dependence and results depend on choise of adequate spatial, angular and energy grids.

b. Segments model

It uses methods of moments, both spatial and angular, to produce transport results. It could be treated as the development of Spencer (36) and Lewis (47) concepts such that results are applicable in a finite medium. It is a deterministic method and uses the continuous slowing down model to calculate energy losses. Angular deflection information is produced from the Goudsmit-Saunderson multiple scattering theory. It uses both spatial and directional moments to calculate electron flux. It is worth mentioning that the deterministic methods are produced from approximate solutions of analytical formulations. Therefore deterministic methods throw away some detailed information. It may be possible to keep some of the detailed information in Monte Carlo calculations at the expense of more computing time.

3. Monte Carlo Methods

A Monte Carlo method is, in general, a statistical

method where the distribution characteristics of a particle population in a system are determined by sampling from appropriate theoretical or measured distributions. For example, in electron transport problems, angular deflections can be sampled from the Goudsmit-Saunderson distribution (23). Similarly, energy losses due to the cumulative effect of inelastic collisions can be chosen from the continuous slowing down approximation or sampled from a Landau distribution which is a convolution with a Gaussian (24,38). This method can be applied to analyze the geometrically complex assemblies (16).

One of the first applications of Monte Carlo methods to electron transport problems was done by Schneider and Cormak (39). They made use of Spencer and Attix (40) schematization to overcome the difficulties associated with very small energy loss collisions (a very large number of collisions are required to reduce energy of an electron to a minimum), and large energy loss random numbers (which do not provide representative samples of large energy losses). In this scheme, a "cutoff" energy is arbitrarily introduced into the model such that an electron collision which results in energy loss less than the "cutoff" energy is treated as if it loses its energy at a "continuous rate." The energy loss rate may be determined from an equation similar to eqn. (2.18). It is probable that some collisions can result in energy losses

greater than "cutoff" energy. Such collisions are called "discrete collisions," and they result in the production of δ-rays, i.e., secondary electron production. This event also results in the "skipping of energy regions" by the primary electron which produces the secondary electron. Hence, a primary electron which undergoes a catastrophic (discrete) collision jumps over a certain segment of the energy scale and reappears with a new initial energy. The magnitude of this new initial energy is determined from the knowledge of the initial energy of a primary electron just before the catastrophic collision and the energy imparted to the δ-ray. The magnitude of energy losses in such individual catastrophic collisions can be as much as $1/2\ E_0$, where E_0 is the kinetic energy of the primary electron before the collision. It is worth mentioning as part of the electron transport theory that after an electron-electron collision the energetic electron is arbitrarily assumed to be the primary electron. This is physically not always true. It is probable that the target electron may acquire most of the kinetic energy of the incident electron and may become the most energetic electron after the collision. It is impossible for us to say which electron is the incident electron after they come out from an electron-electron collision because they are indistinguishable. This knowledge may not be needed to produce transport results, because after the

collision one needs to know which electron has the highest kinetic energy, permitting it to penetrate further, or produce knock-ons (secondary particles). Therefore, after a close investigation of energy transfer from primary electron to target electron, one can see that the possible largest magnitude of energy transfer is E_0, in reality. But, emergent electrons after a collision are indistinguishable, therefore one may prove that the maximum energy transfer to a δ-ray (less energetic emerging electron) is equal to 1/2 E_0 which is the theoretical limit.

The energy loss model discussed above which is based on an arbitrarily defined "cutoff" energy (threshold energy for δ-ray production) can be taken as the two-mechanism model of electron slowing down. The two-mechanism model of electron slowing down can be reduced to a simpler form by taking the limiting case of a very large threshold energy for δ-ray production. This representation suppresses the production of knock-on electrons. In this case all collisions can be said to be of the continuous rate type. This approximate model is called "the Continuous Slowing Down Model" (CSDM), in which all energy losses are included in a "continuous" energy loss curve. The pictorial representation of this theoretical discussion may be given as in Figure (2.1).

The Continuous Slowing Down Model of the Monte Carlo (1) calculations may be discussed in terms of the technique

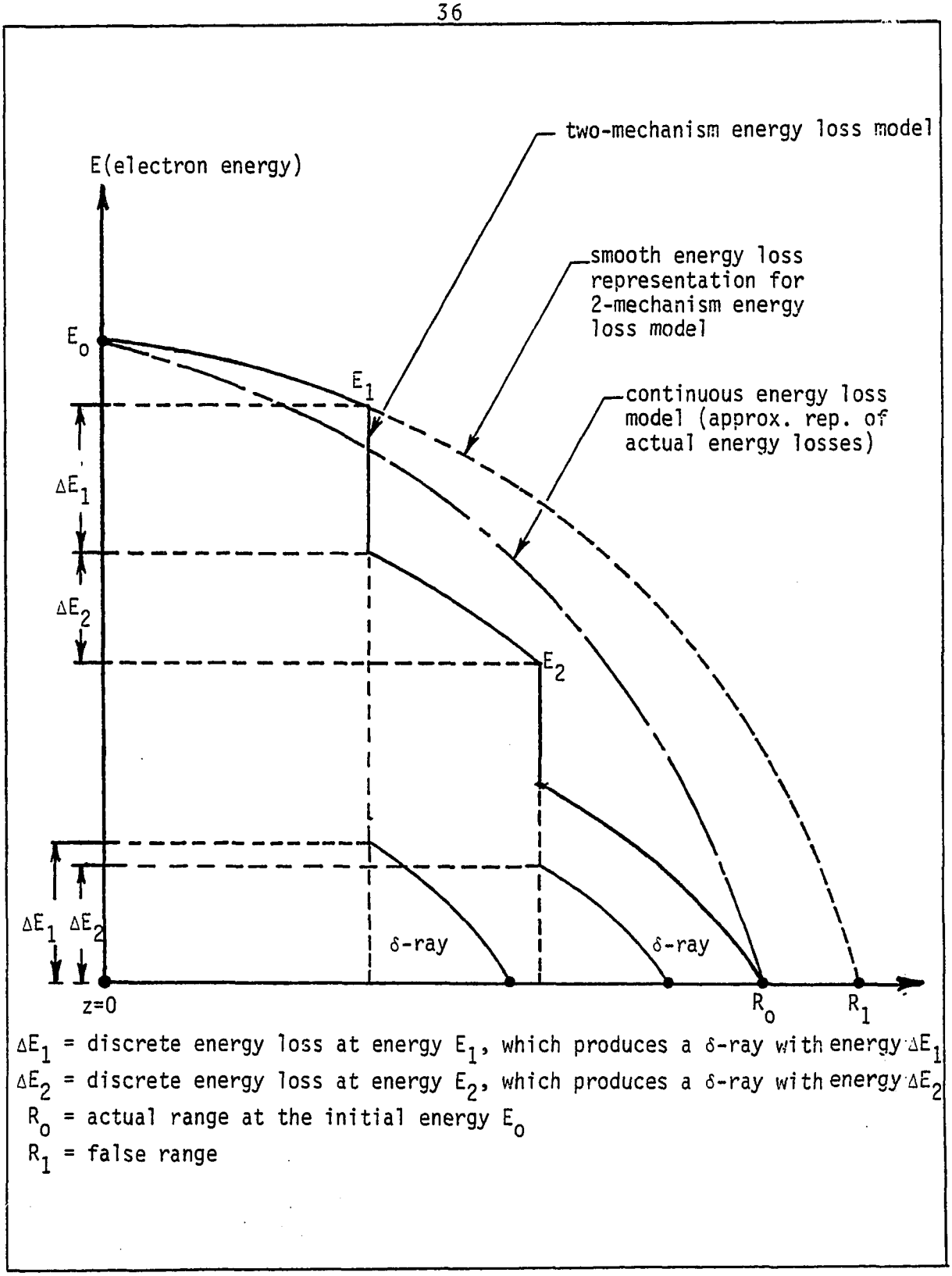

ΔE_1 = discrete energy loss at energy E_1, which produces a δ-ray with energy ΔE_1

ΔE_2 = discrete energy loss at energy E_2, which produces a δ-ray with energy ΔE_2

R_o = actual range at the initial energy E_o

R_1 = false range

Figure (2.1): Energy loss models of electron.

that it defines the states of transported particle in transport medium.

The first scheme involves the selection of pathlengths. The pathlength is determined in such a way that the energy degradation of particle from one step to the next step is related to each other by a fixed factor k. Assuming E_g, ξ_g known then as ξ_{g+1} may be calculated as

$$E_g \times (1-k) = \int_{\xi_g}^{\xi_{g+1}} \left|\frac{dE}{d\xi}\right| d\xi \qquad (2.17)$$

where

$\frac{dE}{d\xi}$ = mean rate of energy loss per unit pathlength due to ionization collisions

$k = (\frac{1}{2})^m$

m = # steps required to reduce initial energy of primary particle by a factor of two without energy loss straggling.

This formulation is called logarithmic spacing procedure.

The energy losses between spatial steps is determined by the continuous slowing down approximation as given below:

$$\int_{\xi_g}^{\xi_{g+1}} \left|\frac{dE}{d\xi}\right| d\xi = \Delta E_g = E_g - E_{g+1} \qquad (2.18)$$

where $E_{g+1} = kE_g$ applies if logarithmic pathlength intervals are used. In the production of cross-section data the

logarithmic spacing in energy reduction is used.

In certain transport problems, such as highly energetic primary electron transport in high Z transport medium, the energy loss by photon production becomes significant. In such a problem the energy loss between spatial steps should be obtained from a distribution in which ionization and photon production energy losses are taken into account. Such a distribution was derived under the assumption that $\Delta E_g/E_g << 1$. The expression of distribution is given as a convolution of ionizational energy loss distribution $W_I(\Delta E)$ with the photon production loss (bremsstrahlung loss) distribution $W_B(\Delta E)$ as follows:

$$W_{IB}(\Delta E_g) = \int_0^{\Delta E_g} W_I(\Delta E_g - U) W_B(U) dU \qquad (2.19)$$

The second scheme involves the specification of energy steps of primary particle reached in the transport process. It is possible to specify a set of preselected energies, such as: E(0),E(1),E(2),...,E(g), such that one may determine the following states of particle which may be represented schematically as follows:

$$\text{----} \begin{pmatrix} \xi_{g-1} \\ E_{g-1} \\ \vec{\Omega}_{g-1} \\ r_{g-1} \end{pmatrix} \rightarrow \begin{pmatrix} \xi_g \\ E_g \\ \vec{\Omega}_g \\ r_g \end{pmatrix} \rightarrow \begin{pmatrix} \xi_{g+1} \\ E_{g+1} \\ \vec{\Omega}_{g+1} \\ r_{g+1} \end{pmatrix} \text{------}.$$

The energy loss structure may be constructed either using logarithmic spacing or uniform spacing. Pathlengths may be evaluated using continuous slowing down approximation as follows:

$$\Delta\xi_g = \xi_{g+1} - \xi_g = \int_{E_{g+1}}^{E_g} \frac{dE}{\left|\frac{dE}{d\xi}\right|} \tag{2.20}$$

In the continuous energy loss model, the assumption is made that a primary electron loses its energy continuously at a rate which is equal to average collisional energy loss. A primary electron passes through all energies below its incident energy. Energy loss is assumed to be deposited in the transport medium. Accurate electron transport results can only be obtained by including the transport of secondary electrons and bremsstrahlung photons. This is required because secondary particles can carry energy away from the spatial point where they are produced. Therefore, secondary particles have their own energy distribution in addition to primary particle energy distribution. Hence, if one wants to produce exact transport results he must take into account transport of secondary particles to produce true spatial distribution of energy deposition. One may conclude from this discussion that the continuous slowing down model of energy loss does not include the transport of secondary particles separately, but rather represents the smooth energy loss and

discrete energy losses in an approximate way.

The continuous slowing down model discussed above is later introduced into the ETRAN (1) computer code family by Berger (38), where this option is used to make comparisons with many older Monte Carlo program results. A large scale application of the probabilistic concepts into electron transport, photon transport problems have been done by Berger (38) and extended by Halbleib and Vandevender (2,3,4, 5), where numerical computation is used as a means of putting the relevant multiple scattering theories into a logically consistent method. The characteristic concept of Berger's electron transport model is the "condensed random walk." This concept may be made clear through the following discussion: The energy range through which an electron slows down is divided into a number of "steps." Each step may represent the cumulative effect of several interactions, and a step is then said to be approximated by a "condensed random walk." A step in the continuous slowing down model may be defined using eqn. (2.18) by assuming that the mean energy loss per unit path length remains constant over the specified pathlength. Then one can obtain, similar form of eqn. (2.20),

$$\Delta\xi(g) = \frac{\Delta E(g)}{(dE/d\xi)_g} \quad \text{cm.} \tag{2.21}$$

From eqn. (2.21) it is obvious that the incremental spatial displacements are linearly related to the incremental energy

loss through stopping power, or vice versa. Probability of producing bremsstrahlung photons is very small, and not many photons are produced per spatial step. Therefore, individual bremsstrahlung photons can be sampled from a distribution without using excess computer time. (If bremsstrahlung photons are simulated their transport will result in photoelectric, Compton and pair production interactions. The choice of interaction is determined by further distribution sampling.) On the other hand, it is not practical to sample successive individual interactions of a primary electron with atoms and atomic electrons because primary electrons undergo many collisions in a small spatial displacement. Therefore, instead of sampling the individual collisions of a primary electron from a distribution, it is useful to group these numerous collisions, and represent them by an average "single collision." This single collision closely represents (i.e., takes into account) the combined effect of overall angular deflections and energy losses of a primary electron which makes many collisions in a short distance. Such a single collision is called a "condensed random walk." An electron track is compowed of several random walk "steps." Each electron track is broken down into many steps. (They may also be called "segments.") This formulation, i.e., condensed random walk concept, is included in ETRAN (1) computer codes and is successfully applied to the practical solutions of the electron/photon transport problems. In this

formulation, it is intended to reduce one-to-one simulation (analog simulation) of electron interactions by using segments. Selection of step sizes depends essentially on the energy loss model used in the calculational procedure. In general, a step size should be large enough so that computer requirements are not excessive. It should be small enough so that the analytical theories predicting the angle and energy changes during a condensed random walk are sufficiently accurate (41,42). The last requirement implies that step size should decrease as energy of primary electron decreases. That is, as an electron becomes less energetic its residual range becomes shorter. It eventually tends to approach zero when kinetic energy of electron vanishes.

An idealized pictorial representation of "condensed random walk model" for one-dimensional slab geometry, is given in Figure (2.2). In this representation, a low energy "cutoff" is defined, terminating the condensed random walk steps at a depth which sufficiently approximates the total range of incident electrons. In Figure (2.2), X(N) is the linear depth after N steps and R_0 is the total range of incident electrons with energy E_0.

The basic computer code which has been used in electron/photon transport problems is the ETRAN family of computer codes. ETRAN is a Monte Carlo computer code system for electron and photon transport through slabs and cylinders

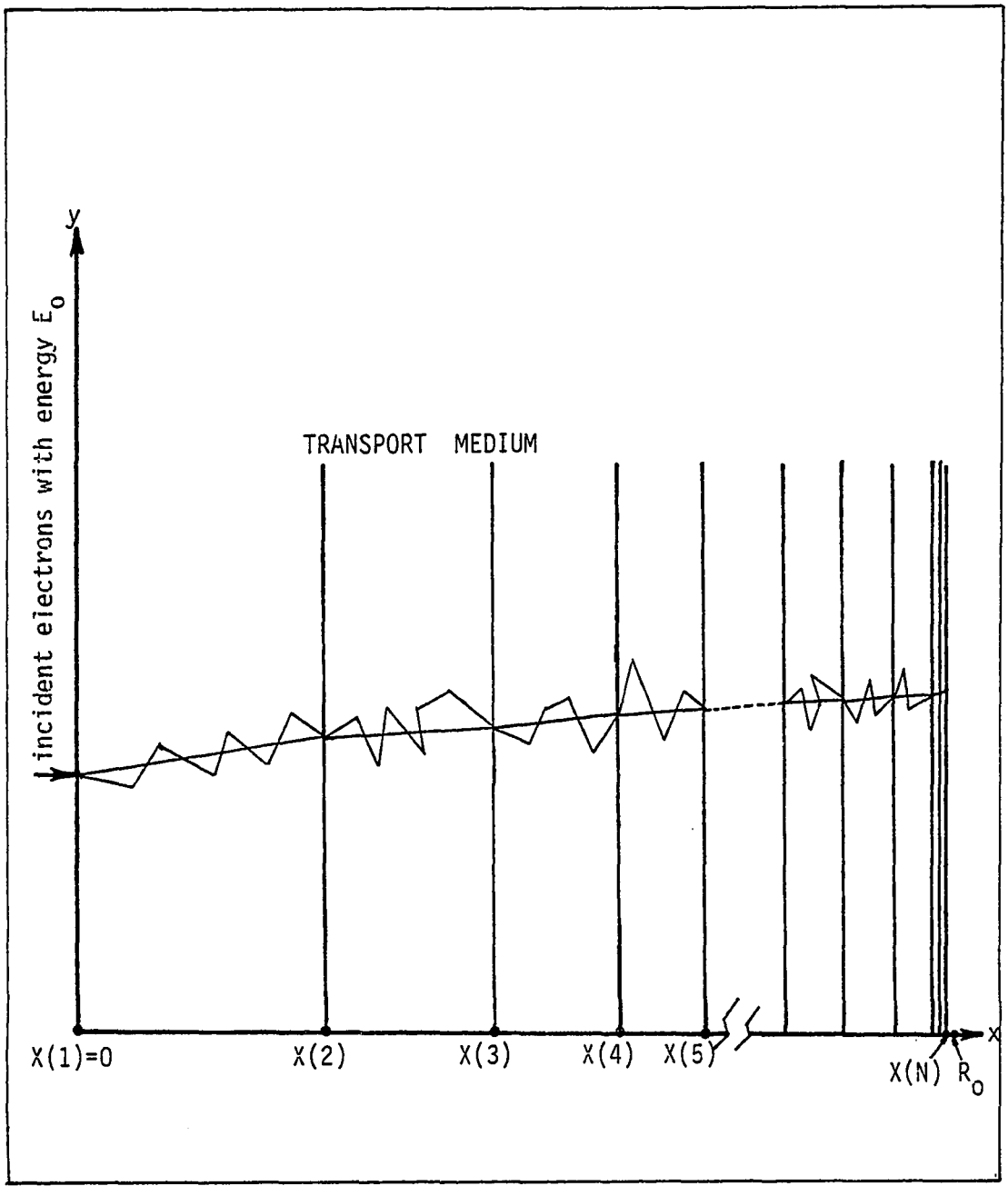

Figure (2.2): Condensed Random Walk Model

(1). It can compute the transport of electrons and photons through plane-parallel slab targets which have a finite thickness in one-dimension but are unbound in the other two dimensions. ETRAN18G, which version is currently used, can be employed to represent two-dimensional geometry by properly specifying the dimensions of nested cylinders. Material properties required by ETRAN18G are provided by the computer code DATAPAC(version 6) which reads its input data from a cross-section library called DATATAPE(version 2C). One can link all of these codes and cross-section libraries as given in Figure (2.3). The functions of the blocks in Figure (2.3) may be outlined as follows:

(i) DATATAPE which includes cross section data and other transport properties for materials with atomic numbers, Z=1,2,...,100.

(ii) DATAPAC reads its input data from DATATAPE then processes and expands these data, and puts them in tabular arrays. It also calculates stopping power with or without a specified cutoff energy for a single collisional energy loss. DATAPAC is a general program to prepare input information for electron transport problems for individual materials, compounds and mixtures.

(iii) ETRAN reads its input data from a file produced by DATAPAC and from cards which specify the

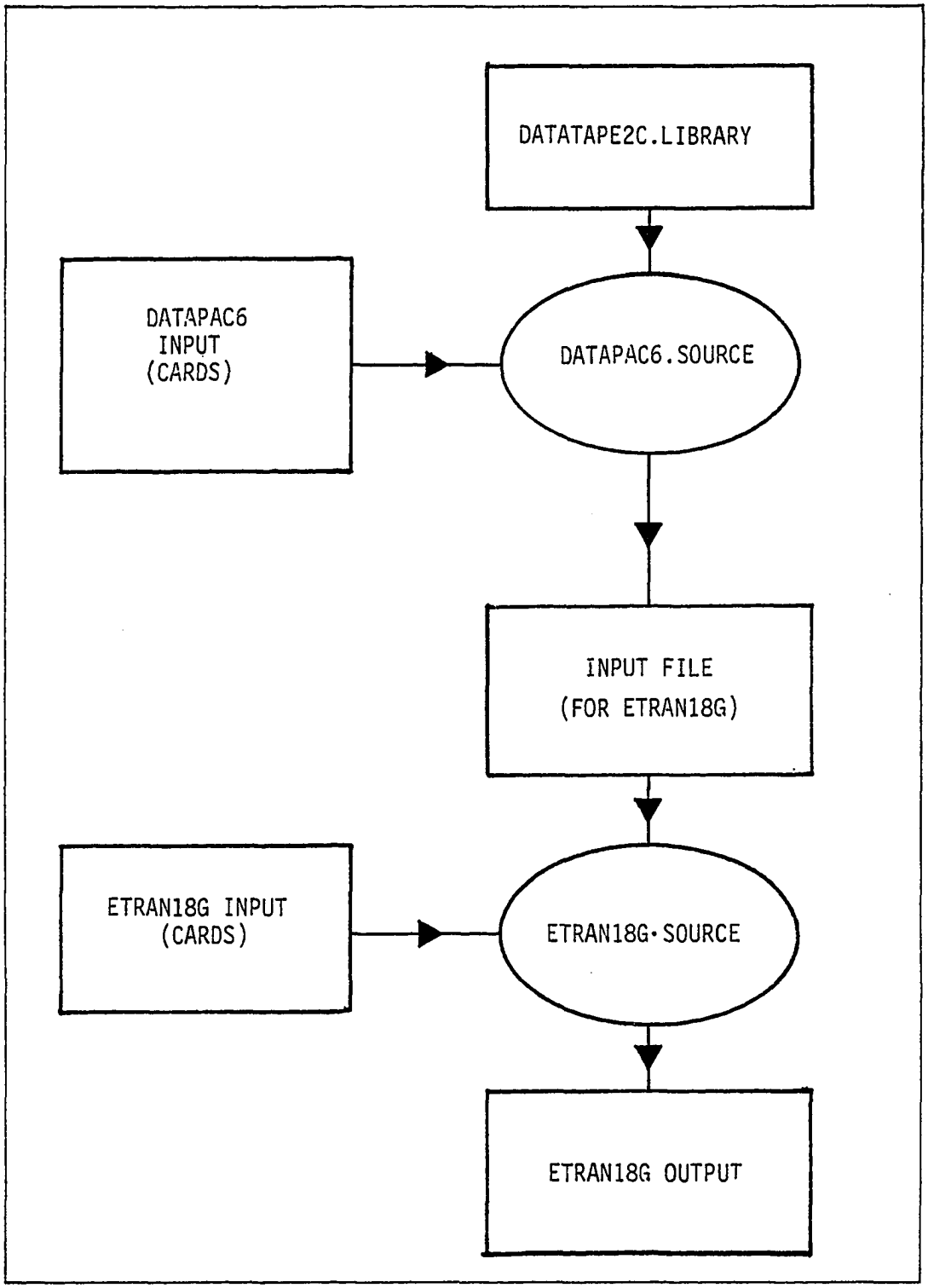

Figure (2.3): Block diagram to produce ETRAN18G output.

particular geometry and options of the problem. It generates large sets of electron and photon histories by random sampling. It calculates transmission and reflection particle currents, energy deposition and particle fluxes.

The calculation models of ETRAN may be outlined as follows:

a. The continuous Slowing Down Model (CSDM):

In this model, energy losses greater than the "cutoff" energy are not treated separately. Collisional energy losses are based on information supplied by DATAPAC using Rohrlick and Carlson (22) formulation for collisional stopping power. The theory of this option is covered in detail in the previous paragraphs of this subsection.

b. Discrete Interactions Model (DIM):

In this model large energy loss interactions are treated separately from the "continuous" small loss interactions. This is the two-mechanism model discussed earlier. The large energy losses in a step due to the cumulative effects of many inelastic collisions is sampled from a Landau (24) distribution. Energy loss in a step consists of two parts. In the first part, electron loses its energy according to continuous slowing down model. Second part includes an energy loss due to a discrete interaction which is sampled from a distribution. The step is terminated after the discrete interaction and after the electron moves into the next spatial interval. The total energy loss per step is the sum

of energy losses due to continuous slowing down and discrete interaction which take place in a step. Discrete interaction does not result in change of spatial step but a significant energy degradation. Depending on the magnitude of total energy loss per step an electron can "skip" to lower energies without changing its spatial segment. It is assumed that each discrete interaction produces a δ-ray. In ETRAN the primary electron is unaffected by a knock-on "δ-ray" electron production but energy losses and angular deflections due to a δ-ray production are approximately included in the primary electron loss sampling and multiple scattering distribution. Skipping to lower energies by an electron is determined by its final energy before it leaves the previous spatial step. Final energy is precisely determined from the knowledge of its energy at the beginning of step and total energy loss over the step. A detailed investigation of relevant subroutines to calculate energy losses shows that the energy group width is the sum of collision and bremsstrahlung energy losses in CSDM of ETRAN18G. Therefore, group skipping of an electron is not possible in CSDM. This is a contrast to the discrete interactions model of ETRAN18G. That is the energy of electron is tested after each scattering in order to determine its next energy group. This idea may be represented mathematically as follows:

One may define the final kinetic energy of primary

electron after an electron-electron collision in energy group g, as follows:

T_f = final kinetic energy of primary electron = $T_{init.} - \Delta E_{loss}^{tot.}$

where $\Delta E_{loss}^{tot.}$ = total energy loss after an inelastic collision

$T_{init.}$ = primary electron initial energy before collision.

If $0 < \Delta E_{loss}^{tot} \leq \Delta E_{g+1}$, primary electron moves into the next energy group.

If $\Delta E_{g+1} < \Delta E_{loss}^{tot} \leq (\Delta E_{g+1} + \Delta E_{g+2})$, primary electron skips the next energy group and moves into (g+2)-nd energy group.

If $(\Delta E_{g+1} + \Delta E_{g+2}) < \Delta E_{loss}^{tot} \leq (\Delta E_{g+1} + \Delta E_{g+2})$, primary electron skips the first two energy groups after g-th energy group, and moves into (g+3)-rd energy group, where ΔE_g's represents the energy group width of the associated energy groups. This procedure shows how the primary electron is classified after an electron-electron collision in the discrete interactions "hard collisions" model. Potential sources of error in Monte Carlo calculations may be discussed as follows:

Analog Monte Carlo calculations may produce exact results whereas it requires very long computer time. The only error associated with this scheme is statistical uncertainty in produced results. Condensed random walk Monte Carlo

calculations provide approximate results. The continuous slowing down and multiple scattering theories result in systematic errors in calculations. In order to get low statistical error one needs relatively long computer time. The statistical and systematic errors are the sources of errors in condensed random walk model calculations. Due to the fact that there exist some difficulties with the statistical accuracy produced in Monte Carlo calculations, a different calculational technique was developed by Bartine, et al.(6) which is a totally deterministic method applied to the solution of electron transport problems. This is the Discrete Ordinates Method (DOM) which was developed for neutron, photon transport. This method does not involve any Monte Carlo statistical approach. DOM uses balance methods in order to solve transport equation. It may possibly include systematic errors but no statistical errors at all. A detailed treatment of the Discrete Ordinates method will be given in the next section.

4. Discrete Ordinates Method (DOM)

Discrete Ordinates method was first developed by Carlson (45) in 1955 to solve neutron and gamma-ray deep penetration transport problems. It has been used successfully to determine detailed distribution of radiation in one- or two-dimensional geometries although some difficulties were reported in two-dimensional geometries. The Discrete

Ordinates Method uses numerical methods (finite difference) to solve approximately the particle transport equation. In this scheme, independent variables of steady-state transport equation are treated discretely. This method applies to the multigroup form of the transport equation to obtain practical results. Practically, the analytical solution of the Boltzmann linear transport equation is impossible due to the fact that the transport parameters, such as total macroscopic cross-section $\Sigma_t(\vec{r},E,t)$ and the scattering cross-section $\Sigma_s(\vec{r},E' \rightarrow E,\vec{\Omega}' \rightarrow \vec{\Omega},t)$ are very much energy dependent. For this reason, one can think of breaking down the energy range into subintervals such that the particle flux could be treated nearly constant over each energy subinterval. One, then, can define average behavior of transport parameters for each energy segment ΔE_g. The size of energy segments are not necessarily the same throughout the energy range of particles. These energy segments "energy subintervals" are called energy groups. They can be numbered from high to lower energies as shown in Figure (2.4). Solution strategy of the multigroup transport equation (will be discussed in Chapter (III)) goes as first solving the equations for the highest energy, energy group 1, and then goes to second energy group, until the last energy group IGM is reached.

The basic idea of the Discrete Ordinates Method is to divide the angular variable into discrete directions and

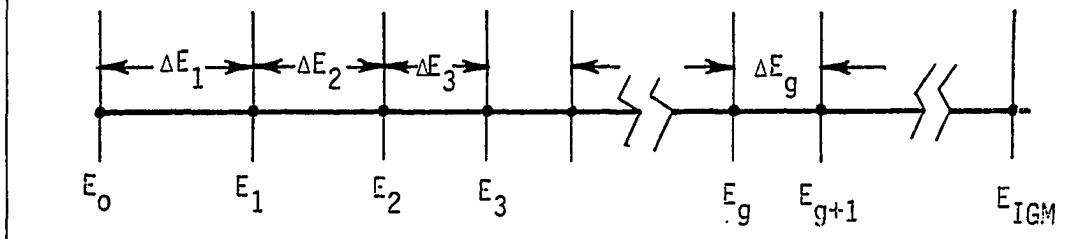

Maximum number of energy groups = IGM

Figure (2.4): Multigroup representation of energy variable E.
E_o = maximum energy of the transport particle.

define "quadratic weights" which correspond to solid angles around these discrete directions. Then, one can treat separately the transport of particles for each of these directions and solve for the associated angular flux. More theoretical discussion of method and derivation of numerical equations from the integro-differential form of transport equation will be given in the next Chapter (III).

Bartine's investigation (6) is generally limited to electron energies below 10.0 Mev in aluminum because of his specific concern for shielding of space systems. The discrete ordinates computer code that Bartine employed to transport electrons is called ANISN. ANISN can be used, by properly defining production cross sections, to calculate the production of secondary particles during the transport of electrons (similar to n,γ coupled transport case). These secondary particles (electrons and bremsstrahlung photons) can be included in the transport calculation. While there is no limit to the production of additional electrons and photons in the code (even from secondary, tertiary, etc. electrons), the production of secondary particles (electrons andpositrons from photons) may be calculated directly.

Bartine's work employed this capability of ANISN but revised the code slightly for convenience in defining transport cross sections. A term was added to the transport equation in the code to account for small energy loss

interactions by electrons in which no angle change are assumed at all. Large energy losses are given in the group skipping formulation of electron transport. That is, electron transfer from an energy group to any other low energy group is determined by integrating the differential Moller energy transfer cross-section over the initial and final energy groups, and averaging over the initial energy group width. The angular redistribution of energy loss collisions has been expressed by expanding the cross-sections in (LMAX+1)-term Legendre series in μ, where μ is the cosine of deflection angle. The basis of approximation on the inelastic cross-sections is not clear.

The key to the application of the discrete ordinates method to electron transport problems is the production of appropriate macroscopic cross-sections. The other electron interactions of importance in transport calculations are the "elastic" collisions that they make with nuclei. These do not change electron energy appreciably, but change their direction. For elastic collisions the energy loss is negligible compared to group width. Electrons remain in the same energy group after the collision. This is called "in-group scattering." These are accounted for, by Bartine (6), in the cross-section, but with an approximation.

The collisions which produce "the small angle changes" occur most frequently, and these are removed from the cross

sections by introducing an approximation called the δ-function correction (such correction is called "extended transport correction" in general). The effect of the δ-function correction may be explained as follows: In group scattering cross-sections are highly forward peaked. Therefore, they can be approximated by a few term (say l_{max} = 25) Legendre series plus a delta function, where the delta function can be expanded into a Legendre series also. Bartine uses the properties of delta function and the Legendre polynomials to determine the few-term expansion coefficients which exclude the effect of in-group scattering collisions from cross-sections. The value of this correction can be very large. For example: the first cross-section expansion coefficient (i.e., P_0 term of $\Sigma_{s_{g\to g}}$), can be about 10^6 before correction, and 10^2 after the δ-function correction. This large correction results from the dominance of forward scattering on in-group scattering. It is desired to have a small P_0 term $\Sigma_{s_{g\to g}}$ (i.e., $\Sigma_{s_{g\to g}}$ physical cross-section) because convergence depends on the magnitude of the in-group scattering cross-section and a small value results in reduced computer time. Derivation of the δ-function correction is included in Chapter (IV).

Bartine, et al., results are in good agreement for low Z (Z=atomic number) transport materials but poor results are observed in high Z transport medium. It is not clearly known yet why their results are poor for high Z transport materials, but recently a recommendation was made by Ligou (9)

to explain the discrepancies observed between experimental data and Bartine's ANISN results. The suggestion made by Ligou may be outlined as follows: Energy losses of charged particles may be classified as (i) large energy transfers, (ii) small energy transfers (also called continuous slowing down). This is a quite arbitrary classification and the angular deflection in small energy transfers is relatively small compared to large energy transfer collisions. If both of these energy losses had been represented together then many terms would have been required in the Legendre expansion of the differential energy loss cross-section. This must be avoided because it requires large input cross-section matrices and more computing time. This difficulty may be removed by breaking the energy transfer operator into two parts in the Boltzmann transport equation according to the energy loss classification defined above. In the final form, small energy transfer is expressed as a deflection operator to account for small angle change and a continuous slowing-down term to account for small energy loss. The elimination of the small energy loss as a cross-section from the transport equation also removes the difficulty of very large cross-sections values which lead to numerical convergence difficulties. At the time this suggestion was made (1979) no code had been written to include deflection operator term in the Boltzmann transport equation.

Another example of an application of the discrete

ordinates method, which is briefly mentioned earlier, is its use in sputtering problems (i.e., ions are incident on the inner wall of a controlled thermonuclear reactor) reported by Hoffman (11). He reported that neutran/photon transport computer codes such as ANISN or DOT can be used in obtaining solution of charged particle transport problems by modifying multigroup cross-section representations.

The accuracy of the developed electron transport model, ANISN-CSDM, will be tested by the standard ANISN computer code. A survey of the basic concepts of the discrete ordinates method and the representation of anisotropic scattering in the general formulation will be discussed in the next chapter. In addition, multigroup form of one-dimensional slab geometry discrete ordinates transport equation will be explained using the general expression. The mathematical derivations given in the next chapter can also be found elsewhere (45,53,54).

CHAPTER III

DISCRETE ORDINATES APPROXIMATION TO TRANSPORT EQUATION AND THE ELECTRON TRANSPORT EQUATION

A. Discussion of Some Basic Discrete Ordinates Concepts

The classification of the methods of solution of the Boltzmann Transport equation may be made as follows:

(i) approximate analytical methods (ordinary diffusion theory, variational methods, perturbation methods, etc.)

(ii) approximate numerical methods (discrete ordinates method, finite element method, etc.) (6,7,8,9,12, 54,54)

(iii) Monte Carlo statistical approach (48,49).

The discrete ordinates method (DOM) is one of the approximate numerical schemes to solve the particle transport equation. The solution procedure of this method to the transport equation requires integration over the angular variable μ. The basis of this integration necessitates partitioning of the continuous variable μ into a set of discrete directions so that the integral in transport equation can be replaced by an approximate sum. Angular fluxes are related

to each other by a linear interpolation between discrete directions and spatial points.

The discrete Ordinates Method is a frequently used method for the solution of neutron transport equation where the results obtained agree with exact solutions within expected error limits. In general, the objective of any proposed solution scheme to the transport equation is to determine the particle distribution function (time dependent angular flux) $\phi(r,E,\vec{\Omega},t)$ associated with the basic assumptions of the model. The following assumptions are considered in the formulation of the transport equations in general:

(i) no energy change or directional change occurs between interactions,

(ii) statistical fluctuations can be neglected because of large number of particles considered,

(iii) no change in material property due to particle interactions.

In a most general geometry, the particle distribution function (angular flux) ϕ is a function of three position variables represented by $\vec{r}(x,y,z)$, two angular variables denoted by $\vec{\Omega}(\theta,\psi)$, the energy of the particle E, and the time t. In this theoretical discussion, only one-dimensional plane geometry is considered because this geometry is adequate to compare with other available results. In one-dimensional geometry, the distribution function $\phi(\vec{r},E,\vec{\Omega},t)$ becomes a function of position variable x, angular variable variable

μ, energy E and time t; where $\mu = \vec{\Omega}.\vec{\Omega}' = \cos\theta$. The vectors $\vec{\Omega}$ and $\vec{\Omega}'$ are the unit vectors representing the direction of particle before and after the interaction with target. The basic idea in the discrete ordinates method is to break down the angular variable into a finite number of discrete directions. One can then rewrite the particle transport equation for each of these discrete directions. The particle transfer between the discrete directions is included in the formulation through coupling terms. The application of discrete ordinates to transport theory was first initiated by G. C. Wick (50) in 1943. Then S. Chandrasekhar developed the idea extensively (51,52).

The discrete ordinates method called S_N method was constructed by Carlson (45,53) in 1953. The characteristic assumption of the S_N method is that the form of angular flux is produced through straight lines between interpolation points of angular and spatial variables. For example, in one-dimensional plane geometry a linear variation of the directional flux is assumed in between (x_j,μ_j) pairs. The discrete ordinates technique solution to the transport equation, in general, requires integration over the angular variable using a numerical quadrature formula. In this technique it is necessary to specify a set of discrete directions, μ_j, and the corresponding weights, w_j. These quadrature parameters, (μ_j,w_j), are given in tables in the literature (12,44,45,46). The discrete directions may be

visualized by a set of points on a unit sphere whose origin is located at $\vec{r}(x,y,z)$. One should note that the sum of weights must be equal to the area of a unit sphere as given below:

$$\sum_{j=1}^{N} w_j = 1.0$$

If directions and weights are chosen symmetric about $\mu = 0$, then it can be expressed as

$$\mu_j = -\mu_{N+1-j} \qquad \text{and,}$$

$$w_j = w_{N+1-j} \quad , \quad j = 1,2,3,\ldots,N$$

Since the integral in the transport equation is always positive then it may be observed that $w_j > 0$ for all j values. For ANISN calculations, a set of symmetric quadrature data sets satisfying various moment conditions were developed and tabulated. Further details and applications of these quadrature data sets may be found in the literature (62).

It must be noted that for highly anisotropic scattering cases one may use nonsymmetrical quadrature sets to provide more discrete directions along a certain orientation for the accurate representation of scattering. Further details of the discrete ordinates method and the historical development can be found elsewhere (45,54).

By using the discrete directions concept the transport definitions of some typical quantities such as total particle flux, particle current in three-dimensional geometry may be defined as follows (54):

$$\Phi(\vec{r}) = \int_{4\pi} \phi(\vec{r}, \vec{\Omega})\, d\Omega \cong \sum_{j=1}^{ISCT} w_j\, \phi(\vec{r},\Omega_j) \qquad (3.1)$$

$$\vec{J}(\vec{r}) \int_{4\pi} \phi(\vec{r}, \vec{\Omega})\, \vec{\Omega}\, d\Omega \cong \sum_{j}^{ISCT} w_j\, \phi(\vec{r},\Omega_j)\vec{\Omega}_j \qquad (3.2)$$

It may be seen that both quantities are derived from the particle angular flux, $\phi(\vec{r}, \vec{\Omega})$.

The discrete ordinates idea is employed in the design of several neutral particle production computer codes such as DTF-IV(LASL), ANISN-ORNL, ONETRAN-LASL, DOT-ORNL, TWOTRAN-LASL, TRIDENT-LASL, etc. These are fairly flexible user-oriented production computer codes which are widely used as research tools in neutral particle transport analyses and could be used as well to produce charged particle transport results.

The discrete ordinates method has been further developed for neutrons/photons for which the phrase "neutral particle" is appropriate. The method is, in general, applicable also to "charged particles" which represent particles that carry at least one electronic charge, such as electron, positron, proton, deuteron, fission fragments, etc.

The behavior of a primary particle in a collision process is governed by the differential scattering cross-section. This cross-section specifies if the collision is an isotropic or anisotropic. The isotropic scattering implies that the scattering cross-section, Σ_s, is independent of direction variable $\vec{\Omega}$ in the laboratory system of collisions.

In fact, the scattering cross-sections are mostly anisotropic. If scattering is isotropic then the contribution to $\phi_j(\equiv\phi(x,\mu_j))$ is the same for all ϕ_j, the appropriate fraction of the scattering from all other ϕ_j's. If scattering is anisotropic then the scattering probability depends on the function $f(\vec{\Omega}_j, \vec{\Omega}_j)$. This is called the scattering probability function.

The stationary form of multigroup discrete ordinates representation of the electron transport equation may be given as follows

$$\vec{\Omega}\cdot\nabla\phi_g(\vec{r},\vec{\Omega}) + \Sigma_{t_g}\phi_g(\vec{r},\vec{\Omega}) = \sum_{g'=1}^{IGM} S_{g'\to g}(\vec{r},\vec{\Omega}) + Q_g(\vec{\Omega}) \tag{3.3}$$

where $Q_g(\Omega)$ = external source. The scattering source term may be represented, in general, as

$$S_{g'\to g}(\vec{r},\vec{\Omega}_j) = \sum_{j'} w_{j'}\, \Sigma_s(g'\to g, \vec{\Omega}_{j'}\to\vec{\Omega}_j)\phi_{g'}(\vec{r},\vec{\Omega}_{j'}) \tag{3.4}$$

In equations (3.3,3.4), it may be identified that Σ_{t_g} is the collision probability per unit pathlength traveled for particles at $\vec{r}$ moving in direction $\vec{\Omega}_j$ with the associated group velocity. The scattering cross-section $\Sigma_s(g'\to g, \vec{\Omega}_{j'}\to\vec{\Omega}_j)$ is the transfer probability from energy group g' into g and from direction $\vec{\Omega}_{j'}$ into $\vec{\Omega}_j$ per unit path length traveled. The weight $w_{j'}$ is the quadrature weight representing the discrete small solid angle element about $\vec{\Omega}_{j'}$ on the unit sphere.

If scattering is highly forward peaked then the contribution to $\phi_j(\equiv\phi(x,\mu_j))$ from all other $\phi_{j'}(\equiv\phi(x,\mu_{j'}))$ depends on the angle between initial direction $\mu_{j'}$ and final direction μ_j. Anisotropic scattering cross-sections are often expanded in terms of Legendre polynomials as follows (in one-dimensional geometry)

$$\Sigma_s(x,E_0,\mu) = \sum_{\ell=0}^{\infty} \left(\frac{2\ell+1}{4\pi}\right) \times \Sigma_{s,\ell}(x,E_0) \times P_\ell(\mu) \qquad (3.6)$$

The coefficients, $\Sigma_{s,\ell}$, are evaluated from angular cross-section data by

$$\Sigma_{s,\ell}(x,E_0) = 2\pi \int_{-1}^{+1} \Sigma_s(x,E_0,\mu')P_\ell(\mu')d\mu' \quad , \qquad \ell = 0,1,2,\ldots,\text{LMAX} \qquad (3.7)$$

The form of scattering cross-section given above is convenient for numerical solutions of the transport equation. So far no scheme has been developed in applying DOM to deep penetration electron transport. As discussed earlier, Bartine (6) and Hoffman (7) succeeded in limited applications for electrons and light ions respectively. Ligou (9) suggested a model which would improve the angular dependence details from approximations of earlier work through incorporation of a deflection operator for highly forward peaked very small energy loss collisions. It may be stated, in general, that angular deflections take place both in-group and down-scattering collisions. For in-group scattering collisions in which energy losses are neglected, the directional changes may be visualized as a cumulative effect of

numerous small angle deflections. These interactions are generally called "elastic collisions." The slowing-down of electrons occur by down-scattering where there exists a significant energy degradation. These interactions are called "inelastic collisions." Angular deflections in inelastic collisions may be defined through energy-angle relationship. A sum of these cross-sections is expected to be a good approximate representation of electron total cross-section. This decoupled approximate representation of total cross-section is included in ETRAN family of computer codes (8). It may be noted that no separate angle change is assumed for inelastic collisions in ETRAN calculational models.

B. General Discrete Ordinates Representation of Transport Equation.

In the following paragraphs an attempt will be made to formulate the general discrete ordinates representation of transport equation and then reduce it into one-dimensional slab geometry case where both energy and spatial meshes will be included. A steady state form of transport equation in three-dimensional space may be given as follows:

$$\vec{\Omega}\cdot\nabla\phi+\Sigma_t\phi=\int_0^\infty dE'\int d\vec{\Omega}'\,\Sigma_s(E'\to E,\vec{\Omega}'\to\vec{\Omega})\phi(\vec{r},E',\vec{\Omega}') + S(\vec{r},E,\vec{\Omega}) \tag{3.8}$$

The angular flux in spherical harmonics may be expanded as

$$\phi(\vec{r},E,\vec{\Omega}) = \sum_{\ell=0}^{\infty} \sum_{m=-\ell}^{+\ell} \left(\frac{2\ell+1}{4\pi}\right)^{\frac{1}{2}} \phi_{\ell,m}(\vec{r},E)\ Y_{\ell,m}(\vec{\Omega}) \qquad (3.9)$$

Similarly, expand the scattering cross-section in terms of Legendre polynomials as follows

$$\Sigma_s(E'\to E,\vec{\Omega}'\to\vec{\Omega}) = \sum_{\ell=0}^{L} \left(\frac{2\ell+1}{4\pi}\right) \Sigma_{s,\ell}(E'\to E)\ P_\ell(\vec{\Omega}'\cdot\vec{\Omega}) \qquad (3.10)$$

Using the addition theorem of spherical harmonics, i.e.,

$$P_\ell(\vec{\Omega}'\cdot\vec{\Omega}) = P_\ell(\mu_0) = \sum_{m=-\ell}^{+\ell} \left(\frac{4\pi}{2\ell+1}\right) Y^*_{\ell,m}(\vec{\Omega}')\ Y_{\ell,m}(\vec{\Omega}), \qquad (3.11)$$

one may rewrite the scattering cross-section as

$$\Sigma_s(E'\to E,\vec{\Omega}'\to\vec{\Omega}) = \sum_{\ell=0}^{L} \left(\frac{2\ell+1}{4\pi}\right) \Sigma_{s,\ell}(E'\to E) \sum_{m=-\ell}^{+\ell} \left(\frac{4\pi}{2\ell+1}\right) Y^*_{\ell,m}(\vec{\Omega}')Y_{\ell,m}(\vec{\Omega}) \qquad (3.12)$$

which can be reduced into

$$\Sigma_s(E'\to E,\vec{\Omega}'\cdot\vec{\Omega}) = \sum_{\ell=0}^{L} \sum_{m=-\ell}^{+\ell} \Sigma_{s,\ell}(E'\to E)\ Y^*_{\ell,m}(\vec{\Omega}')\ Y_{\ell,m}(\vec{\Omega}) \qquad (3.13)$$

Using the definitions given above one can reduce the general form of transport equation into the following form

$$\Omega\cdot\nabla\phi+\Sigma_t\phi = \int_0^{\infty} dE' \int d\vec{\Omega}' \sum_{\ell=0}^{L} \sum_{m=-\ell}^{+\ell} \Sigma_{s,\ell}(E'\to E)Y^*_{\ell,m}(\vec{\Omega}')Y_{\ell,m}(\vec{\Omega})\ \phi(\vec{r},E',\vec{\Omega}') + S(\vec{r},E,\vec{\Omega}) \qquad (3.14)$$

For the moment consider one-speed transport equation. Then one may bring equation (3.14) into the form as given below:

$$\Omega\cdot\nabla\phi\ (\vec{r},\vec{\Omega})+\Sigma_t\ \phi(\vec{r},\vec{\Omega}) = \sum_{\ell=0}^{L} \sum_{m=-\ell}^{+\ell} \Sigma_{s,\ell}\ Y_{\ell,m}(\vec{\Omega}) \int d\vec{\Omega}'\ Y^*_{\ell,m}(\vec{\Omega}')\ \phi(\vec{r},\vec{\Omega}') + S(r,\vec{\Omega}) \qquad (3.15)$$

where $Y^*_{\ell,m}$ is the complex conjugate of $Y_{\ell,m}(\theta,\psi)$ which is defined as

$$Y_{\ell,m}(\theta,\psi) = Y_{\ell,m}(\vec{\Omega}) = \left[\left(\frac{2\ell+1}{4\pi}\right)x\frac{(\ell-m)!}{(\ell+m)!}\right]^{\frac{1}{2}} P^m_\ell(\cos\theta)e^{im\psi} \quad (3.16)$$

The algorithm to solve equation (3.15) requires the selection of a set of MM discrete directions Ω_m, m = 1,2,3,...,MM (MM=ISN+1, ISN=order of angular quadrature of problem being investigated). Then the corresponsing angular quadrature weights w_m, m = 1,2,3,...,MM needs to be defined; where numerical integration is performed over angle. Now include these definitions into equation (3.15) to write

$$\vec{\Omega}_m\cdot\nabla\phi(\vec{r},\vec{\Omega}_m) + \Sigma_t\ \phi(\vec{r},\vec{\Omega}_m) = \sum_{\ell=1}^{LMAX}\ \sum_{n=-\ell}^{+\ell} Y_{\ell,n}(\vec{\Omega}_m)\ \Sigma_{s,\ell}\int d\vec{\Omega}'\ Y^*_{\ell,n}(\vec{\Omega}')$$
$$x\ \phi(\vec{r},\vec{\Omega}') + S(\vec{r},\vec{\Omega}_m) \quad (3.17)$$

The determination of integral term in equation (3.17) may be achieved through preassigned set of discrete directions and angular quadrature weights, $\{\Omega_m,W_m\}$. It may be evaluated as follows:

$$\int d\vec{\Omega}\ Y^*_{\ell,n}(\vec{\Omega})\phi(\vec{r},\vec{\Omega}) \cong \sum_{m=1}^{ISN+1}\ w_m Y^*_{\ell,n}(\vec{\Omega}_m)\ \phi(\vec{r},\vec{\Omega}_m) \quad (3.18)$$

One can insert equation (3.18) into equation (3.17) to write equation (3.15) in discrete directions as follows:

$$\vec{\Omega}_m\cdot\nabla\phi(\vec{r},\vec{\Omega}_m) + \Sigma_t\ \phi(\vec{r},\ \vec{\Omega}_m) =$$
$$\sum_{\ell=1}^{LMAX}\ \sum_{n=-\ell}^{+\ell} Y_{\ell,n}(\vec{\Omega}_m)\ \Sigma_{s,\ell}\ \sum_{m=1}^{ISN+1} w_m\ Y^*_{\ell,n}(\vec{\Omega}_m)\phi(\vec{r},\vec{\Omega}_m) + S(\vec{r},\vec{\Omega}_m) \quad (3.19)$$

where, LMAX = ISCT + 1 = (maximum order of scatter in any zone) +1. In order to obtain an algebraic system of equations for the angular fluxes at the local points it is required to introduce discrete spatial mesh and and explicit finite difference representations of derivatives appear in equation (3.19). After that, equation (3.19) can be reduced into a matrix equation form, which is solvable by computer, as given below in its general form:

$$A_1\phi(r_i,\vec{\Omega}_m) = A_2\phi(r_i,\vec{\Omega}_m) + S(r_i,\vec{\Omega}_m) \qquad (3.20)$$

where,

A_1 and A_2 represent coefficient matrices. The matrix "A_1" may be treated as a discretized streaming-collision term, and "A_2" as a discretized form of inscatter term. $S(r_i, \vec{\Omega}_m)$ may be called directional source term. The shell source is the form of source used in this study. It requires source strength specification of each energy group for all possible preselected discrete directions in appropriate spatial intervals. A normal source on slab face is assumed in producing the transport results in this work.

C. Simple Geometry Cases

1. One-Dimensional Plane Slab Geometry

For this particular application of equation (3.19) the integral of equation (3.15) becomes

$$\int d\vec{\Omega}' \; Y^*_{\ell,n}(\vec{\Omega}')\psi(r,\vec{\Omega}') = \left(\frac{2\ell+1}{4\pi}\right)^{\frac{1}{2}} \times 2\pi \int_{-1}^{+1} d\mu' \; P_\ell(\mu')\psi(x,\mu') \qquad (3.21)$$

for one spatial dimension. Legendre polynomials can be seen to replace the spherical harmonics in one-dimensional problems. (to verify equation (3.21) one may use the definitions of spherical harmonics and the associated Legendre polynomials (14,17)). Observe that the particle flux becomes a function of x,μ in one-dimensional geometry as given by the transformation in equation (3.21). The integral term in equation (3.21) can be approximated by a numerical quadrature formula as follows:

$$\int_{-1}^{+1} d\mu' \; P_\ell(\mu')\phi(x,\mu') \cong \sum_{m=1}^{ISN+1} w_m P_\ell(\mu'_m)\phi(x,\mu'_m) \qquad (3.22)$$

Now one may combine equations (3.19, 3.21, 3.22) to obtain the one-dimensional slab geometry discrete ordinates form of the transport equation as given below:

$$\mu_m \frac{d\phi(x,\mu_m)}{dx} + \Sigma_t \; \phi(x,\mu_m) \cong \sum_{\ell=1}^{LMAX+1} \left(\frac{2\ell+1}{4\pi}\right)^{\frac{1}{2}} P_\ell(\mu_m) \; \Sigma_{s,\ell} \sum_{m=1}^{ISN+1} w_m \; P_m(\mu'_m) \; x \; \phi(x,\mu'_m) \; x \; \left(\frac{2\ell+1}{4\pi}\right)^{\frac{1}{2}} x \; 2\pi + S(x,\mu_m) \qquad (3.23)$$

which may be reduced into the following form:

$$\mu_j \frac{d\phi(x,\mu_j)}{dx} + \Sigma_t \; \phi(x,\mu_j) = \sum_{\ell=1}^{LMAX+1} \sum_{j'=1}^{ISN+1} \left(\frac{2\ell+1}{2}\right) \Sigma_{s,\ell} \; P_\ell(\mu_j) P_\ell(\mu_{j'}) \; x \; w_{j'} \phi(x, \mu_{j'}) + S(x,\mu_j) \qquad (3.24)$$

Equation (3.24) is called the in-group transport equation; i.e., the one-speed transport equation. In equation (3.24) j' represents an inner loop over all initial directions to

make a contribution to the angular flux at the direction of μ_j which also represents the final direction. This is done for each ℓ, the Legendre polynomial expansion order, ℓ=1,2,3, ...,LMAX.

2. Multigroup Form of One-Dimensional Slab Geometry Discrete Ordinates Transport Equation

A more general form of steady-state particle transport equation in plane geometry with anisotropic scattering may be given as

$$\mu \frac{\partial \phi(x,E,\mu)}{\partial x} + \Sigma_t(x,E)\phi(x,E,\mu) = \int_0^\infty dE' \int d\vec{\Omega}' \, \Sigma_s(x,E'\to E,\vec{\Omega}'\to\vec{\Omega})\phi(x,E',\mu) + S(x,E,\mu) \tag{3.25}$$

where flux $\phi(x,E,\mu)$ satisfies appropriate boundary conditions on both sides of the slab and

$$\Sigma_t(x,E) = \Sigma_s(x,E) + \Sigma_a(x,E) = \Sigma_s(x,E);$$

i.e., $\Sigma_a(x,E) = 0$ and, $\Sigma_s(x,E) = \Sigma_s(x,E\to E) + \Sigma_s(x,E'\to E)$

for electron transport problems. In order to solve equation (3.25) one needs to define the anisotropic scattering cross-section. For example, it can be expanded in terms of the scattering angle cosine $\mu_0 = \vec{\Omega}'\cdot\vec{\Omega}$ as

$$\Sigma_s(x,E'\to E,\vec{\Omega}'\cdot\vec{\Omega}) = \sum_{\ell=0}^{\infty} \left(\frac{2\ell+1}{4\pi}\right) \Sigma_{s,\ell}(x,E'\to E)\, P_\ell(\mu_0) \tag{3.26}$$

where the Legendre polynomials expansion coefficients $\Sigma_{s,\ell}(x,E'\rightarrow E)$ are given as

$$\Sigma_{s,\ell}(x,E'\rightarrow E) = 2\pi \int_{-1}^{+1} d\mu'_0 \quad \Sigma_s(x,E'\rightarrow E,\mu'_0)\ P_\ell(\mu'_0). \tag{3.27}$$

In order to prove equation (3.27) one may use the orthogonality properties of Legendre polynomials in equation (3.26).

Now one may substitute equation (3.26) into the transfer term of equation (3.25); i.e., the double-integral term, to obtain the collision source term as

$$S_1 = \int_0^\infty dE' \int d\vec{\Omega}' \sum_{\ell=0}^{\infty} \left(\frac{2\ell+1}{4\pi}\right) \Sigma_{s,\ell}(x,E'\rightarrow E)\ P_\ell(\mu_0)\phi(x,E',\mu') \tag{3.28}$$

The addition theorem of Legendre polynomials, which will be used in equation (3.28), given as

$$P_\ell(\mu_0) = P_\ell(\mu)P_\ell(\mu') + 2\sum_{m=1}^{\ell} \frac{(\ell-m)!}{(\ell+m)!}\ P_\ell^m(\mu)\ P_\ell^m(\mu')\ \cos m(\psi-\psi') \tag{3.29}$$

where ψ, ψ' are the azimuthal angles and μ, μ' are the direction cosines. $P_\ell^m(\mu)$ are associated legendre polynomials (see Appendix). $\vec{\Omega}'$ and $\vec{\Omega}$ are the directions of particle before and after scattering and are specified by azimuthal angles and direction cosines. Insert equation (3.29) into equation (3.28) and integrate over ψ' and μ'. One can show that the terms containing $\cos m(\psi - \psi')$ vanish upon integration over ψ'. Therefore equation (3.28) becomes

$$S_1 = 2\pi \int_0^{\infty} dE' \int_{-1}^{+1} d\mu' \sum_{\ell=0}^{\infty} \left(\frac{2\ell+1}{4\pi}\right) \Sigma_{s,\ell}(x,E' \to E) P_\ell(\mu) P_\ell(\mu') \phi(x,E',\mu') \tag{3.30}$$

It may be rearranged to obtain

$$S_1 = \int_0^{\infty} dE' \sum_{\ell=0}^{\infty} \left(\frac{2\ell+1}{2}\right) P_\ell(\mu) \Sigma_{s,\ell}(x,E' \to E) \int_{-1}^{+1} d\mu' \phi(x,E',\mu') P_\ell(\mu') \tag{3.31}$$

The integral term in equation (3.31) can be evaluated approximately using a numerical quadrature formula. It gives

$$\int_{-1}^{+1} d\mu' \; P_\ell(\mu') \phi(x,E',\mu') \cong \sum_{m=1}^{ISN+1} w_m P_\ell(\mu_m) \phi(x,E',\mu_m) \tag{3.32}$$

Now insert equation (3.32) into equation (3.31) to write collision source term as

$$S_1(x,E,\mu_j) = \int_0^{\infty} dE' \sum_{\ell=0}^{\infty} \left(\frac{2\ell+1}{2}\right) P_\ell(\mu_j) \Sigma_{s,\ell}(x,E' \to E) \sum_{m=1}^{ISN+1} w_m P_\ell(\mu_m) \phi(x,E'\mu_m) \tag{3.33}$$

where μ_m's and μ_j's indicate initial and final discrete directions of scattered particle. In practical applications the truncated expansion of Legendre polynomials are used instead of infinite expansion as in equation (3.33). Therefore an approximate representation of collision source term may be given as

$$S_1(x,E_g,\mu_j) \cong \sum_{g'=1}^{g} \sum_{\ell=1}^{LMAX+1} \left(\frac{2\ell+1}{2}\right) P_\ell(\mu_j) \Sigma_{s,\ell}(x,E_g' \to E_g) \sum_{m=1}^{ISN+1} w_m P_\ell(\mu_m) \phi(x,E_g',\mu_m) \tag{3.34}$$

In order to perform the summation over ℓ it is necessary to specify LMAX expansion coefficients. For LMAX = 0, problem

reduces to the isotropic scattering case. By including the discretization idea into energy and spatial independent variables one can obtain the one-dimensional discrete ordinates form of equation (3.25) as given below. Here one may note that this formulation results in an entirely discrete point representation of the transport equation which can be solved directly by standard numerical methods.

$$\mu_j \frac{d(x_i,E_g,\mu_j)}{dx} + \Sigma_t(x_i,E_g)\phi(x_i,E_g,\mu_j) =$$

$$\sum_{g'=1}^{IGM} \sum_{\ell=1}^{LMAX+1} \sum_{m=1}^{ISN+1} \left(\frac{2\ell+1}{2}\right) P_\ell(\mu_j)\, \Sigma_{s,\ell}(x_i,E_{g'}\rightarrow E_g)$$

$$w_m\, P_\ell(\mu_m)\phi(x_i,E_{g'},\mu_m) + S(x_i, E_g,\mu_j) \qquad (3.35)$$

where i = 1,2,3,...,IM+1 (IM = number of spatial mesh intervals), IGM = number of energy groups. Initial and final discrete directions are represented by the direction cosines μ_m and μ_j respectively. $\{\mu_j\}$ and $\{w_m\}$ are the appropriate set of quadrature points and weights. One may observe that it is possible to obtain the simple geometry (one-dimensional) transport equation either from the most general form of transport equation using proper transformations between spherical harmonics and Legendre polynomials, or by starting with one-dimensional transport equation and then expanding the scattering cross-section in terms of Legendre polynomials. Equation (3.35) can be put into a compact form by defining an "effective source term" which represents the right hand side of equation (3.35) as given below:

$$\mu_j \frac{d\phi(x_i,E_g,\mu_j)}{dx} + \Sigma_t(x_i,E_g)\phi(x_i,E_g,\mu_j) = Q(x_i,E_g,\mu_j) \quad (3.36)$$

The multigroup form of one-dimensional discrete ordinates equations, equation (3.35), are solved by iterating on the source term. In this study it is not intended to cover the solution procedure of equation (3.35) in detail. It gives a set of ordinary differential equations in x. Solution of equation (3.35) provides the values of angular fluxes along the discrete directions for each spatial mesh interval.

The one-group model, given by equation (3.24), clearly shows how elastic collisions ("in-group scattering") and inelastic collisions ("down scattering") appear in the one-dimensional transport equation. The one-group model which is derived in this section clearly represents the "angular-dependent structure of the electron transport equation" that is employed in this study. The in-group scattering term, the first term on the right hand side of equation (3.24), indicates the contribution from all other discrete directions μ_j, into a final direction μ_j. No energy degradation occurs in the in-group scattering interactions, and these collisions make the only contribution to the angular distribution of scattered electrons. The source term of the one-group model transport equation may be taken as a "sum" of the external source and the down scattering terms. The down scattering terms represent the contribution to the effective

source term from all collisions which occur above the reference energy of the one-group model. The down scattering terms in general, represent energy and change. If no angle change is assumed the source term of equation (3.24) may be represented by a delta function notation as given below:

$$S(x,\mu_j) = S(x)\,\delta(\mu_j-\mu_{j'}) \tag{3.37}$$

The multigroup model of the transport equation in one-dimensional space is given by equation (3.35). One may observe that the expansion coefficients of directional fluxes are energy dependent. That is, the coefficients, $\Sigma_{s,\ell}(x_i, E_{g'}\rightarrow E_g)$ represent particle transfer from energy group g' to energy group g for each x_i. The coefficient for any order ℓ, can thus be distinguished as follows. For in-group scattering $E_g = E_{g'}$, for down scattering $E_{g'} > E_g$ for a number of values of $E_{g'}$. One may observe that $\Sigma_{s,\ell}(x_i, E_{g'}\rightarrow E_g)$ represents a contribution into final energy group g from all g' which are the higher energy groups with respect to final energy group g. Therefore one can consider the "sum" of the external source and the collision source terms as an "effective source" of final energy group g. Then the effective source term may be defined as follows:

$$S_{eff.}(x_i,E_g,\mu_j) = S_{ext.}(x_i, E_g, \mu_j) + S_{col.} \tag{3.38}$$

where

$$S_{col.} = \sum_{g'=1}^{g} \sum_{\ell=1}^{LMAX+1} \sum_{m=1}^{ISN+1} \left(\frac{2\ell+1}{2}\right) P_\ell(\mu_j)\Sigma_{s,\ell}(E_{g'}\rightarrow E_g) w_m P_\ell(\mu_m)\, \phi(x_i,E_{g'},\mu_m) \tag{3.39}$$

which can be given in terms of in-group scattering and down scattering as follows:

$$S_{col} = \sum_{\ell=1}^{LMAX+1} \sum_{m=1}^{ISN+1} \left(\frac{2\ell+1}{2}\right) P_\ell(\mu_j) w_m P_\ell(\mu_m) \phi(x_i, E_g, \mu_m) \Sigma_{s,\ell}$$

$$(x_i, E_g \rightarrow E_g) + \sum_{g'=1}^{g-1} \sum_{\ell=1}^{LMAX+1} \left(\frac{2\ell+1}{2}\right) P_\ell(\mu_j) \Sigma_{s,\ell}(x_i E_{g'} \rightarrow E_g) \sum_{m=1}^{ISN+1}$$

$$w_m P_\ell(\mu_m) \phi(x_i, E_{g'}, \mu_m) \qquad (3.40)$$

The first term on the right hand side of equation (3.40) represents the collision term in which energy group does not change but angle changes. Therefore it is the collision term which appears in the one-group electron transport equation. The second term on the right hand side of equation (3.40) represents the terms which result in energy change and are expressed as part of the "source term" in one-group transport equation, equation (3.24). Since angle change occurs in these terms, the down-scattering expansion coefficients should be chosen to express the corresponding angular deflections. In fact, inelastic collisions are more forward than elastic collisions. In order to produce proper ANISN transport results some modifications may be needed in the formulation to generate energy loss expansion coefficients. For example, if there exists no significant angle deflection for a fraction of inelastic collisions then they would be removed from the angular part of energy transfer cross-sections. Further details of the expansion

coefficients generation algorithm for inelastic collisions will be covered in Chapter IV.

CHAPTER IV

THE THEORY OF THE CROSS-SECTION PRODUCTION

A. Introduction of the Average Energy Loss and the Formulation of the Multigroup Energy Group Structure

The production of the total (Σ_{g_t}), in-group ($\Sigma_s(g \rightarrow g)$), and the group transfer ($\Sigma_s(g \rightarrow g+1)$) cross-sections will be introduced in this chapter. In this subsection definitions of the average properties of ANISN-CSDM electron transport model will be introduced. Also, analytical form of energy transfer differential cross-section and the normalized angular expansion coefficients of energy transfer cross-sections will be discussed. In addition, the construction of the multigroup structure of the electron transport model which has been developed on this study will be presented.

It is the property of the ANISN-CSDM that the particle is transported to the next lower energy group by one average inelastic collision. Therefore, this electron transport model may also be called the "one collision model." Similarly, there has been defined one effective elastic collision which is equivalent to many in-group scatters. For this

electron transport model, every particle loses the amount of energy necessary to reach the next lower energy group. The magnitude of this energy loss is the average energy loss from inelastic collisions and may be expressed as follows:

$$\langle \Delta W(E_0) \rangle = \Delta E_{loss}(E_0) = E_0 - \langle W(E_0) \rangle_{inel} \qquad (4.1)$$

where $\langle W(E_0) \rangle_{inel}$ represents the average energy of the scattered particles after having undergone all possible energy loss collisions at the initial energy E_0. The average energy of the scattered electron can be calculated by the following expression for a given initial energy E_0:

$$\langle W(E_0) \rangle_{inel} = \frac{N \int_{E_0/2}^{E_0-\eta} W \frac{d\sigma_{inel}(E_0,W)}{dW} dW}{N \int_{E_0/2}^{E_0-\eta} \frac{d\sigma_{inel}(E_0,W)}{dW} dW} \qquad (4.2)$$

Here N is the number density of electrons of the transport medium. It may be noted that the differential energy loss cross-section applies, provided that the target electron is a free electron. This cross-section tends to infinity at $W = E_0$ which is not a physical case. The cross-section becomes manageable for a value of η which is about the magnitude of mean ionization potential of transport medium. In fact, a bound electron becomes a free electron if the

energy imparted to it is equal to or greater than its ionization potential. The magnitude of $\langle W(E_0)\rangle_{inel}$ is defined as the "average energy of the scattered particle." This quantity is one of the significant properties of the electron transport model which has been developed in this study. The $\langle \Delta W(E_0)\rangle$ which was defined by equation (4.1) represents the "average energy loss" of the primary particle. This can be determined using the result of equation (4.2) for a given initial energy E_0. It should be noted that the average energy loss calculation takes into account those inelastic collisions where energy losses are greater than η. The minimum value of η may be set equal to I (ionization potential of the transport medium) in the process of producing transport results. The differential energy transfer cross-section given by Bethe (21) in the Møller's approximation can be cast into the following form:

$$\frac{d\sigma_{inel}(E_0,W)}{dW} = 2\pi r_0^2 \times \frac{(1+\frac{1}{T})^2}{T+2} \times \left[\frac{1}{(\frac{W}{E_0})^2} - \frac{1}{\frac{W}{E_0}(1-\frac{W}{E_0})} \times \frac{2K-1}{K^2} + \frac{1}{(1-\frac{W}{E_0})^2} + (\frac{K-1}{K})^2 \right] \quad (4.3)$$

where

$r_0 = e^2/mc^2 = 2.818\times10^{-13}$ cm = classical electron radius

$T = \frac{E_0}{mc^2}$

$$K = \frac{E_0+mc^2}{mc^2} = T + 1$$

$E_0 - W$ = net energy loss in electron-electron collision

E_0 = initial kinetic energy of the primary particle

W = kinetic energy of the scattered particle

This form of the energy transfer cross-section is appropriate for numerical calculations, and has been used in this study to produce associated transport properties. The average energy loss which was defined in equation (4.1) can be used to generate the energy group structure of the electron transport problem for ANISN-CSDM model.

In the evaluation of average energy loss a primary particle is permitted to make all possible inelastic collisions in which the maximum energy loss is determined by the theoretical limit, $E_0/2$. In other words, a primary particle is permitted to lose its initial energy up to $E_0/2$ in a single electron-electron collision. The probability of occurrence of large energy transfer collisions is relatively small. Electrons make rather small energy transfer collisions in electron-electron interactions. In the ANISN-CSDM model of electron transport a primary particle is permitted to make only one average inelastic collision which results in the energy loss that is equal to average energy loss of a particle due to all inelastic collisions.

Since the constructed energy group width is relatively small, it is possible to define the average properties of the electron transport model at the mean energies of established group structure. In addition to defining energy group structure by average energy loss, test calculations have shown that one may define a constant energy reduction factor which can determine the entire multigroup structure. For example, for 1.0 MeV electrons, average energy of the scattered particle may be used as an energy reduction factor. This factor may be used with DATAPAC6 to produce multigroup data which can be revised to the form of elastic and inelastic cross-sections needed for discrete ordinates calculations. Using the mathematical energy loss model of DATAPAC6, one may obtain the following relationship between the number of steps required in reducing the energy of a primary particle by a factor of two.

$$m \cong \frac{\log 2}{\log(1/k)} \tag{4.4}$$

where m is an integer and

$$k \approx \frac{\langle W(E_0)\rangle_{inel}}{E_0}$$

This relationship indicates that the multigroup structure of DATAPAC6 may be reflected to ANISN-CSDM calculations using the constant energy reduction factor, k. It may also be observed that the data produced by DATAPAC6 and CRXPC are in

agreement in terms of the energy group structure for multi-group electron transport calculations. Part of the mathematical discussions given in this subsection and next subsection also applies to DATAPAC6 calculations. The expansion coefficients of the cross-sections which are responsible for the angular redistribution of "model elastic" and "model inelastic collisions" must be calculated for each energy group based on the average energy loss model defined above. This energy loss model will also be designated the "squashed collision electron transport model" in this study. This terminology means that all possible inelastic collisions are treated as if each loses the same amount of energy which is equal to model average energy loss. The magnitude of such energy losses is $<\Delta W(E_0)>$ in the squashed collision electron transport model, which has one unique value for a given upper bound in the integration over the final energies.

The squashed collision electron transport model approximates all possible inelastic collisions by one average inelastic collision at the mean values of each energy group E(g), g = 1,2,3,...,IGM. This average inelastic collision produces the energy loss which is the average of all possible inelastic collisions at a given energy which result in energy loss equal to or greater than η. The inelastic single scattering law states that there exists a corresponding angular deflection associated with each of these inelastic collisions. The angle-energy relationship for inelastic

collisions is given as follows for the initial energy E_0 (21):

$$\mu_h(\Delta E_{loss}) = \left[\frac{W \times (E_0 + 2mc^2)}{(E_0 \times (W + 2mc^2)} \right]^{1/2} \tag{4.5}$$

$$\mu_\ell(\Delta E_{loss}) = \left[\frac{(E_0 - W) \times (E_0 + 2mc^2}{E_0 \times (E_0 - W + 2mc^2)} \right]^{1/2} \tag{4.6}$$

The subscripts h and ℓ denote primary (high energy) and secondary (low energy) particles after electron-electron collisions. E_0 and W are the kinetic energies of the primary particle before inelastic collision and after inelastic collision with $\Delta E_{loss} = E_0 - W$ = energy loss in a single collision.

The developed electron transport model uses the angular expansion coefficients of cross-sections in transport calculations. It may be appropriate to introduce the second average property of the squashed collision electron transport model. This is the "average angular deflection" of all possible individual deflections due to all individual inelastic collisions. This average angular deflection may be evaluated by the expression

$$\langle \mu(E_0) \rangle_{inel} = \frac{\int_{\mu_{lower}(E_0/2)}^{+1.0-\Delta\mu} \mu \frac{d\sigma_{inel}(E_0,\mu)}{d\mu} d\mu}{\int_{\mu_{lower}(E_0/2)}^{+1.0-\Delta\mu} \frac{d\sigma_{inel}(E_0,\mu)}{d\mu} d\mu} \tag{4.7}$$

Here one should note that if $d\sigma_{inel}(E_0,\mu)/d\mu$ is derived from the equivalent relationship of Møller (equation 4.3), then its value goes to infinity as μ goes to 1. For this reason a $\Delta\mu$ must be removed from the range of integration to achieve a value of $\langle\mu(E_0)\rangle_{inel}$ which is less than 1.0. This $\Delta\mu$ corresponds to η in the energy domain.

The lower bound of μ-integration may be determined using $\mu_h(\Delta E_{loss})$ expression, equation (4.5), at $W=E_0/2$. This represents the maximum theoretical energy loss in electron-electron collisions. If $W = E_0$, then $\mu_h = 1, \mu_\ell = 0$, because $\Delta E_{loss} = 0$. No energy loss results in no angular deflection in inelastic collisions. The $\langle\mu(E_0)\rangle_{inel}$ may be interpreted as the average $\cos\theta$ of all possible individual $\cos\theta$'s of all inelastic collisions that can occur at energy E_0. It is a measure of the overall angular behavior of all inelastic collisions. It should be noted that the angular behavior of inelastic collisions is attached to group-transfer cross-sections through energy dependent expansion coefficients. The expansion coefficients are normalized to the inelastic scatter cross-section.

The explicit form of the Møller differential energy transfer cross-section given by equation (4.3) may be expressed in terms of the initial kinetic energy of a primary particle and $\mu = \cos\theta$ (θ being the scattering angle of the scattered particle), by using the energy-angle relationship (equation 4.5). From this one can deduce the angle-

dependent differential energy loss cross-section

$$\frac{d\sigma_{inel}(E_0,\mu)}{d\mu} = 8\pi r_0^2 \times (1+\frac{1}{T})^2 \times \left\{(\frac{1}{2\mu^2})^2 + \frac{2K-1}{K^2} \times \frac{1}{2\mu^2(\mu^2-1)(T+2)}\right.$$

$$\left. + \left(\frac{1}{(\mu^2-1)(T+2)}\right)^2 + (\frac{K-1}{K})^2 \times \frac{1}{(T\mu^2-T-2)^2}\right\} \times \mu \qquad (4.8)$$

The constants r_0, K and T are the same as before. The equation (4.8) will be employed to generate the angular expansion coefficients of energy transfer cross-sections.

The multigroup structure of ANISN-CSDM electron transport model has been constructed based on the approximation that the energy losses less than η are excluded from the average energy loss calculation of a primary particle. This means that the calculation of average energy loss which has been evaluated using the Møller cross-section requires the integration of cross-section up to $E_0-\eta$ in final energy. The magnitude of average energy loss, $<\Delta W(E_0)>$, in inelastic collisions depends on the value of the upper bound of the integration variable, W. The removal of small energy losses from average energy loss calculations results in loss of energy deposition. This requires that the energy loss cross-section has to be slightly increased to compensate the neglected energy loss in energy conservation analysis. Magnitude of the average energy loss, $<\Delta W(E_0)>$, is a measure of fraction of inelastic collisions which has been excluded

from the calculations. This means that if $<\Delta W(E_0)>$ is very small, then the energy loss model includes most of the small energy transfer collisions which are highly forward. In this situation energy transfer cross-section becomes fairly large. If $<\Delta W(E_0)>$ is relatively large then it indicates that the energy loss model does not include very small energy transfer collisions. This results in small energy transfer cross-sections. The magnitude of energy losses which are excluded from the average energy loss calculation is relatively smaller than the $<\Delta W(E_0)>$. These very small energy loss collisions could be called "inelastic ingroup scatters." This classification of small energy transfer collisions represents the degree of approximation made on the energy transfer cross-section. Note that the energy losses associated with those small energy transfer collisions which do occur are retained in the total stopping power. In order to achieve a complete energy conservation in transport calculations it is necessary to define ANISN-CSDM cross-sections to take into account the exclusion of small energy transfer collisions from average energy loss calculations. This requires us to define "corrected cross-sections" in the cross-section matrix. The corresponding exclusion of η in the process of generating the angular expansion coefficients of energy transfer cross-sections has been made as described below: The angular deflections which correspond to small energy losses,

whose magnitude is less than or equal to η, are removed from the calculation of angular expansion coefficients of energy transfer cross-sections. The neglected angular deflections are extremely forward, and it is necessary to apply this approximation to the expansion coefficients in reducing the size of cross-section matrices to a manageable level. These small energy transfer collisions are thus assumed not to occur, and therefore no angle change occurs. They keep their original direction at the initial energy. Since energy losses of a primary particle are completely modeled in ANISN-CSDM cross-section production, then no modification of the Boltzmann transport equation is necessary to get correct energy deposition. The correct energy deposition has been achieved by adjusting the cross-sections rather than adding term to the Boltzmann transport equation as Bartine et al. did.

As discussed in the theory, there is no hard and fast rule for drawing a line between soft collisions and hard collisions. It is generally agreed that the upper bound of small energy transfer collisions, η, should be large compared to the ionization potential, I(eV), of the transport medium. If the medium is a multimaterial transport medium, then the value of I should be equal to the ionization potential of the highest Z material. In the discrete ordinates method literature of electron transport, the upper bound of small energy transfer collisions is taken to be from $\eta = I$ to

100I (6), where η was fixed for all energy groups. The results produced by Bartine et al. show that the angular distribution of transmitted electrons per MeV per incident electron becomes less forward for small η values. If the value of η becomes larger than the distribution becomes more forward (6). This happens due to the fact that no angle change is assumed for small energy transfer collisions, and such collisions occur more frequently as η increases (6).

An increase in η allows more forward-directed flow since the soft collisions are not deflected in Bartine et al. work. In ANISN-CSDM an increase in η permits forward directed flow in place of soft collisions but also increase the probability of hard collisions to conserve energy depositions. Since hard collisions have greater deflection, there may be an increased width of the peak of energy distribution of transmitted particles with greater η.

In this study the squashed electron transport model is based on a variable energy group width. The group width decreases as one proceeds to lower energies. For a typical case, the first energy group width is approximately 8 - 10 times greater than the final energy group width. A variable η is introduced into the squashed collision electron transport model rather than keeping it fixed for all energy groups, as was done by Bartine et al. (6). The magnitude of η may be related to the established group width. For example, one

may wish to choose η to be a small fraction of the energy group width. The choice must be made in defining the group structure, since it is affected by the magnitude of η, as defined in equation (4.2). Therefore, the group width and η are interrelated. Test calculations have shown that if E_0-η is close to E_0 then η becomes a small fraction of the average energy loss which is equal to group width at E_0. If E_0-η is not close to E_0 then the ratio of group width to η becomes relatively large. The most detailed transport results can be produced by calculations using small η values. In the cases where the expansion order of elastic scattering cross-section could become large η would be chosen large enough so that the cross-section matrix size remains manageable. A parametric study on η has shown that the electron transport results which have been produced by ANISN-CSDM are essentially independent of the magnitude of η. Some change in angular distribution, as previously noted, is caused by the choice of η. More detailed discussions on the selection of η will be given in the next chapter. The relative size of η may be understood more clearly if one pictorially represents the squashed collision electron transport model as shown below. Figure (4.1) represents all possible inelastic collisions that can occur at energy E_0, where the average energy of scattered particles due to inelastic collisions is denoted by $\langle W(E_0)\rangle_{inel}$. By noting the

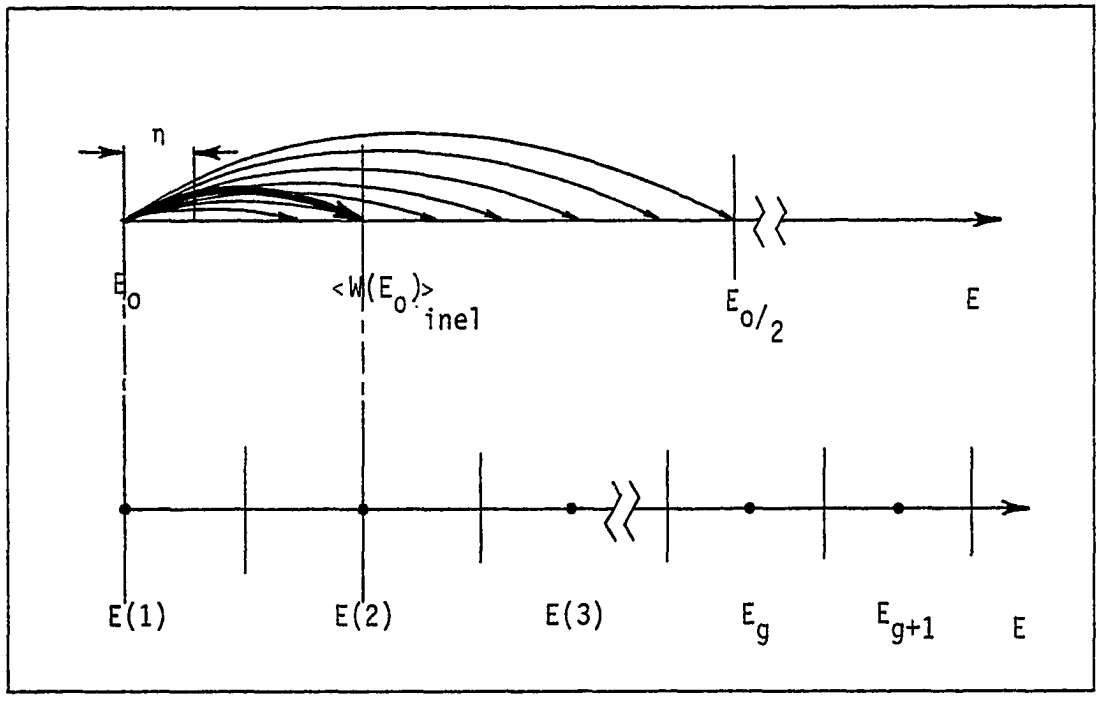

Figure (4.1) Construction of the multigroup energy structure by average inelastic collisions. The E_g represents the mean energy of energy group g.

average energy of scattered particle, $\langle W(E_0)\rangle_{inel}$, from the corresponding energy scale, Figure (4.1), one can construct the associated multigroup structure of the squashed electron transport model. This procedure is valid, provided that this process can be repeated at the average energy of the scattered particles in order to determine the mean energy of the next energy group, etc. It is evident from the Figure (4.1) that the choice of η affects the energy group structure and that the value of η is always less than the value of the mean energy loss.

Angular distributions of scattered electrons is represented by the expansion of cross-sections in Legendre polynomials as previously discussed. Normalized angular expansion coefficients for slowing-down cross-sections may be given as follows:

$$V(E(K),\ell) = \frac{2\pi}{\bar{C}(E(K),0)} \int_{\mu_{lower}(E(K)/2)}^{\mu_{mod}} \frac{d\sigma_{inel}(E(K),\mu)}{d\mu} P_\ell(\mu)\,d\mu \quad (4.9)$$

where

$K = 1,2,3,\ldots,IGM$

$L = 1,2,3,\ldots,LMAX$

and $\mu_{mod} = 1 - \Delta\mu$, and the differential cross-section was given by equation (4.8). The value of $\Delta\mu$ corresponds to η on the μ-domain versus energy-angle relationship. Equation (4.9) may be obtained from the general expression of cross-section expansion into Legendre polynomials (equation (3.7)). The $\bar{C}(E(K),0)$ represents the physical inelastic scattering cross-section of energy group K since $P_0(\mu) = 1$. This is also known as the first unnormalized expansion coefficient of energy group K. The value of μ_{mod} in equation (4.9) may be determined using the angle-energy expression given earlier in this chapter. For a selected η, the final energies of the scattered particle fall in the domain of $(E_0-\eta,\ E_0/2)$. Therefore, the μ_{mod} can be obtained from equation (4.5) as

follows:

$$\mu_{mod} = \left[\frac{(E_0-\eta) \times (E_0+2mc^2)}{E_0 \times (E_0-\eta+2mc^2)} \right]^{1/2} \qquad (4.10)$$

where

E_0 = initial kinetic energy of primary particle (MeV)

$2mc^2$ = 1.022 MeV.

In multigroup calculations the E_0 must be replaced by the mean energy of the associated energy group. The η has been internally produced for each energy group, and thus one can generate the group dependent $\mu_{mod}(E(K))$, K = 1,2,3,...,IGM. The production of the group dependent η, $\eta(K)$, could be explained as follows: The average energy of the scattered particles can be calculated for various η values. Then the size of the problem could be judged by equation (4.4), which determines the number of steps required to reduce initial energy by a factor of two. Thus the choice of η determines the number of energy groups between an initial high electron energy and a low energy cutoff. In the numerical integration this has been achieved by subtracting a few fine energy intervals from the initial energy of the primary particle. If one applies this rule consistently to the remainder of the energy groups, then it can be seen that the ratio $\eta(K)/\Delta E(K)$ is essentially constant. This means that a fixed fraction of inelastic collisions is excluded from the calculation of the $\langle W(E(K))\rangle_{inel}$ in a regular manner. Here the $\Delta E(K)$ designates the energy

group width of energy group K. It may be noted that a fixed number of energy intervals has been employed for each energy range of E(K)/2, which is the maximum theoretical energy loss in electron-electron collisions in energy group K. One may also note that the energy mesh size decreases as particles slow down to lower energies. This happens because E(K)/2 becomes smaller as particles slow down from group to group. Test calculations have shown that if the values of $\eta(K)$ which are generated as defined above are used in the average energy loss calculations for an arbitrary energy group K, they can produce the same energy group width, $\Delta E(K)$, as calculated by DATAPAC6.

As stated earlier, the differential inelastic scattering cross-section, the Møller cross-section, used in multigroup Legendre polynomials expansion coefficients V(E(K),L), tends to infinity as $\mu \to +1$. In that case the number of terms in the Legendre series expansion needs to be infinity. This represents an absolute forward distribution. Such a case would require infinite computer storage and infinite computer time, and hence is not a possible engineering solution of the transport problem. This solution difficulty arises because the extremely forward scattering is being retained in the calculations. Therefore, there is a need for a convenient approximation to remove the effect of highly forward scattering from the calculations. We have seen that the most strongly forward of the scatters, for which the energy loss

would be less than the ionization energy, do not occur in nature, even though predicted in the Møller formulation. It is convenient, in terms of computing requirements to exclude some collisions with energy loss greater than I so that the computed scattering is less forward than may really occur and allow some additional electrons to remain unscattered to compensate for this. This is the effect of η upon scattering angle as used in computing the Legendre coefficients for angular redistribution. The further use of η will be given in the next subsection in conjunction with the formulation of the macroscopic cross-sections for the use of ANISN-CSDM calculations.

The in-group and group transfer cross-sections are generated using the data produced by the DATAPAC6 computer code. Some of the data transferred to the Cross-Section Processing Code (CRXPC) are collisional and radiative stopping powers, multiple elastic scattering expansion coefficients, and point values of the energy group structure.

The expansion coefficients of the macroscopic elastic cross-sections, H(K,L), are generated by DATAPAC6. The calculational model of H(K,L) uses a multiple scattering approximation to modify single-scatter angular distribution coefficients. Since several elastic scatters may occur in a single spatial interval in this model, the wider angular distribution resulting from the multiple scattering approximation is used instead of that associated with a single

scatter. If scattering is isotropic, a Legendre expansion formulation produces a single expansion coefficient, as expected, and it is equal to unity. If scattering behaves as a δ-function (i.e., $\mu = 1$), a scattering cross-section may be represented as

$$\sigma(E_0 \rightarrow E, \mu \rightarrow \mu_0) = \sigma(E_0 \rightarrow E)\ \delta(\mu-1), \qquad (4.11)$$

which results in an infinite set of expansion coefficients each of which is equal to unity. In these cases, no broadening effect is observable for any expansion order and the single scatter and multiple scatter coefficients are identical. For all other cases, the multiple scatter coefficients predict a broadened distribution, as indicated by smaller values of high order coefficients. The mathematical details of this discussion may be obtained from the expression (16, 23,36,56)

$$f(\psi)\sin\psi\ d\psi = \sum_{\ell=0}^{\infty} \left(\frac{2\ell+1}{4\pi}\right) \exp\left(-2\pi N \int_0^{\xi}\int_0^{\pi} \sigma(\theta,\xi)(1-P_\ell(\cos\theta))\sin\theta d\theta d\xi\right)$$
$$\times\ P_\ell(\cos\psi)\ \sin\psi\ d\psi \qquad (4.12)$$

It should be noted that if $\sigma(\theta,\xi) = 0$ everywhere except at $\theta=0°$, where it tends to infinity, this represents scattering which behaves as a δ-function. Since $(1-P_\ell(\cos\theta))$ in equation (4.12) is zero when $\sigma(\theta,\xi)$ is non-zero for a δ-function and $\sigma(\theta,\xi)$ is zero when $(1-P_\ell(\cos\theta))$ is non-zero, the exponential part of equation (4.12) is always unity for a δ-function. The $f(\psi)$

may be interpreted as a normalized probability that the primary particle will be deflected into the angular interval $(\psi, \psi + d\psi)$. Here, the ψ is the multiple scattering angle of the primary particle. The $\sigma(\theta,\xi) = \sigma(\theta,\xi(E))$ is a single elastic scattering cross-section, and enters into the multiple scattering distribution in the form of expansion coefficients representing the exponential part of equation (4.12). The energy dependence of this cross-section is represented by its dependence on the pathlength ξ through the continuous slowing down approximation. This may be expressed as

$$\xi = \frac{\Delta E}{(-\frac{dE}{d\xi})} \tag{4.13}$$

In equation (4.12) the multiple scattering expansion coefficients of Legendre polynomials may be identified as given below:

$$H(\ell) = \exp(-2\pi N \int_0^{\xi} \int_0^{\pi} \sigma(\theta,\xi)\ (1-P_{\ell}(\cos\theta))\sin\theta d\theta d\xi). \tag{4.14}$$

Here N is the number of scattering atoms per cm^3. The ξ is the pathlength being traveled by the primary particle. The angular distribution of multiply scattered particles after crossing a given material thickness, ξ, is not limited to small angle scatters (equation (4.12)). Originally, multiple scattering was formulated by Moliere (68), and similar derivations were given by Bethe (68) as well. Both of their derivations are based on a small angle approximation. That is,

all scattering angles are small so that $\sin\theta$ may be replaced by θ. The multiple scattering law derived by Gaudsmith-Saunderson (23), as used here, is valid for any deflection angle θ.

The ETRAN family of codes employs the condensed random walk concept. In this method one representative interaction replaces several interactions and the scattered particle distribution is constructed using a multiple scattering approximation. The ANISN-CSDM has a similar transport structure. ANISN-CSDM employs equally probable elastic and inelastic collision. The elastic part results in angular deflections and the inelastic part involves both energy and angle changes. The angle change from an elastic scatter approximates the change from many actual elastic collisions and the inelastic scatter energy change transfers a particle from energy group g to g + 1. In an inelastic collision the particle is subject to angle deflection associated with energy relationship. In order to maintain the angle-energy relationship consistency, group transfer cross-sections include inelastic scatter expansion coefficients for each energy group. These are called multigroup group-transfer expansion coefficients for inelastic collisions and are produced using the general theory of cross-section expansion into the Legendre polynomials and the Møller cross-section representation. Each entry in the expansion coefficients may be treated as an angular redistribution

coefficient of Legendre polynomials.

There are two major developments in this study: (1) the application of the condensed random walk model of ETRAN into the discrete ordinates method (DOM); and (2) the formulation of the inelastic cross-sections by the collisional average energy loss model. The latter development will be introduced in the next subsection of this chapter. These developments are tested in producing the electron transport results using ANISN-CSDM.

The application of the condensed random walk concept into the discrete ordinates method has been done for the first time in this study. The condensed random walk model was introduced in Chapter (II) in detail, and its pictorial representation was given in Figure (2.2). From the previous discussions it may be seen that the application of the condensed random walk model into DOM allows relatively large spatial intervals with multiple scattering. The multiple scattering approximation replaces the detailed small interval calculations of Bartine et al. This approximation permits more efficient approximate calculations and makes the deep penetration radiation transport analyses possible within computer storage and time limitations. This deep penetration radiation transport analysis application of the multiple scattering approximation has been tested in this study. The produced transport results have shown that ANISN-CSDM of electron transport produces the experimental data better

than the ETRAN18G models do. The comparison of ANISN-CSDM model of electron transport with the model of Bartine et al. indicates that Bartine was constrained to small intervals by the mathematical limitation of a few scatters per spatial interval for good numerical approximations. It is relatively inefficient to produce deep radiation penetration transport results using Bartine's method. The ANISN-CSDM electron transport model completely removes this difficulty because of the incorporation of the condensed random walk concept into the production of the cross-section matrices for ANISN calculations. The mathematical representation of the "one effective elastic collision model" will be developed further in subsection (C) of this chapter.

B. Modeling of the Inelastic Ingroup Scattering and the Squashed Collision Electron Transport Model

In the following paragraphs, standard expressions of total stopping power, collisional total energy loss cross-section, and average energy loss will be introduced. In addition, the relationship between total stopping power and energy loss cross-section will be given. Then these basic parameters will be redefined by excluding the extremely forward inelastic collisions in order to formulate the corrected macroscopic cross-sections used in the discrete ordinates method. The differential energy transfer cross-section, which will be used in the following expressions,

was defined by equation (4.3).

The energy transferred to a bound atomic electron (target particle) from a primary particle has been classified based on the magnitudes of energy transferred to the target electron. From a theoretical point of view, energy loss mechanisms of charged particles to a target electron are essentially the same, but the analytical forms of the energy transfer differential cross-sections vary from one charged particle to another (30). In this study the primary charged particle is assumed to be an electron, but the discussion of the theoretical concepts of energy loss mechanisms may apply to all charged particles in general. From previous discussions, the total collisional stopping power of inelastic collisions may be given as

$$-\frac{dE}{dx} = N \int_{E_0/2}^{E_0} (E_0-W) \times \frac{d\sigma_{inel}(E_0,W)}{dW}\, dW \qquad (4.15)$$

Assuming the validity of $\frac{d\sigma_{inel}(E_0,W)}{dW}$ from equation (4.3) over the range of integration. The collisional total energy transfer cross-section may be calculated as follows:

$$\sum_{t,inel}^{cols} = N \int_{E_0/2}^{E_0} \frac{d\sigma_{inel}(E_0,W)}{dW}\, dW \qquad (4.16)$$

again assuming the validity of equation (4.3).

By using the notations of equation (4.15) the collisional average energy loss of the primary particle may be given by the expression

$$\langle \Delta W(E_0) \rangle = \frac{N \int_{E_0/2}^{E_0} (E_0 - W) \frac{d\sigma_{inel}(E_0, W)}{dW} dW}{N \int_{E_0/2}^{E_0} \frac{d\sigma_{inel}(E_0, W)}{dW} dW} \qquad (4.17)$$

which results in

$$\langle \Delta W(E_0) \rangle = E_0 - \langle W(E_0) \rangle_{inel} \quad \text{for } W < E_0.$$

Here it has to be noted that the true integration in equations (4.15) through (4.17) must be performed in two parts. The first part includes the energy losses which are less than or equal to η, where the integration should be carried out over the interval $(E_0-\eta, E_0)$. The second part includes energy losses which are greater than η, where the integration should be carried out over the interval $(E_0/2, E_0-\eta)$. These were discussed in Chapter (II) in detail, where complete expressions for the energy losses for each part were also given. In the next paragraph it will become clear that ANISN-CSDM does not directly deal with the first part of the integration mentioned above. This part, rather, has been included in the transport calculations by a correction.

The energy loss collisions were classified into two

groups, those which result in an energy loss less than η, and those which result in an energy loss greater than η. The choice of the value of η was made somewhat arbitrarily. In ANISN-CSDM let us denote the upper bound of energy losses of small energy loss collisions by η. Those energy loss collisions which result in energy losses up to η are treated as "no collision" interactions in ANISN-CSDM. A primary particle is treated as remaining at its initial energy as long as its energy losses are less than the abritrary η value. Since no energy change is assumed in such collisions, there will be no angle change, so that these collisions will retain their original angular direction. Therefore, a correction should be made on the cross-sections to account for the neglected small energy transfer inelastic collisions. This correction will result in less inelastic scattering because small energy transfer collisions are being removed. The discussion given above essentially comprises the mathematical basis of the electron transport model which has been developed in this study.

The pictorial representation of the average energy losses with $\eta = 0$ and with $\eta \neq 0$ may be shown in Figure (4.2) and Figure (4.3), respectively. Earlier, it was mentioned that non-zero energy loss occurs if $\eta \neq 0$. This is the basis of the multigroup formulation of the electron transport problem in the ANISN-CSDM. Figure (4.2) represents the case where $\eta = 0$, which cannot be used for

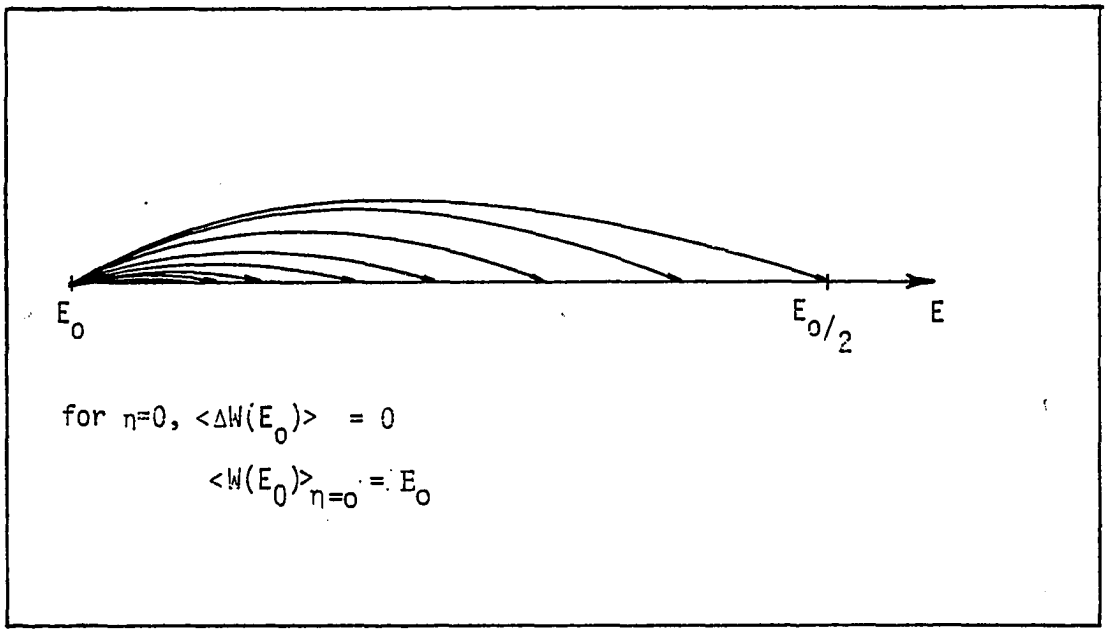

Figure (4.2): Energy loss of inelastic collisions with $\eta=0$.

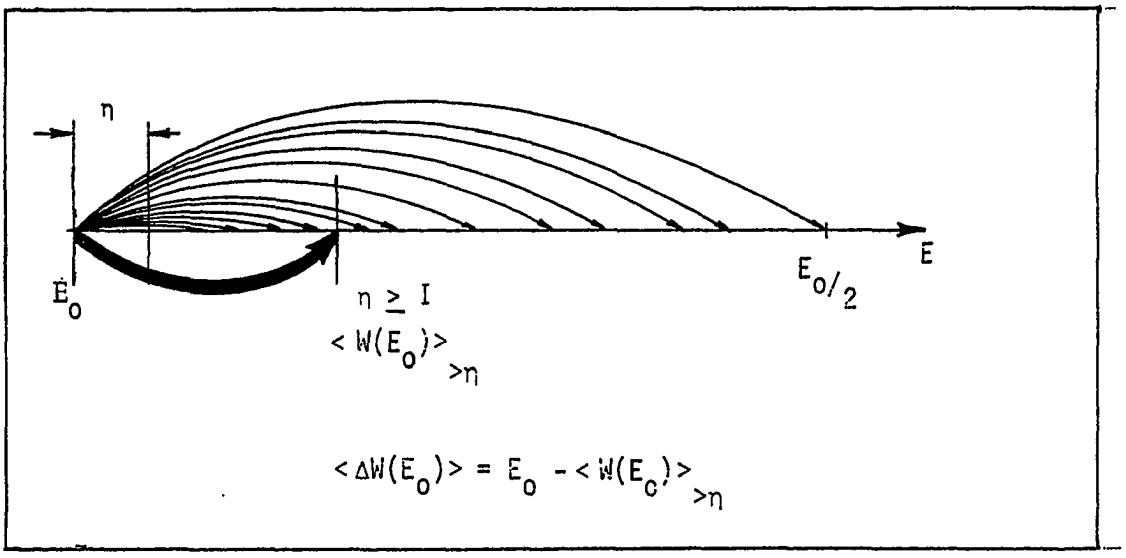

Figure (4.3): Energy loss of inelastic collisions with $\eta \geq I$

calculations. Figure (4.3) represents the case where small energy transfer collisions (energy loss less than or equal to η) are excluded from inelastic collisions. Figure (4.3) also depicts "one average inelastic collision" which approximates all possible inelastic collisions whose energy losses are greater than η. This energy loss model was called "the squashed collision electron transport model," where possible magnitudes of energy losses are in the domain of $(E_0/2,\ E_0-\eta)$. The $\langle W(E_0)\rangle_{>\eta}$ is the average energy of the scattered particle where energy losses greater than η are retained in the calculation. This energy loss is evaluated as

$$\langle W(E_0)\rangle_{>\eta} = \frac{N\int_{E_0/2}^{E_0-\eta} W\,\frac{d\sigma_{inel}(E_0,W)}{dW}\,dW}{\int_{E_0/2}^{E_0-\eta} \frac{d\sigma_{inel}(E_0,W)}{dW}\,dW} \qquad (4.18)$$

The equation (4.18) provides the basic knowledge to generate the multigroup energy structure of the ANISN-CSDM calculations for a given initial energy E_0. Similarly, the average energy loss of the large energy transfer collisions (energy loss greater than η) is given by

$$<\Delta W(E_0)>_{>\eta} = \frac{N\int_{E_0/2}^{E_0-\eta} (E_0-W)\,\frac{d\sigma_{inel}(E_0,W)}{dW}\,dW}{N\int_{E_0/2}^{E_0-\eta} \frac{d\sigma_{inel}(E_0,W)}{dW}\,dW} \qquad (4.19)$$

which may be rewritten as

$$<\Delta W(E_0)>_{>\eta} = E_0 - <W(E_0)>_{>\eta}$$

It may be noted that $<\Delta W(E_0)>_{>\eta} \to 0$ as $\eta \to 0$.

Then one can relate this average energy loss, $<\Delta W(E_0)>_{>\eta}$ to be "restricted" (excluding small energy loss) collisional stopping power by the following expression:

$$<\Delta W(E_0)>_{>\eta} = \frac{(-\frac{dE}{dx})_{>\eta}}{\Sigma_{>\eta}} \qquad (4.20)$$

From equation (4.20) it can be seen that if $<\Delta W(E_0)>_{>\eta} = 0$, which is the $\eta = 0$ case, then $\Sigma_{>\eta} \to +\infty$ where $\Sigma_{>\eta}$ may be called the "restricted collisional macroscopic energy transfer cross-section." This may be evaluated by

$$\Sigma_{>\eta}(E_0) = N\int_{E_0/2}^{E_0-\eta} \frac{d\sigma_{inel}(E_0,W)}{dW}\,dW \qquad (4.21)$$

The energy loss model which has been used to calculate the restricted collisional macroscopic cross-sections (equation (4.21)) does not provide complete energy conservation because

it completely neglects the energy loss due to small energy transfer collisions. It does, however, correctly evaluate the mean energy loss and angular distribution of these restricted collisions. The results of the test calculations of $\Sigma_{>\eta}(E_0)$ versus η are given in Table (4.1), and the data is plotted in Figure (4.4). From the plotted data, it is observed that the rate of change of $\Sigma_{>\eta}$ is relatively small for large η values, and it becomes fairly large at small η values. The value of $\Sigma_{>\eta}$ tends to $+\infty$ as $\eta \to +0$. A larger η value would result in small $\Sigma_{>\eta}$. This may accomplish a large energy loss per average inelastic collision, since large η value results in small cross-sections and therefore it means less scattering. Small cross-sections produce large spatial intervals which directly result in the reduction of the total number of energy groups for a particular transport case. The magnitude of η functions as a basic controlling parameter to determine the actual computing requirements of the problem which can be solved by ANISN-CSDM.

The best approximate collisional cross-section which takes into account all collisional energy losses may be defined as

$$\Sigma_t^{col} = \frac{(-\frac{dE}{dx})^{col}_{total}}{<\Delta W(E_0)>_{>\eta}} \qquad (4.22)$$

where $(-\frac{dE}{dx})^{col}_{total}$ represents the total stopping power due to soft ($<\eta$) and hard ($>\eta$) collisions. This formulation

TABLE (4.1)

Restricted Total Energy Transfer Cross-Section

$\Delta W = 0.005$MeV		$\Delta W = 0.002$MeV		$\Delta W = 0.01$MeV	
η(MeV)	$\Sigma_{>\eta}$(1/cm)	η(MeV)	$\Sigma_{>\eta}$(1/cm)	η(MeV)	$\Sigma_{>\eta}$(1/cm)
2.25010×10^{-2}	10.5	3.700×10^{-2}	5.65	2.50×10^{-2}	10.381
1.75001×10^{-2}	14.18	2.5×10^{-2}	8.735	1.5×10^{-2}	20.319
1.25010×10^{-2}	21.35	1.900×10^{-3}	11.824	5.0×10^{-3}	110.25
7.501×10^{-3}	41.30	9.00×10^{-3}	27.249	1.0×10^{-7}	0.20722×10^{12}
2.501×10^{-3}	221.4	5.0×10^{-3}	54.401		
1.0×10^{-7}	0.10361×10^{12}	1.0×10^{-6}	0.379×10^{12}		

where

ΔW = mesh size (in final energies) of energy integration.

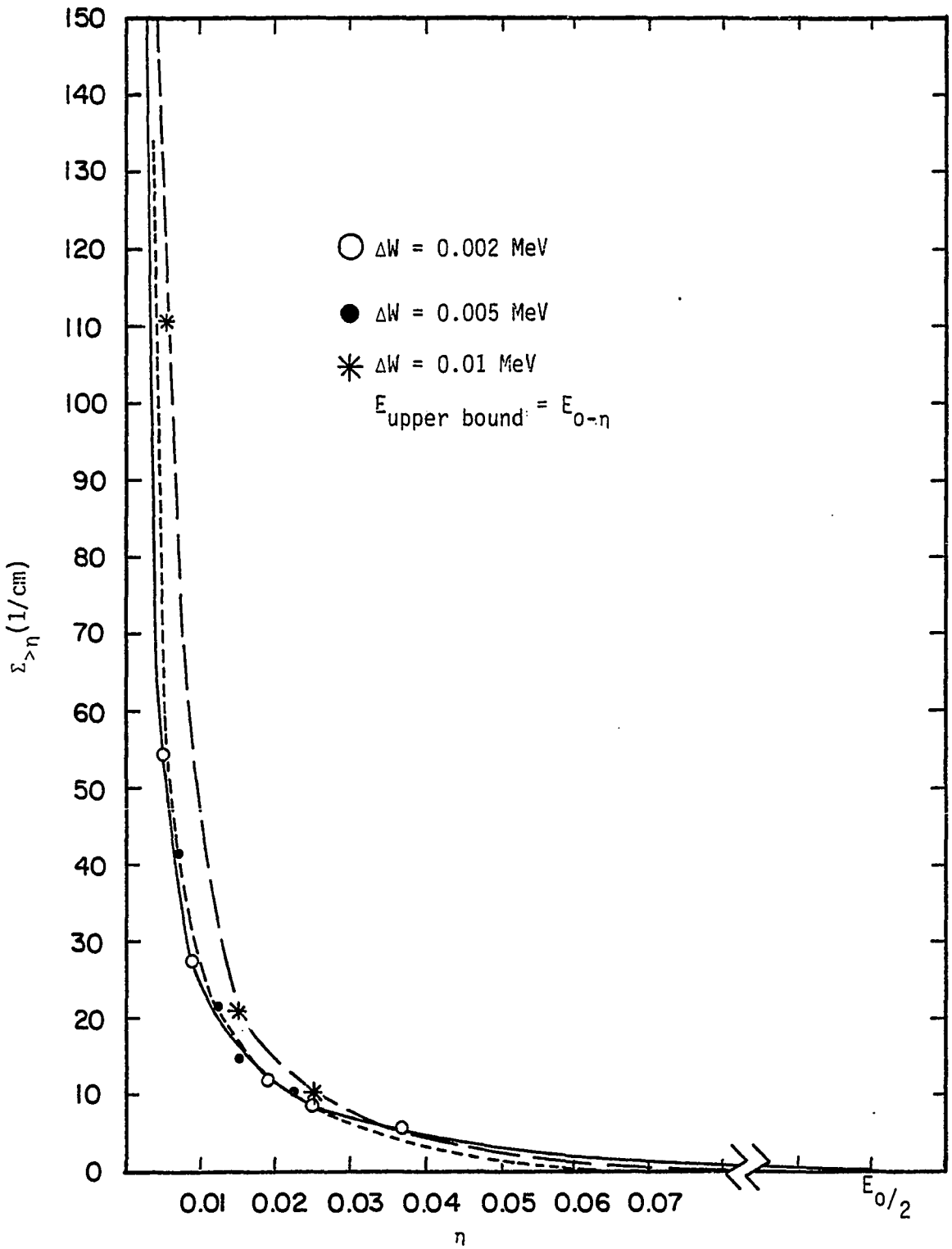

Figure (4.4): The variation of the total energy transfer cross-section as a function of η.

of the energy transfer cross-section represents the best collisional transport model in terms of energy conservation, if the energy loss by photon production is treated separately. Here it may be noted that the angular distribution of the hard collisions applies to these "corrected collisional cross-sections" which are defined by equation (4.22). Thus the angular distribution due to the added effect of soft collisions is approximated by the angular distribution of hard collisions per unit of energy deposited. This approximation results from using the expansion coefficients of equation (4.9) for all inelastic electron-electron scattering.

In the production cross-section formulation of ANISN-CSDM (i.e., cross-sections which produce the electron transport results), it is necessary to include all energy losses due to soft, hard and photon production (rediative) collisions. This is the total energy loss model which will be used in ANISN-CSDM electron transport calculations to produce the transport results. One may note that the energy lost by photon production is negligible compared to the total collisional energy loss in this study. The angular information which is included into these production cross-sections has been generated by using the equation (4.9) for each energy group. For a complete energy analysis, by using the total correct stopping power (the sum of total collisional and radiative) along with the collisional average energy loss, the macroscopic inelastic cross-sections, in general, may be

given as,

$$\Sigma_s(g \to g+1) = \frac{(-\frac{dE}{dx})^{correct}_{tot,g}}{\Delta E(g)} \qquad (4.23)$$

here $\Delta E(g) = <\Delta W(E_g)>_{>\eta}$. Equation (4.23) means that the macroscopic cross-sections should be corrected because of the removal of very small energy loss and radiative collisions from the average energy loss calculations. This correction maintains the complete energy conservation by the correct stopping power, and increases the magnitudes of the macroscopic cross-sections. The increase in cross-sections is because of the contribution of small energy transfer and radiative collisions are being included into the correct total stopping power which has been used in equation (4.23). One may observe the following relationship by comparing equations (4.21, 4.22, 4.23):

$$\Sigma_{>\eta} < \Sigma_t^{col} < \Sigma_s(g \to g+1).$$

Here, one may note that the angular distribution due to the added effect soft and photon production collisions is approximated by the angular distribution of hard collisions. The angular distribution of hard collisions was defined by equation (4.9). In other words, the angular distribution of all energy loss collisions (the soft, hard, and photon production collisions) has been approximated by the angular distribution of the hard collisions in which energy losses are greater than η.

The energy loss formulation for one average inelastic

collision assures energy conservation due to all inelastic and radiative collisions. The energy range considered here assumes that the hard collision energy loss dominates the total energy loss. The secondary electrons and photons are to have relatively low energies compared to the initial energy of the primary particle. Their transport has not been separately taken into account. They are assumed to deposit their energy in the spatial region where they are created. Thus it may be possible to formulate a consistent energy group structure in ANISN-CSDM and produce a consistent energy analysis. The macroscopic cross-sections which will be used in ANISN-CSDM calculations will be discussed in detail in the ANISN-CSDM terminology.

C. Formulation of the Macroscopic Cross-Sections Used in the ANISN-CSDM Calculations

The macroscopic cross-sections which are required for the ANISN input file are produced by using the particle flux conservation. The energy grid structure of the ANISN-CSDM of electron transport may be represented as shown in Figure (4.5). It has been assumed that the interactions take place at the mean energy of the energy groups g = 1,2,3,...,IGM. The ε_g can be defined as the mean energy loss due to interactions occurring in energy group g. It is the property of this electron transport model that

$$\Sigma_a = 0 \text{ for } g = 1,2,3,\ldots,IGM-1 \text{ and } \Sigma_{a,IGM} > 0.$$

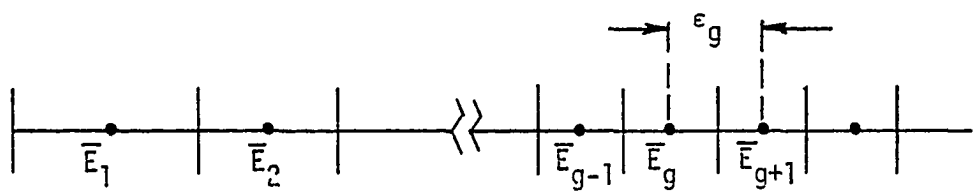

ε_g = (mean energy loss of a particle in energy group interval g)

$= \frac{1}{2}(E_g - E_{g+2})$

$\overline{E}_g = \frac{1}{2}(E_g + E_{g+1})$

$\overline{E}_{g+1} = \frac{1}{2}(E_{g+1} + E_{g+2})$

Figure (4.5): Energy group structure representation of the electron transport model (ANISN-CSDM).

A non-zero absorption cross-section for the final energy group means that the particles are assumed to be removed from the final group by an absorption process. Therefore, all particles which can reach the final energy group are assumed to deposit all of their remaining energy. The magnitude of $\Sigma_{a,IGM}$ can be relatively large, so that the energy deposition occurs promptly at g = IGM (IGM = total number of energy groups).

From the previous discussions one may proceed as follows to formulate the macroscopic cross-sections which are employed in producing the electron transport results using ANISN-CSDM:

From the earlier discussions one may observe that there is "one effective elastic scatter" per spatial interval. This one effective elastic collision represents several individual elastic scatters which can occur in a single spatial interval. A set of successive individual elastic scatters results in wider angular distribution. This effect has been included in the cross-sections for one effective elastic collision by the use of multiple scattering expansion coefficients, $H(E(g),\ell)$. This wider angular distribution which results from the multiple scattering approximation is used in ANISN-CSDM instead of the narrower angular distribution associated with an individual single scatter. The use of one effective elastic collision per spatial interval allows a large interval size whereas the use of single elastic scatters which have large cross-sections requires small intervals. In

general, one may express the representative in-group (elastic) cross-section which results in one collision per spatial interval as

$$\Sigma_s(g \rightarrow g) = \frac{1}{\Delta x_g} \tag{4.27}$$

for the energy group g. Here, the spatial interval size Δx_g is determined by the following equation:

$$\Delta x_g = \frac{1}{\Sigma_s(g \rightarrow g+1)} \quad \text{for energy group g.} \tag{4.28}$$

This allows one spatial interval to be the distance associated with the primary electron slowing down to the next lower energy group. In equation (4.28) $\Sigma_s(g \rightarrow g+1)$ represents the group transfer (inelastic) cross-section of energy group g. This group transfer cross-section can be given as

$$\Sigma_s(g \rightarrow g+1) = \frac{1}{\epsilon_g} \times \left(-\frac{dE}{dx}\right)_g \tag{4.29}$$

By comparing the equations (4.27, 4.28, 4.29) it may be seen that

$$\Sigma_s(g \rightarrow g) = \Sigma_s(g \rightarrow g+1) \tag{4.30}$$

Equation (4.30) shows the mathematical representation of the one-collision nature of the ANISN-CSDM electron transport model. Using the definitions of the elastic and inelastic cross-sections, then the total cross-section may be given by

$$\Sigma_{t_g} = \Sigma_s(g \rightarrow g) + \Sigma_s(g \rightarrow g+1) \tag{4.31}$$

where the in-group scattering and down scattering

cross-sections are given by equations (4.27, 4.29) respectively. For g = IGM the total cross-section should be modified as follows:

$$\Sigma_{t,IGM} = \Sigma_s(IGM \rightarrow IGM) + \Sigma_{a,IGM} \qquad (4.32)$$

The cross section $\Sigma_{a,IGM}$ will be discussed in following paragraphs.

The cross-sections of ANISN-CSDM which are given by equations (4.27, 4.29) are attached to the angular information in the cross-section matrices as expressed below in their general form:

(i) in-group scattering cross-sections

$$(2\ell+1) \times H(E(g),\ell) \times \Sigma_s(g \rightarrow g) \qquad (4.33)$$

(ii) down-scattering cross-sections

$$(2\ell+1) \times V(E(g),\ell) \times \Sigma_s(g \rightarrow g+1) \qquad (4.34)$$

for each energy group, with $\ell = 1,2,3,\ldots,LMAX$. Here $H(E(g),\ell)$ and $V(E(g),\ell)$ are as previously defined. In equations (4.33, 4.34) the $\ell = 0$ case corresponds to the physical in-group and group transfer cross-sections. As discussed earlier, one may note that:

$$H(E(g),\ell) = 1 \quad \text{for } \ell = 0, \text{ and}$$
$$V(E(g),\ell) = 1 \quad \text{for } \ell = 0. \qquad (4.35)$$

The macroscopic energy absorption cross-section (the activity cross-section) may be obtained from the following: The total energy absorption rate, R_g, of the energy group g may be expressed as

$$R_g = \Phi_g \left(\frac{\#particles}{cm^2.sec}\right) \times \left(-\frac{dE}{dx}\right)_g \quad MeV/cm^3.sec \qquad (4.36)$$

where the total particle flux, Φ_g, is produced by ANISN per spatial interval for each energy group. It may be seen that the product $\Phi_g \times \left(-\frac{dE}{dx}\right)_g$ represents the energy deposition density per unit volume for the energy group g. Thus, one may observe that the total activity cross-section is given as

$$\Sigma_{activity,g} = \left(-\frac{dE}{dx}\right)_g \frac{MeV}{cm} . \qquad (4.37)$$

Here, the $\left(-\frac{dE}{dx}\right)_g$ represents the total stopping power of the primary particle in transport medium.

A detailed analysis must be done for the final energy group cross-section calculations because the developed radiation transport model requires complete absorption of particles in the final energy group. Particles which reach the lowest energy without leaking from the material, and do not leak while at that energy, must deposit all the remaining energy in that energy group because there exists no lower energy group into which particles can scatter and deposit the rest of their energy. The out-scatter in the last energy group should be zero because of the reasons stated above. Therefore, the cross-sections of the final energy group, IGM, may be constructed according to the following procedure:
Define some arbitrarily large total cross-section, $\Sigma_{t,IGM}$, for the final energy group IGM. By using equation (4.32) one may write the total particle absorption cross-section

of the final energy group as

$$\Sigma_{a,IGM} = \Sigma_{t,IGM} - \Sigma_s(IGM \rightarrow IGM) \qquad (4.38)$$

Here the $\Sigma_{t,IGM}$ is defined as large enough that the $\Sigma_{a,IGM}$ assures complete absorption of particles which have arrived at the final energy group. A complete absorption of particles in the final energy group means that no particle outscatters from the energy group IGM. Similarly, the activity cross-sections, the energy absorption cross-section, for g = IGM should be defined so that the code indicates that the particles which have arrived at the final energy group have deposited all of their remaining energy. This cross-section may be given as

$$\Sigma_{activity,IGM} = [\Sigma_{t,IGM} - \Sigma_s(IGM \rightarrow IGM)] \times \overline{\Delta E}_{IGM}. \qquad (4.39)$$

Here $\overline{\Delta E}_{IGM}$, all of which must be deposited, is the average total energy of the particles at g = IGM. The cross-sections which are constructed by equations (4.38, 4.39) meet the requirements of the final energy group in ANISN-CSDM model of electron transport.

The macroscopic cross-sections which have been described in the previous paragraphs using the particle flux formulation will be used in the ANISN-CSDM calculations. These cross-sections are based on the squashed collision electron and condensed random walk transport models. The production of these macroscopic cross-sections includes the use of correct total stopping power. In the theoretical

discussion of the squashed collision model, it was necessary to define an average energy loss due to all inelastic collisions. This means that in the calculations one has to specify an η value in calculating average energy loss at a given initial energy, E_0. This means that those inelastic collisions where energy losses are less than or equal to η are excluded from the average energy loss calculations. Such collisions are extremely low energy loss collisions with practically no angular changes occurring. In order to include the correct energy deposition of these low energy transfer collisions in the macroscopic cross-sections it has been stated that the corrected macroscopic cross-sections should be used in the ANISN-CSDM calculations.

On the mathematical formulation of the macroscopic cross-sections one may conclude as follows: If one wants to use the restricted total energy transfer cross-section, $\Sigma_{>\eta}(E(K))$, with the multigroup energy structure, which is determined by $<\Delta W(E(K))>_{>\eta}$, one has to correct the energy group width to maintain complete energy deposition. It is not physically consistent to use the group structure defined by excluding energy losses less than or equal to η along with the $\Sigma_{>\eta}(E(K))$ cross-section as in equation (4.20). This is due to the fact that it completely neglects the energy contribution effect of small energy loss collisions on the total cross-sections. Hence it results in incomplete energy conservation.

The multigroup energy structure specified by $<\Delta W(E(K))>_{>\eta}$

can be used with the total cross-sections which include small energy loss collisions and bremsstrahlung, as in equation (4.23). This combination of cross-sections and energy group structure will assure the conservation of energy deposited.

Choice of small η may improve transport results since more of the "hard" electron-electron collisions (energy losses $> \eta$) are included in the calculation of the angular distribution coefficients. The accuracy may be limited, however, by the use of the same distribution during bremsstrahlung photon production. A small η value may produce detailed transport results, but it requires many energy groups, large core storage, and more computing time. It may not be necessary to use a very small η value to produce reasonably good physical results. A parametric study on η indicates that the transport results are somewhat independent of the selection of η. This makes ANISN-CSDM model economical and user-oriented. This will be discussed later in detail.

A general block diagram for producing the ANISN-CSDM results is given in Figure (4.6). Currently, the production of the electron transport results by ANISN-CSDM represents a multi-step process. The first step is the generation and storage of the basic macroscopic cross-section data, UNIT(20) in DATAPAC6, for Cross-Section Processing Computer Code (CRXPC). The CRXPC has been designed and developed for this research. In the second step the CRXPC processes the input data and produces an ANISN input file in the Group Independent Tape (GIT)

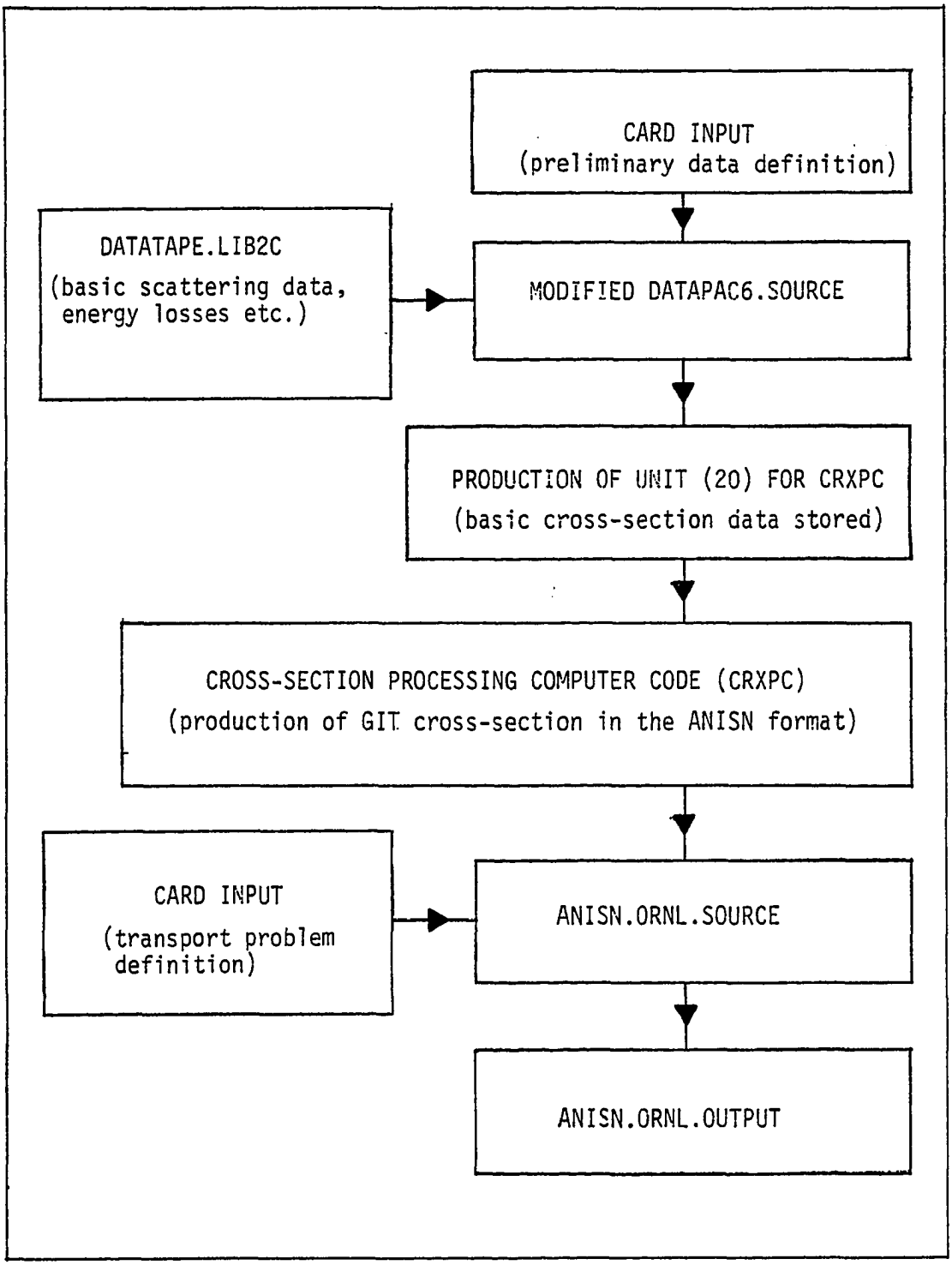

Figure (4.6): The block diagram of a typical ANISN-CSDM calculations.

format. The third step involves the normal ANISN run with the card inputs plus the input file (GIT) which has been produced by CRXPC. This work required up to 5 minutes of computing time to produce cross-sections and 2-29 minutes per ANISN run on an IBM 370-158. For comparison, Bartine's calculations required 15-24 minutes for processing and 11-44 minutes per ANISN on an IBM 360-91

D. Theory of the Extended Transport Cross-Section

The idea in in-group scattering can be visualized as a scatter such that after the scattering collision the scattered particle remains in the same energy group as it was in before the collision. Elastic scattering collisions, in general, result in in-group scattering. But also a fraction of inelastic collisions may result in small angular deflection and energy change and therefore may stay in the same energy interval after the collision. These collisions may also be treated as in-group scattering collisions. All in-group scattering collisions are called highly forward peaked scattering interactions. In electron transport, such collisions occur very frequently, and their effect may be removed from the total scattering cross-section by a correction known as δ-function correction (6,8). Using the δ-function expansion as a correction term, one may obtain the corrected scattering cross-sections as given below.

In general $\Sigma_s(\mu_0)$ may be expanded into Legendre polynomials as

$$\Sigma_s(\mu_0) = N\sigma_s(\mu_0) = \sum_{\ell=0}^{\infty} \left(\frac{2\ell+1}{4\pi}\right) \Sigma_{s,\ell} P_\ell(\mu_0) \tag{4.40}$$

where

$$\Sigma_{s,\ell} = 2\pi \int_{-1}^{+1} \Sigma_s(\mu_0) P_\ell(\mu_0) d\mu_0 \,. \tag{4.41}$$

If $\Sigma_s(\mu_0)$ is highly forward peaked, then one may approximate it as

$$\Sigma_s(\mu_0) \cong \sum_{\ell=0}^{N} \left(\frac{2\ell+1}{4\pi}\right) \Sigma'_{s,\ell} P_\ell(\mu_0) + \frac{K_0}{2\pi} \delta(\mu_0-1) \tag{4.42}$$

where

$$\delta(\mu_0-1) = \sum_{\ell=0}^{\infty} \left(\frac{2\ell+1}{2}\right) P_\ell(\mu_0) \tag{4.43}$$

then equation (4.42) becomes

$$\Sigma_s(\mu_0) \cong \sum_{\ell=0}^{\infty} \left\{ \left(\frac{2\ell+1}{4\pi}\right) \Sigma'_{s,\ell} P_\ell(\mu_0) + K_0 \left(\frac{2\ell+1}{4\pi}\right) P_\ell(\mu_0) \right\}. \tag{4.44}$$

This equation may be rewritten as

$$\Sigma_s(\mu_0) \cong \sum_{\ell=0}^{\infty} \left(\frac{2\ell+1}{4\pi}\right) [\Sigma'_{s,\ell} + K_0] P_\ell(\mu_0) \tag{4.45}$$

where

$$\Sigma'_{s,\ell}\Big|_{\ell \geq N+1} = 0. \tag{4.46}$$

One may calculate the expansion coefficients of $P_\ell(\mu_0)$ in equation (4.45) by assuming the equation (4.44) is exact to

the order of N+1. That is, one may equate equation (4.45) to equation (4.40) to write

$$\Sigma_{s,\ell} = \Sigma'_{s,\ell} + K_0 \quad \text{for } \ell = 0,1,2,3,\ldots,N+1. \tag{4.47}$$

Using equation (4.46), one may determine K_0 as follows:

$$\Sigma_{s,\ell}\Big|_{\ell=N+1} = [\Sigma'_{s,\ell} + K_0]_{\ell=N+1} = \Sigma'_{s,N+1} + K_0 = K_0 \tag{4.48}$$

Therefore, it follows that

$$\Sigma'_{s,\ell} = \Sigma_{s,\ell} - \Sigma_{s,N+1} \quad \text{for } \ell=0,1,2,3,\ldots,N \tag{4.49}$$

It is assumed that $\Sigma_s(\mu_0)$ is highly forward peaked and may be adequately represented by a few term expansions of Legendre polynomials as given in equation (4.42). It is observed that $\Sigma_{s,0}$ is not much greater than $\Sigma_{s,N+1}$. Therefore, one may observe that the transport-corrected scattering cross-section is smaller than $\Sigma_{s,\ell}$. This also means that the transport-corrected cross-section is less forward peaked than $\Sigma_{s,\ell}(\mu_0)$ (6,8). In literature, $\Sigma'_{s,\ell}$ are called the P_{N+1} transport-corrected P_N expansion of $\Sigma_{s,\ell}$. One may note that the transport corrected in-group scattering cross-sections provide less forward scattering and result in wider distribution of multiply scattered particles. The fundamental idea in the extended transport corrected cross-section formulation is that the ingroup scattering is assumed as no scattering. This means that no appreciable energy loss occurs in such collisions. In practical calculations it is impossible to

input the angular representation of such collisions into ANISN cross-section matrices because this representation requires many terms in the Legendre polynomial expansion of these in-group scattering cross-sections. Further details of the theory of the extended transport correction may be found in the literature (6,8).

E. A Preliminary Discussion of the Electron Group Skipping Model

From the previous discussions of energy loss mechanisms in electron collisions, one may visualize an electron-electron collision as follows. The primary particle with an initial energy E_0 comes away from the collision with an energy W. The energy of the second electron is then given by

$$E' = E_0 - W. \tag{4.50}$$

Now there exist two electrons, one with energy W and the other with energy E', $(W > E')$. It can be seen that the probability of the scattering into low energy groups is relatively small for the primary particles. This means that the magnitude of energy losses in electron-electron collisions is small, and that the primary particle usually moves into adjacent energy groups. The further energy loss interactions of the two particles which came from the previous interaction are governed by $\frac{d\sigma_{inel}(E_0,W)}{dW}$, which was

defined earlier in this chapter by equation (4.3). It may be seen that $\frac{d\sigma_{inel}(E_0,W)}{dW}$ is in the differential form of the final energy of the scattered particle, but the initial energy represents a point value. In deep penetration radiation transport problems (e.g., shielding design), one must employ a fine energy group structure to produce detailed transport results. In this case the mean energies of the established energy group structures are approximated as the initial energies of the primary particle for that particular energy group. Then it is possible to define the group skipping cross-sections as

$$\sigma(g \to g') = \left[\int_{E_{g'+1}}^{E_{g'}} \frac{d\sigma_{inel}(E(g),W)}{dW} \, dW \right]_{E(g)=\frac{1}{2}(E_g+E_{g+1})} \tag{4.51}$$

where

$g = 1,2,3,\ldots,IGM-1$

$g' \geq g+1.$

The group skipping cross-section formulation which is given above indicates that the initial energy of the primary particle is assumed to be equal to the mean energy of the associated energy group. The numerical integration should be performed over the final energy group width. The angular information should be attached to those group skipping cross-sections based on the energy-angle relationship which was also given earlier in this chapter, but a different

approximation may be required than was used for ANISN-CSDM.

CHAPTER V

RESULTS AND COMPARISONS

In this chapter, the validity of the Continuous Slowing Down Model (ANISN-CSDM) of electron transport which has been developed in the previous chapters will be tested. There are two kinds of test calculations. The first part is the one-group electron transport calculations. The second part is the multigroup calculations. The multigroup calculation results may be classified as follows:

(i) energy and angle distribution of transmitted particles in one dimensional slabs (aluminum, gold, water)

(ii) distribution of energy absorption as a function of depth in transport medium (water, aluminum).

Each of those calculations has been performed in one-dimensional slab geometry; where the slab has a finite thickness along the x-axis but it is treated as infinite along the y- and z-axes. Therefore, leakage is observable at the boundaries of the slab and no leakage from the sides. Calculations are performed with the vacuum boundary conditions at each side of the slab with a unit source at the incident (left boundary). The source is so placed that it approximates

normally incident particles falling on the slab from the negative x-axis direction. The x = 0 represents the left boundary of the slab and x = d represents the right boundary of the slab as shown in Figure (5.1). The problem has been solved for different transport mediums at different thicknesses for the different initial energies. The type of problem which is solved here is generally classified as a fixed source problem in the Discrete Ordinates Method.

A. One Group Calculations

Morel (8) has investigated the relationship between the variation of the scalar flux as a function of the electron energy, the magnitude of the removal cross-section, and the thickness of the slab in scattering mean-free-paths. Initial energy of electron is used as a measure of the anisotropy included into transport calculations. The problem which was solved represents vacuum boundary conditions. Morel's calculations include only a one-group model of electron transport. This is an accurate representation of the highly anisotropic scattering cross-sections requiring high order Legendre polynomial expansion (LMAX $\approx$ 150 at E_0= 1.0 MeV). The need for high order is one of the major drawbacks in producing good electron transport results. High expansion orders require relatively large computer storage and computing time. Morel has employed the concept of the

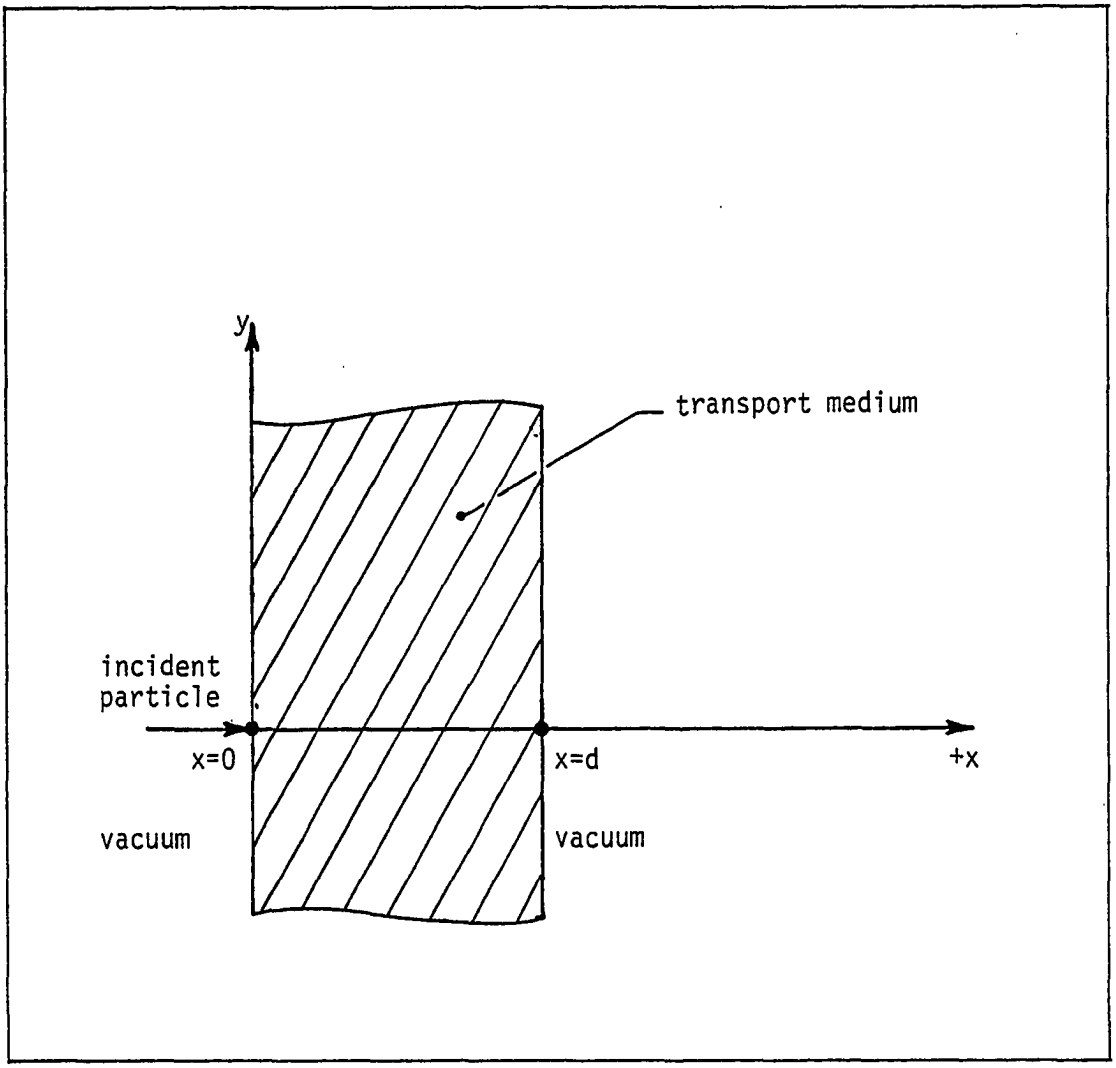

Figure (5.1): Geometry of the ANISN-CSDM calculations.

extended transport corrected cross-section formulation in reducing such a high expansion order and made the calculations manageable. Characteristics of Morel's calculations may be stated as follows: For a given energy one may vary the slab thickness (in removal mean free-paths, or scattering mean free-paths) and then observe the variation of the electron scalar flux, $\phi(E_0, x_i)\frac{\#particles}{cm^2 \cdot sec}$, as a function of the penetration depth. Here penetration depth is given in terms of the scattering mean-free paths. The electron transport results have been produced by Morel using the DTF69 (A Sandia Laboratories version of the DTF transport code) and a Monte Carlo computer code which was designed using standard analog techniques (8). The results obtained using these two schemes show very good agreement. Morel's calculations include P_{12} transport-corrected P_{11} expansions of the ingroup scattering cross-sections. No energy loss collisions were considered in his calculations, because he performed one-group electron transport calculations.

The ANISN-CSDM formulation for electron transport which has been discussed in the previous sections was adjusted to represent the problem solved by Morel for one-group calculations. One may note that ANISN-CSDM involves multiple scattering approximation in the formulation of the macroscopic cross-sections. This formulation significantly

reduces the computer storage requirement and the computing time. The appropriate angular redistribution of the elastically scattered particles was achieved by multiple scattering expansion coefficients. The general theory of the formulation of such expansion coefficients is given by Goudsmit-Saunderson (23).

The results from ANISN-CSDM for one-group calculations are given in Figure (5.2) and Figure (5.3) along with the results obtained by Morel (8). The results show that there exists an excellent agreement between them. The characteristics of the calculations are: incident electrons of the energy E = 1.0 MeV normally fall on an aluminum slab of the thickness d = 1000 x λ_s where λ_s represents the scattering mean-free-path of electron which may be defined as follows:

$$\lambda_s = \frac{1}{\Sigma_s(1\rightarrow 1)}$$

In ANISN format, $\Sigma_s(1\rightarrow 1)$ is the total in-group scattering cross-section of electrons. The variable parameter in the two ANISN-CSDM transport calculations is the d/λ_{R_1} ratio; where λ_{R_1} represents the mean-free-path of the removal cross-section and d the slab thickness. The λ_{R_1} may be defined as follows:

$$\lambda_{R_1} = \frac{1}{\Sigma_{R_1}(1 \rightarrow 2)}$$

where in this case group 2 represents all energies below group 1, so that

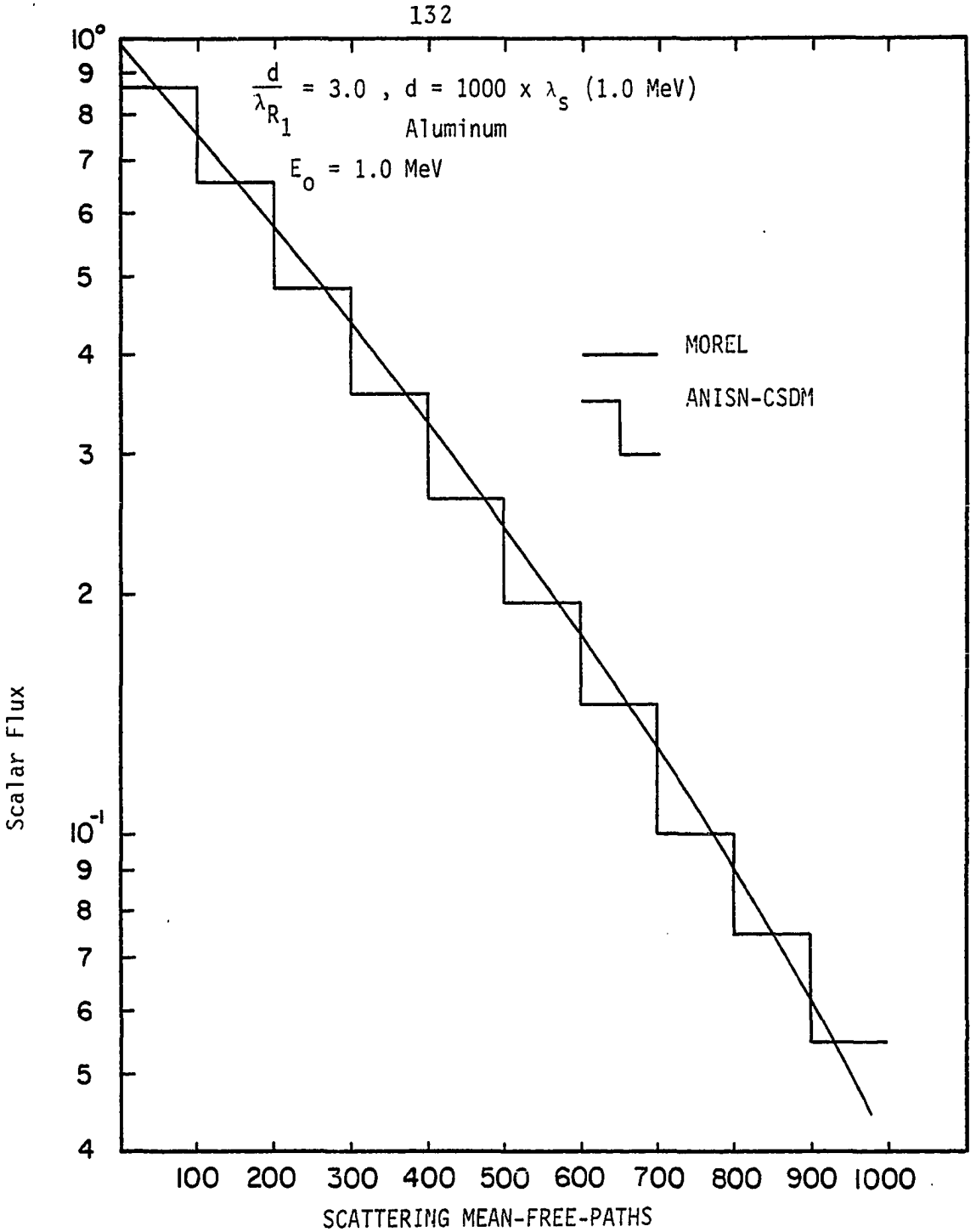

Figure (5.2): Scalar flux comparison at E_o = 1.0 MeV in aluminum.

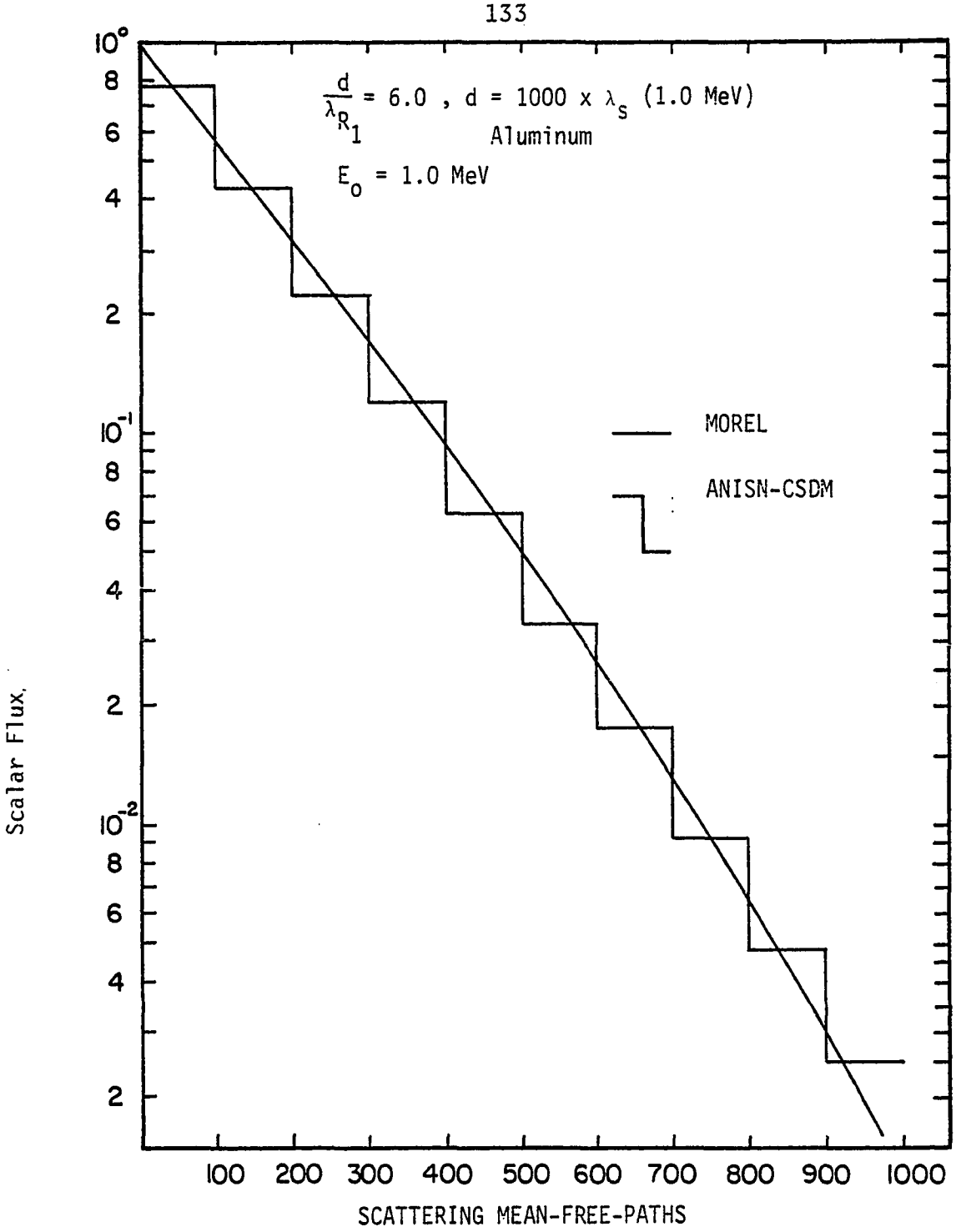

Figure (5.3): Scalar flux conparison at E_o = 1.0 MeV in Aluminum.

$$\Sigma_s(1 \rightarrow 2) = \Sigma_{R_1}(1 \rightarrow 2) = \Sigma_{t_1} - \Sigma_s(1 \rightarrow 1).$$

The transport medium thickness, the thickness of the slab, has been kept constant for the particular transport cases which are chosen for the comparisons. In Figure (5.2), $d/\lambda_{R_1} = 3.0$ with $d = 1000 \times \lambda_S$, and in Figure (5.3) $d/\lambda_{R_1} = 6.0$ with the same slab thickness. The electron transport results which have been produced by both of these schemes have shown that the scalar electron fluxes, $\phi(E_0, x_i)$ #electrons/cm^2·sec, fall off almost linearly on a semi-log scale, as a function of the depth of penetration. In Figure (5.2) and Figure (5.3) Morel's results are given by continuous lines and the ANISN-CSDM results are given by step-lines. The ANISN-CSDM results given on Figures (5.2,5.3) used 11 spatial mesh intervals and P_{10} transport-corrected P_9 expansion of the Legendre polynomials with a standard S_{48} Gaussion quadrature set. This problem is equivalent to a P_{146}/S_{48} case without using the transport-corrected cross-sections. Overall calculation time is about 3.0 minutes on an IBM370-MODEL158. In this case P_{146}/S_{48} took 5.0 minutes, but in all other cases the convergence becomes a very significant problem. This difficulty has been removed by using the transport corrected cross-sections in those cases which require high expansion orders. This comparison with Morel confirms the validity of the multiple scattering approximation in the ANISN-CSDM formulation and confirms the accuracy of the extended transport

cross-section correction as well. As discussed earlier, the concept of the extended transport correction is to remove those collisions which result in no appreciable energy-angle change from cross-sections. The extended transport correction implies the reduction of cross-sections due to the removal of frequent small energy/angle collisions from transport calculations. This approximation results in less forward peaked distribution and eases the ANISN-CSDM calculations from the convergence point of view.

B. Multigroup Calculations

In this subsection a validity test of the electron transport model, ANISN-CSDM, will be made. The electron transport results which have been produced using the model developed in this paper will be compared with the experimental results of Rester/Derrickson (57) and Anderson (59). In addition, some comparisons will be made with the results of ETRAN18G and Bartine et al. These comparisons required the development of cross-section sets and transport calculations in aluminum, gold, and water.

1. Transmitted Electron Energy Distributions

a. 1.0 MeV Electrons Normally Incident on Variable Aluminum Slab Thicknesses

The ANISN-CSDM of electron transport is here tested on a low Z transport medium. Electron transport results are

given on Figures (5.4,5.5,5.6) along with the experimental results of Rester/Derrickson. The ETRAN18G results are also given separately for the energy straggling and continuous slowing down options. Figure (5.4) represents an aluminum thickness of 0.1815 of the full range of incident particle. Figure (5.5) represents an aluminum thickness of 0.3993 of the full range of incident particle. Figure (5.6) represents an Aluminum thickness of 0.5809 of the full range of incident particle. From Figure (5.4) one may observe that the experimental results and the ETRAN18G-straggling results are slightly higher than the ANISN-CSDM results at the peak value of the energy distribution of the transmitted particles. There is good agreement along the high energy and the low energy edges of the distribution. Also there exists a good agreement in predicting the location of the peak of the transmitted energy distribution. A consistent η value has been used for all Figures (5.4,5.5,5.6). From Figure (5.5) one may observe that the ANISN-CSDM produces very much the same result as ETRAN18G-energy straggling (best ETRAN model) model. The agreement between the ANISN-CSDM and the experiment becomes better in Figure (5.6). The Figure (5.6) represents a relatively deep penetration ratiation transport problem. For this deep radiation penetration problem the ANISN-CSDM produces relatively good electron transport results, as ETRAN18G does. The

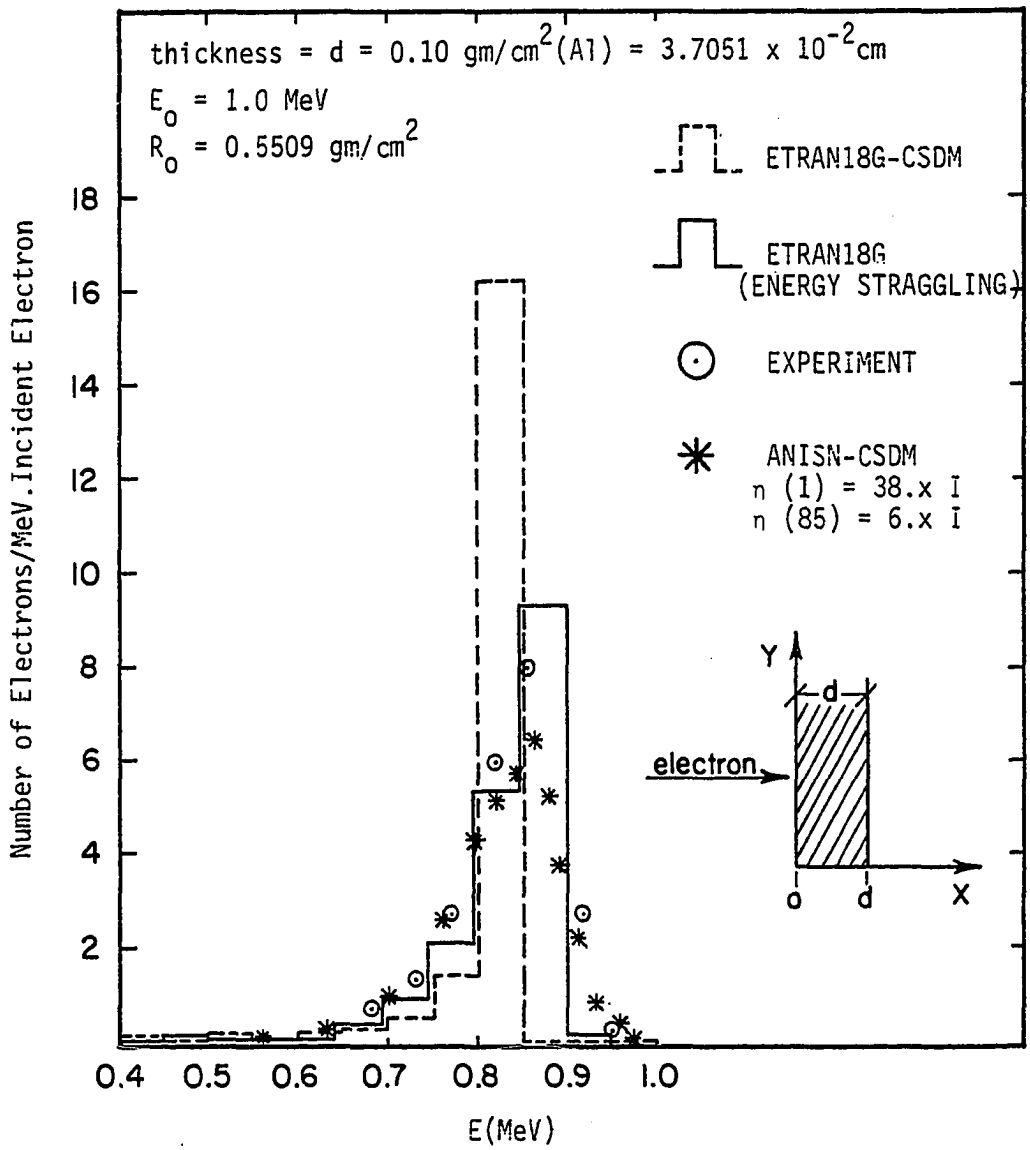

Figure (5.4): Transmitted electron energy distribution per unit energy per electron in aluminum of thickness 0.10 gm/cm^2.

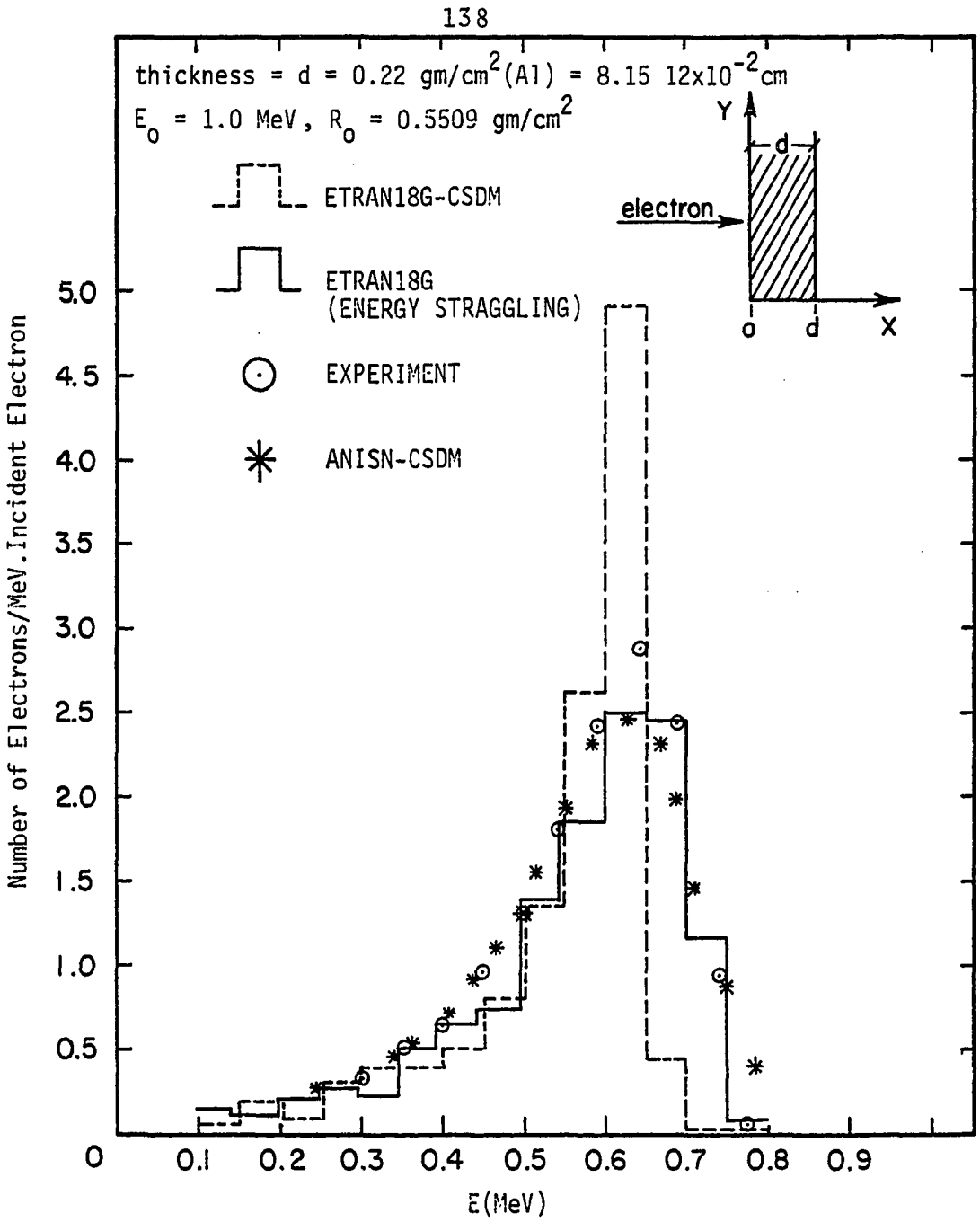

Figure (5.5): Transmitted electron energy distribution per unit energy per electron in aluminum of thickness 0.22 gm/cm^2.

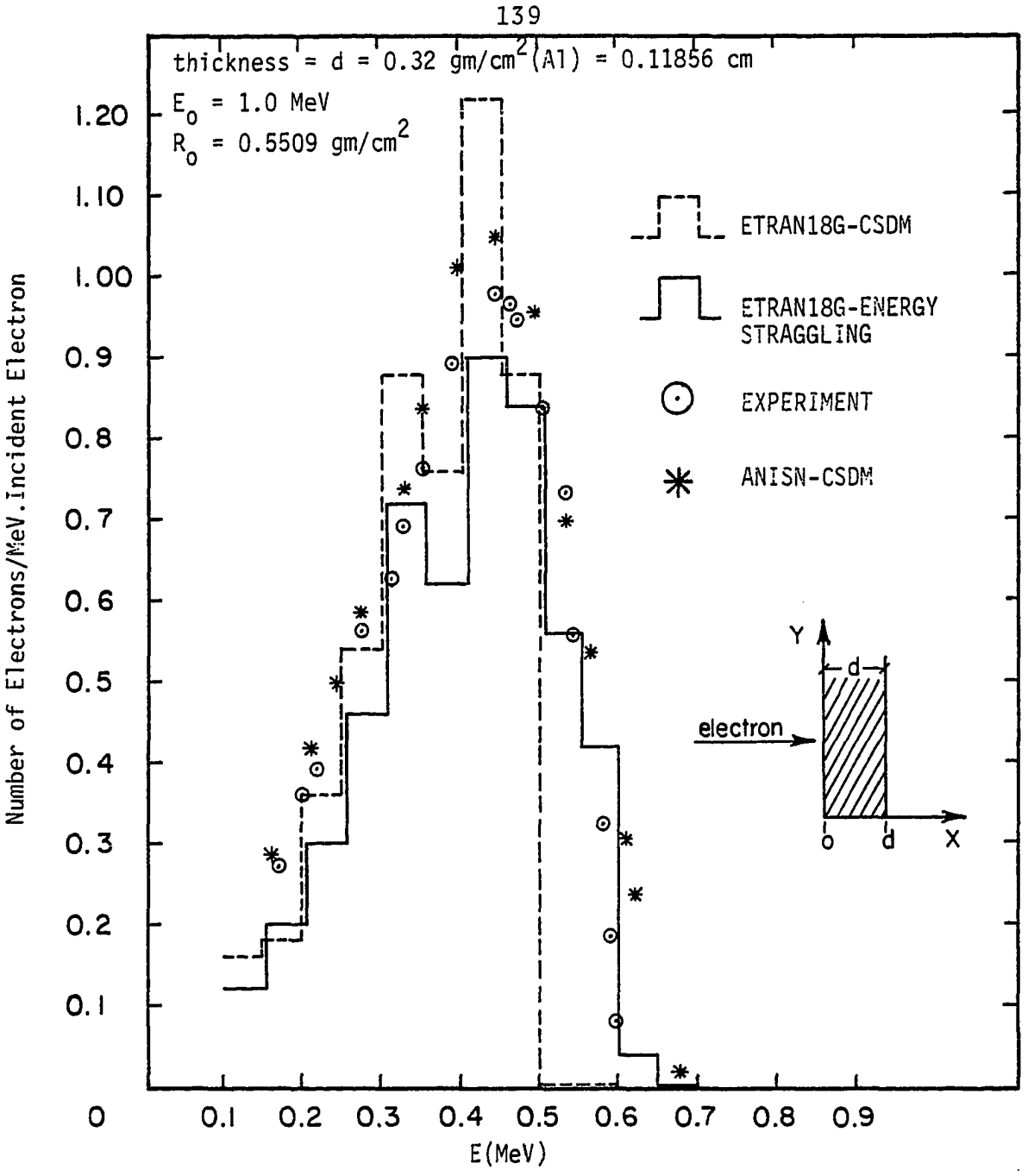

Figure (5.6): Transmitted electron energy distribution per unit energy per electron in aluminum of thickness 0.32 gm/cm^2.

analysis of the electron transport results in aluminum (a low Z and low energy transport problem) demonstrates good agreement between the ANISN-CSDM and the experimental results. This agreement comes from the accurate representation of the probabilistic energy losses of the primary particle based on the average energy loss model of ANISN-CSDM. In Figures (5.4,5.5,5.6) it may be seen that the agreement between ANISN-CSDM and the experimental results becomes better at the peak of the distributions of transmitted particles for greater slab thickness.

In general, an inelastic collision results in the production of a secondary electron with an energy above the η value (minimum η value is I). The energy loss and the deflection of the primary particle in the production of a secondary particle with energies above cut-off energy option of ETRAN18G is not in effect. The ETRAN18G currently assumes that the primary electron is unaffected by the production of a secondary electron. The energy loss of the primary electron and the angular deflections are included, approximately (see: ETRAN18G MANUAL (DATAPAC6, SUBROUTINE INELS)) in the inelastic scattering correction to the multiple elastic scattering angular distributions. The ANISN-CSDM produces the inelastic scattering expansion coefficients which are to be attached to the energy transfer cross-sections separately. The analytical equations

associated with the production of the expansion coefficients of the energy transfer cross-sections were given in detail in Chapter (IV).

The comparisons of the ANISN-CSDM results with the ETRAN18G and the experimental results for angular distributions of the transmitted electrons per unit solid angle for aluminum slabs of different thicknesses resulting from a primary electron at the initial energy $E_0 = 1.0$ MeV, are plotted on Figures (5.7,5.8,5.9). These figures correspond to the d = 0.10 gm/cm^2, 0.22 gm/cm^2 and 0.32 gm/cm^2 transport cases, respectively. In each case, the ANISN-CSDM data is in relatively good agreement with the experimental and the ETRAN18G results. For the 0.32 gm/cm^2 case, given in Figure (5.9), some small disagreement may be apparent at smaller angles. This is especially true when comparing ETRAN18G and experiment, possibly indicating that ANISN-CSDM is better than ETRAN18G for deep penetration radiation transport problems. In general, all three results (experimental and calculated results) are relatively in good agreement in terms of predicting the angular distributions of the transmitted particles at the right boundary of the aluminum slabs. Similar good agreements are observed in water, and will be given later in this chapter.

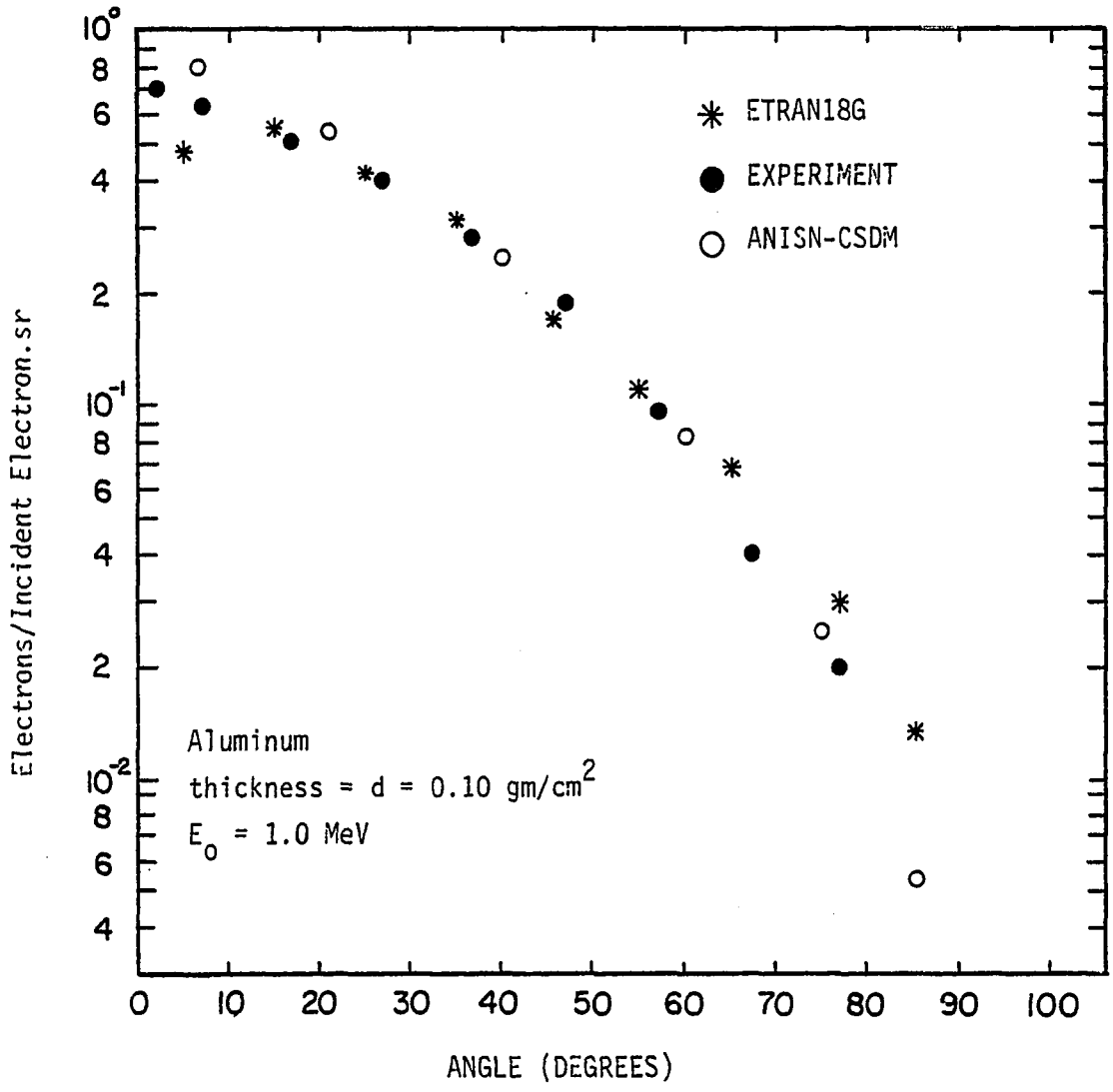

Figure (5.7): Angular distributions of transmitted electrons in aluminum of thickness 0.10 gm/cm^2.

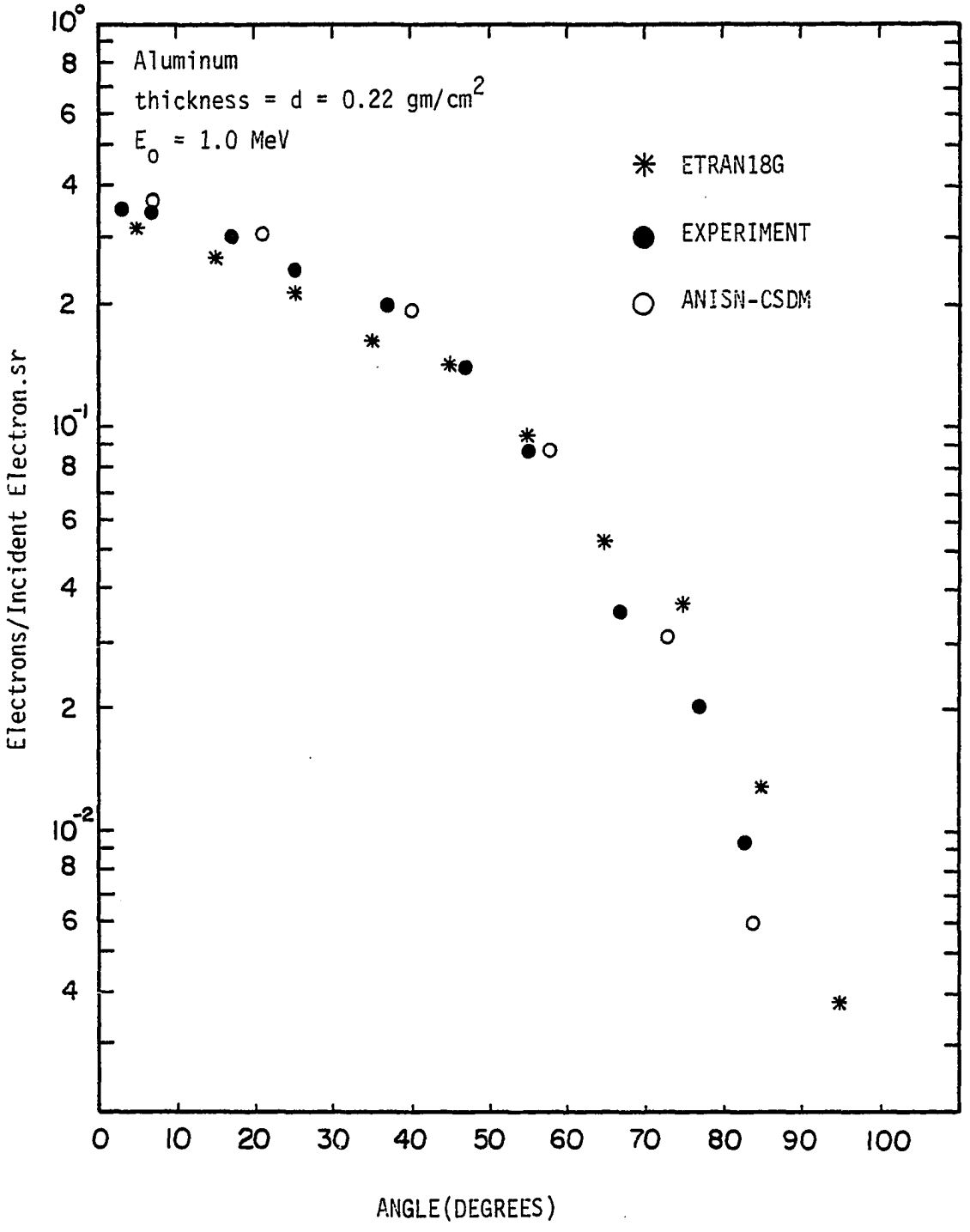

Figure (5.8): Angular distributions of transmitted electrons in aluminum of thickness 0.22 gm/cm^2.

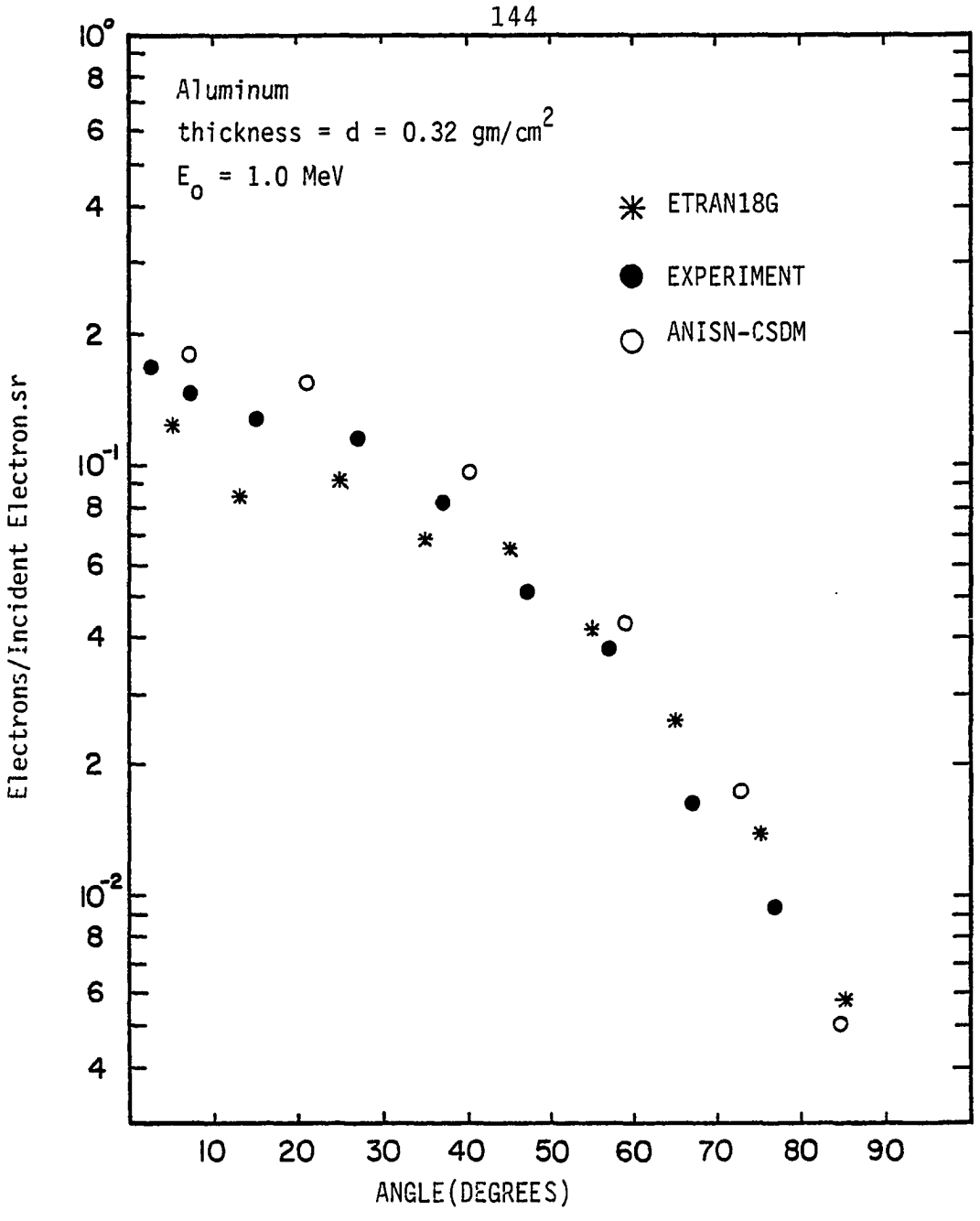

Figure (5.9): Angular distributions of transmitted electrons in aluminum of thickness 0.32 gm/cm^2.

b. 1.0 MeV Electrons Normally Incident on a Gold Slab

The ANISN-CSDM has been tested in a high Z transport medium, gold. The results are given in Figure (5.10). This is a comparison of the energy distribution of the transmitted particles at the right boundary of the gold slab. Three different ANISN-CSDM results are shown in Figure (5.10) along with the experimental result of Rester/Derrickson (57). The slab thickness is 0.15 gm/cm^2. From Figure (5.10) it can be seen that the ANISN-CSDM results for different η values, are relatively in good agreement with the experimental result along the high energy and low energy edges. However, the peak value of the energy distribution of the transmitted particles is relatively higher than the experimental results. The ANISN-CSDM transport results correspond to IGM = 25, IGM = 61, and IGM = 85 respectively (IGM = total number of energy groups in ANISN transport calculations). This series of calculations represents a parametric study of η where $\eta(1)$ is equal to 32.9 x I, 10.97 x I, and 7.8 x I respectively, where I is the ionization energy of an electron. The characteristic data for the parametric study of η in gold is given in Table (5.1). It may be observed that one can produce essentially the same transport result while reducing the computing time by a factor of three through the proper selection of an η value. The corresponding gold result which was produced by

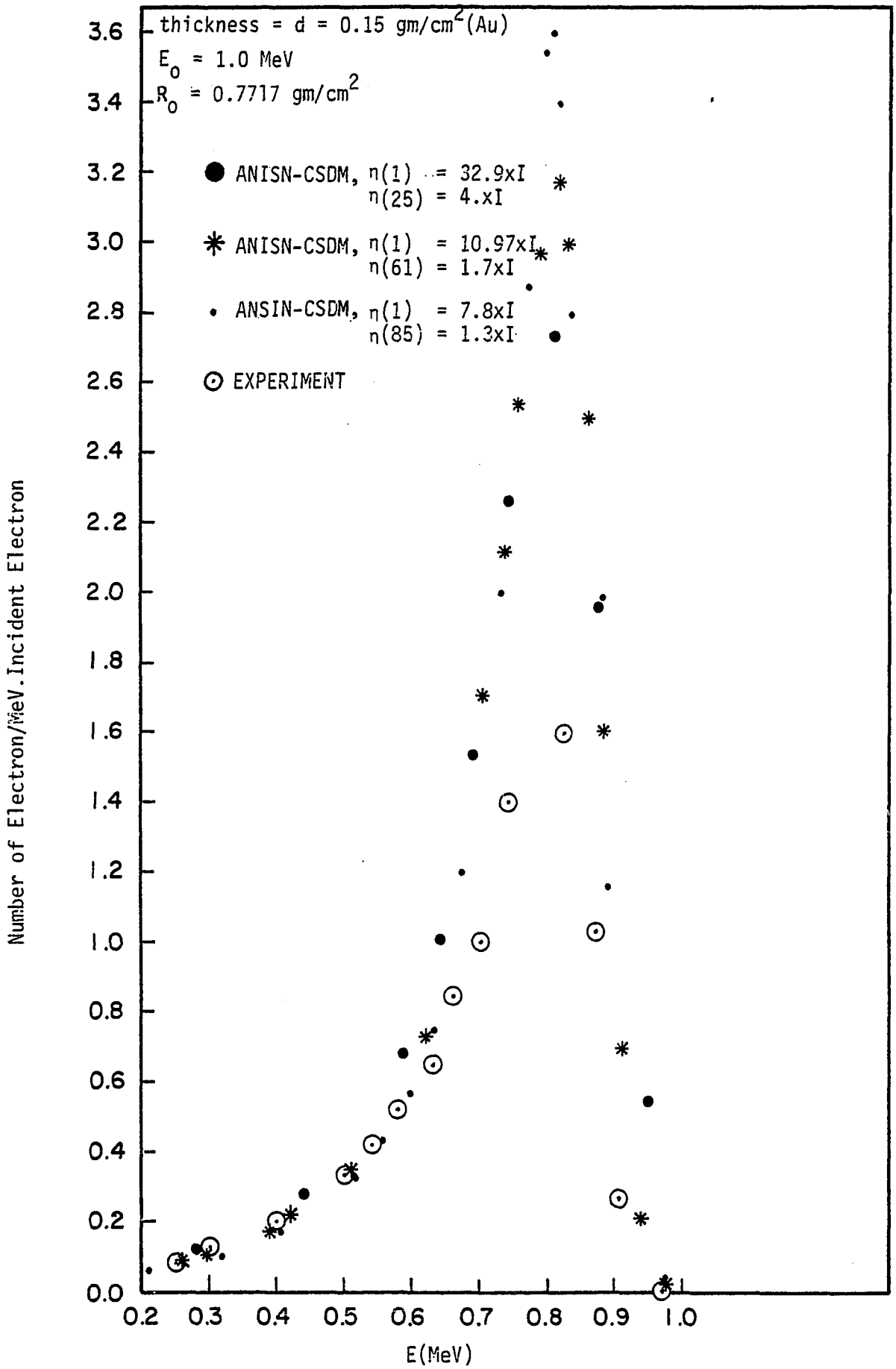

Figure (5.10): Transmitted electron energy distribution in gold.

TABLE (5.1)

Characteristic data for the parametric study of η in gold for the results given in Figure (5.10)

Legend	IGM	$\eta(1)$	η(IGM)	IM	ISCT	CPU time[(a)] (minutes)
●	25	32.0 x I	4. x I	4	15	2.26
✳	61	10.9 x I	1.7 x I	7	30	4.16
•	85	7.8 x I	1.3 x I	9	39	6.35

where

IGM = total number of energy groups

IM = number of spatial intervals

ISCT = Maximum order of scatter found in any zone

The ISN (order of angular quadrature) is 48 for all ANISN-CSDM runs.

(a) on IBM370-MODEL158

Bartine et al. (6) relatively underestimates the energy distribution of the transmitted particles near the peak and along high energy edges of the spectrum while ETRAN18G results agree fairly well with experiment. This is shown in Figure (5.11(a)).

It has also been observed that if one increases the number of spatial intervals independently (not shown), the value of the peak may be reduced. Relatively few intervals were used in the reported calculations (see Table (5.1), so further improvements might be possible. The number of intervals used were consistent with those of other tests, so this was not pursued. Since the ANISN-CSDM is a "one collision model" in terms of energy losses, the spatial intervals adequate for the model are used in the calculations. It has also been observed in test calculations that if one inputs "a wider distribution of inelastic expansion coefficients " (not implied by the model) then it is possible to produce the electron transport results which are in good agreement with the experimental and the ETRAN18G-energy straggling model results.

From study of Figure (5.11(a)) it may be seen that Bartine's model underestimates the experimental result by about 40%, but the ANISN-CSDM model overestimates the experimental result by about 25% (based on areas under curves). This difference comes from the fact that the ANISN-CSDM model

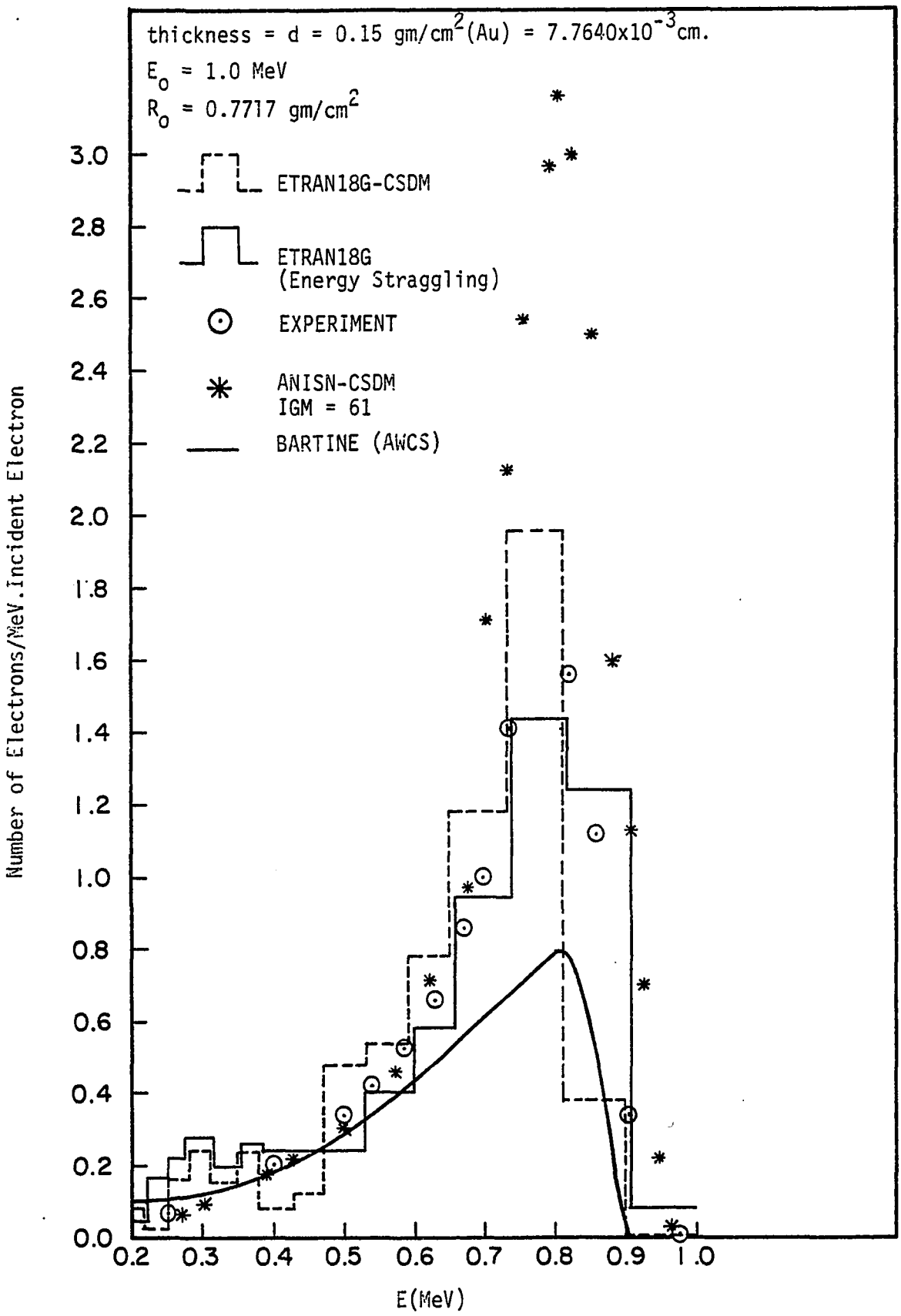

Figure (5.11(a)): Transmitted electron energy distribution in gold.

results in more forward angular distribution leaking from the gold slab as shown in Figure (5.11(b)). This situation may be taken as a limitation of the ANISN-CSDM model in high Z transport mediums, and could be related to the separation of variables. More detailed discussions will be given in Chapter (VI) along with the observations made in test calculations.

Here it may be noted that in the ETRAN18G models the angular effect of the inelastically scattered particles is incorporated into the multiple elastic scattering angular distribution by replacing Z^2 with $Z(Z+1)$ in the single elastic scattering cross-section. The test calculations with the modified DATAPAC6 have shown that such a correction is very small. In ANISN-CSDM separate angular expansion coefficients have been used for energy transfer cross-sections. A comparative study between angular distributions of the transmitted particles has shown that (water results will be given in the next subsection) the ANISN-CSDM angular redistribution model is, in general, in good agreement with experimental and Monte Carlo results except in gold (a high Z transport medium).

The parametric study of η in gold indicates that when η gets larger the peak value of the energy distribution of transmitted particles becomes smaller. This could be explained as follows: The energy from small energy transfer collisions has been included in inelastic scatter energy deposition. Thus, the modeled angular deflections are the same

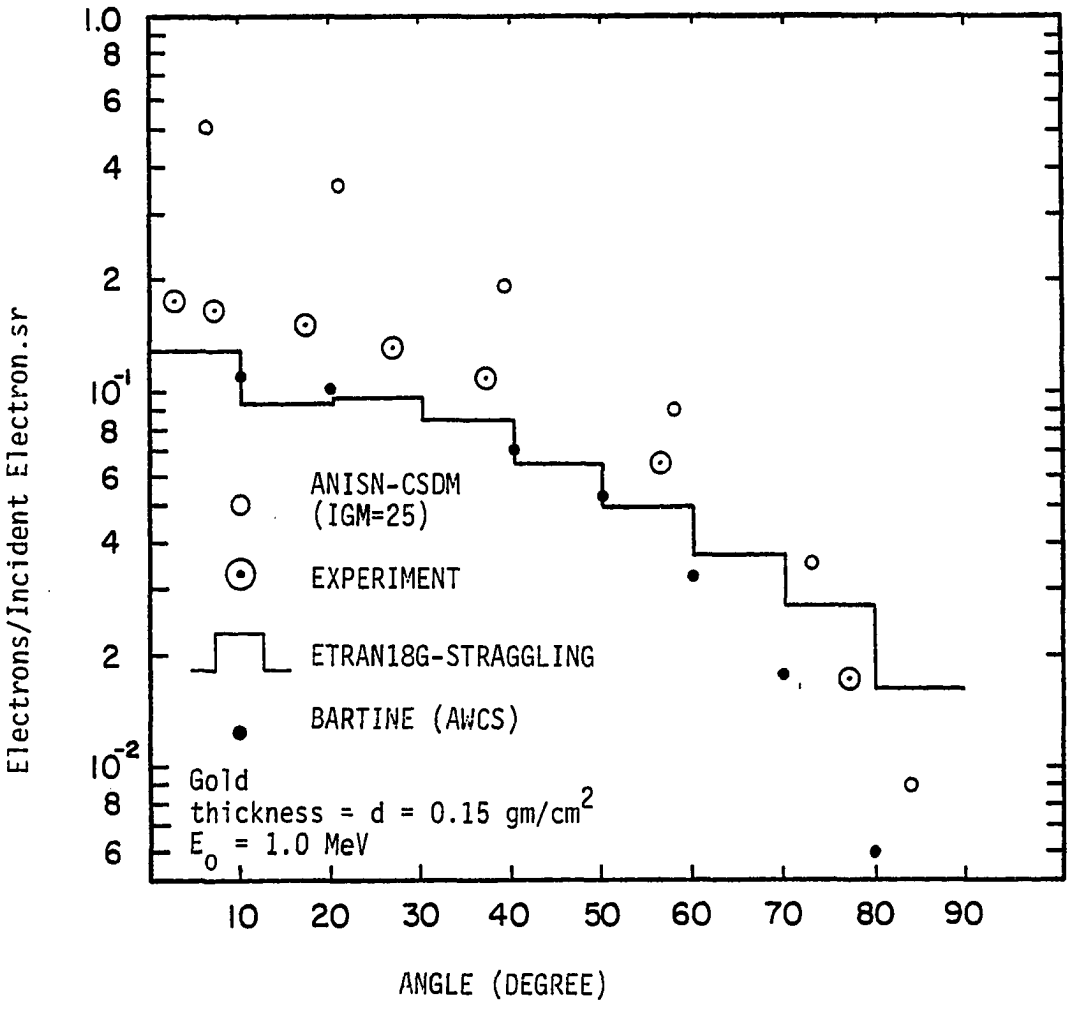

Figure (5.11(b)): Angular distributions of transmitted electrons in gold.

as those of inelastic scatters depositing the same energy. This requires fewer scatters than actually occur, so that other small-angle scatters are replaced by non-scatters with original direction retained. This combination of large-angle scatters and non-scatters, while retaining the correct energy deposition, increases somewhat the effect of the large-angle scatters for greater values of η. One might expect that smaller values of η would result in better agreement with experiment. Since this is not the case, other causes for the disagreement must be sought. The use of a non-zero η is essential to the model, since it greatly reduces the collision cross-section, thus reducing the number of spatial intervals that must be used and reduces the scattering order that must be used. This greatly reduces computer time and storage requirements, making many calculations (especially for thick materials) possible.

Energy loss by photon production is treated approximately by ANISN-CSDM. This approximation could be important at very high energies. In the results given in Figure (5.10) the energy loss to photon production is 9%. Therefore, the effect of energy loss by photon production upon the production of expansion coefficients for energy transfer cross-sections may not be significant. Note that the angular distribution expansion coefficients of energy transfer cross-sections are generated by considering the energy losses (greater than η) which are governed by Møller cross-section.

These expansion coefficients are generated using equation (4.9). The Møller cross-section represents the most important mode of energy loss in electron-electron collisions for the energy range considered in this study. This is due to the fact that energy losses by inelastic scatters account for about 91% of the energy deposition for gold at 1.0 MeV, and for about 92% for water at 10.0 MeV. It is unlikely that the observed differences are caused by this approximation. The following section will test the use of the model against other models and experimental results on water.

2. Energy Deposition Distributions

a. 10.0 MeV Electrons Normally Incident on a Water Slab

The total electron energy deposition as a function of the penetration depth in water from 10.0 MeV electrons is given in Figure (5.12) obtained by ANISN CSDM. In this figure ETRAN18G results are also shown. This represents the transport case in which the water slab thickness is greater than the range of the primary particle. That is, the water slab thickness is at least 5.0 cm, which is the approximate range of an electron at 10.0 MeV in water. Experimental energy deposition data for water at 10.0 MeV is unavailable. The experimental distribution of deposited energy (normalized energy deposition) is available, and is shown in later figures.

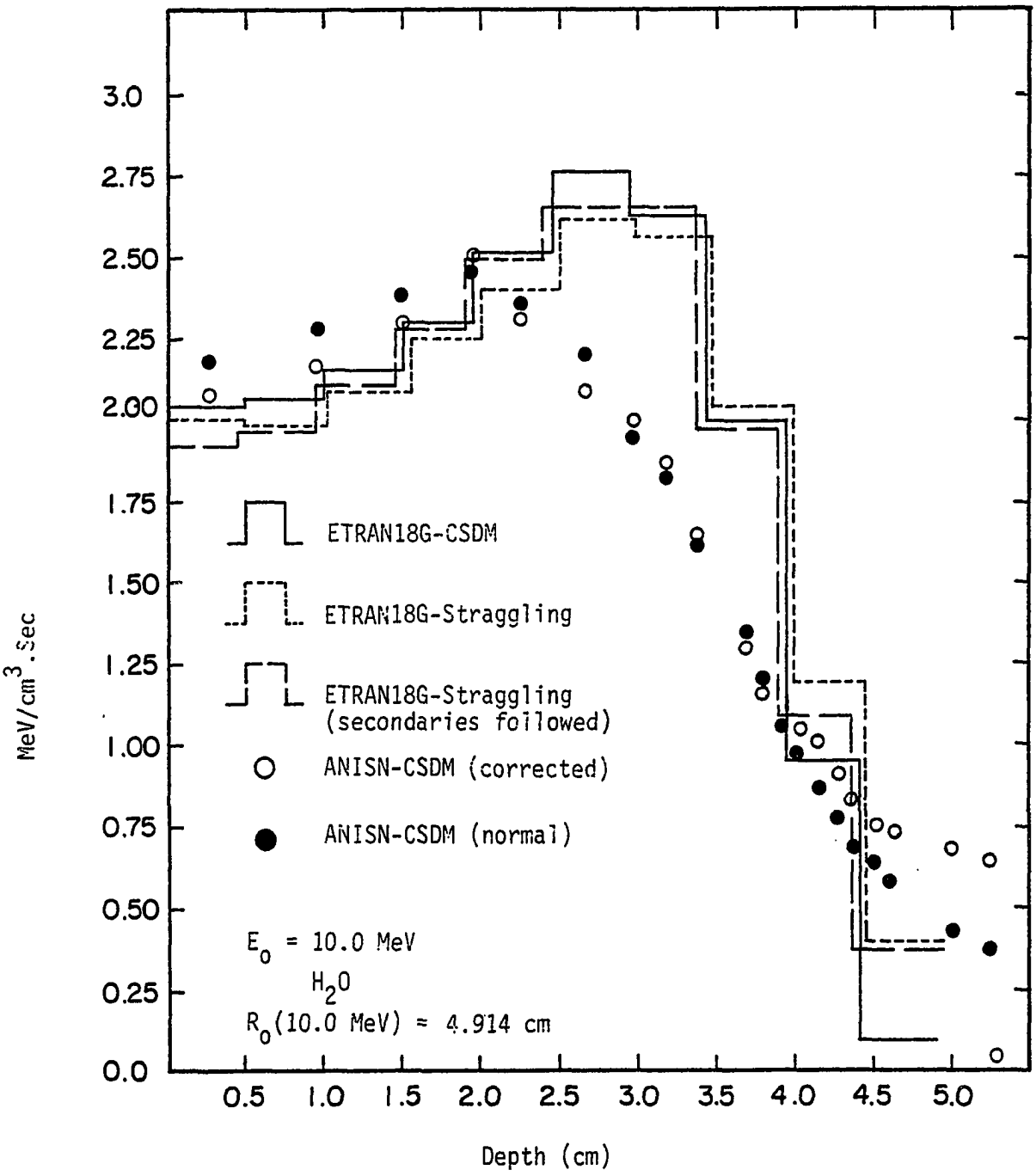

Figure (5.12): Total unnormalized energy deposition in H_2O.

Three ETRAN18G results are plotted in Figure (5.12) in addition to two ANISN-CSDM results. The ETRAN18G results may be described as: (a) The ETRAN18G-CSDM data represents the transport case where the energy losses of the primary particle are determined by the continuous slowing down model, (b) the ETRAN18G-straggling curve represents the transport case where some energy straggling has also been taken into account, and the secondaries are not followed, (c) the second ETRAN18G-straggling (the best ETRAN18G electron transport model) represents the transport case in which the secondaries are followed and the energy straggling is permitted. From Figure (5.12) it may be noted that all the ETRAN18G results have shown an energy deposition peak at about the same penetration depth. There is not a significant difference among the energy deposition distributions of the ETRAN18G results. This may mean that the particles behave similarly in the ETRAN18G calculational models because of the basic continuous slowing down model of the ETRAN18G calculational schemes.

Two ANISN-CSDM results are plotted in Figure (5.12). The curve denoted by the shaded circles represents the normal ANISN-CSDM result which has been produced by the standard model for the problem. Since this model does not include energy straggling (i.e., group skipping) and does not follow secondaries, an estimate of the effect of these may be useful. The ANISN-CSDM curve which is denoted by the unshaded circles represents an approximation of the ANISN-CSDM results

if the primary particle were permitted to undergo energy straggling and secondaries were followed. This ANISN-CSDM (corrected) curve may be taken as corresponding to the best ETRAN18G calculational model. It has been produced from the normal ANISN-CSDM result by adding an approximate correction. The magnitude of this correction is obtained from the corresponding ETRAN18G results on a point by point basis as shown in Figure (5.12), and then added to ANISN-CSDM result to produce the corrected ANISN-CSDM transport result. The corrected ANISN-CSDM result agrees relatively well with the best ETRAN result along the high and low energy edges of the energy deposition distribution. There exists a significant difference between ANISN-CSDM and the ETRAN18G results at depths of 2 to 4 cm. This difference must relate to the basic CSDM models for both techniques and will be explained in following paragraphs of this subsection. Other comparisons indicate further differences which will also be discussed.

In the ETRAN18G-CSDM electron transport model any spatial displacement of electrons in the medium must result in the deposition of energy predicted by the stopping power. That is, for a minimum distance traveled by an electron, Δx, equal to the depth at which the electron is found, the energy deposition must be at least equal to Δx times the stopping power. Greater energy deposition results from paths which are greater than the depth due to deflections caused by

intermediate scatters.

Other ETRAN18G models use this continuous slowing down model as their basis. For instance, in the ETRAN18G-straggling model (also called Class (II) by Berger (38)), the history of a particle is divided into sections. Each section is called a step and is terminated by a catastrophic collision. Since the energy loss in these collisions vary magnitude, they produce "energy straggling." Within the section the energy loss is determined by using a continuous-slowing-down-model approximation (see: Figure (2.1)). The particle then suffers an energy loss due to a catastrophic collision at the end of the step. The catastrophic collision energy loss is obtained by sampling from an energy loss distribution.

In Figure (5,12) we can see that this model difference does not significantly affect the result. In all ETRAN18G cases it can be seen that the energy deposition curve sharply decays beyond the peak and practically approaches zero. The ANISN-CSDM energy deposition result does not show such a sharp drop beyond its peak. This occurs because ANISN-CSDM does not require an energy loss in each spatial interval, but permits a probabilistic energy loss. When this loss occurs, it always has the value of one energy group width, and can be considered as a continuous slowing down model. It does not always occur, however, distinguishing it from the ETRAN18G continuous slowing down

model, which requires a minimum energy loss for all versions. The difference between the energy deposition curves (Figure (5.12)) of ANISN-CSDM and ETRAN18G comes from the energy loss models of these two electron transport calculational tools. The difference between the energy deposition curves has been justified by hand calculations in addition to the results given in Figure (5.12). Hand calculations have indicated that ETRAN18G models deposit about 5% more energy than ANISN-CSDM electron transport model at depths of 2 to 4 cm. For sufficiently thick slabs the total energy deposition predicted by the ANISN-CSDM and ETRAN18G must be the same.

The energy deposition at the surface of the slab (also called "surface dose") has been estimated by each calculational scheme by using the energy deposition in the first spatial interval. One should note that the true energy deposition at the surface of a slab should be essentially model independent. Each electron transport model should result in essentially the same energy deposition per unit volume at the surface of the slab; i.e., $x = 0$. The results which have been produced by the transport models shown in Figure (5.12) are tabulated in Table (5.2). One column of results gives the doses for the first spatial interval. An additional column gives results which are obtained by approximately correcting these to produce a true surface dose.

TABLE (5.2)

Surface energy deposition in water calculated by different electron transport models (see Figure (5.12)).

Calculational Model	MeV/cm^{3}sec. (first interval, Figure (5.12))	MeV/cm^{3}sec. (corrected to surface*)
ANISN-CSDM (normal)	2.18488	1.9896
ANISN-CSDM (corrected[1])	2.06	1.980
ETRAN18G-CSDM	2.04	1.910
ETRAN18G-straggling[2]	2.00	1.910
ETRAN18G-straggling[3]	1.910	1.910

(*) This means that the energy depositions in the first interval which are predicted by the calculational models are corrected to yield the energy deposition on the surface of the slabs. This may be done as follows: First find the magnitudes of the energy depositions at x = 0 by extrapolating the energy distribution curves which are given in Figure (5.12). These extrapolated values are not shown in Table (5.2). The ANISN-CSDM (normal) extrapolated data should then be corrected for "energy-straggling and following secondaries." It amounts to a 6.4% correction on the extrapolated ANISN-CSDM (normal) data. The ANISN-CSDM (corrected) data should not be corrected again, because it is obtained from the ANISN-CSDM (normal) data after "energy straggling and following secondaries" correction. The ETRAN18G-CSDM data should be corrected for "energy-straggling and following secondaries." This correction amounts to 6.4% of the extrapolated value of the energy deposition. The ETRAN18G-straggling(2) data, the fourth data from the top of the first column of Table (5.2), should only be corrected for the secondaries. This correction amounts to 4.5% of the extrapolated value of the energy deposition. The ETRAN18G-straggling(3) data need not be corrected, because it includes the

Table (5.2) (Cont'd)

effect of "energy-straggling and following secondaries."

[1]Corrected for energy straggling and following secondaries by comparing appropriate ETRAN18G results.

[2]Straggling is taken into account, but secondaries are not followed.

[3]Energy straggling is taken into account and the secondaries followed.

In Figure (5.13) the measured energy deposition (normalized to 100 at the peak) (59) and ANISN-CSDM results are given along with the three ETRAN18G results (also normalized to 100 at the peak). It may be observed again that all ETRAN18G transport results are essentially the same. The results for the "best" ETRAN18G model are joined by a solid line. In Figure (5.14) the simpler ETRAN18G models are excluded. One may observe that ANISN-CSDM agrees very well with the measured energy deposition. The best ETRAN18G result does not agree as well with the measured data, especially at the incident surface of the slab. This is not because ETRAN18G does not predict the surface dose accurately. As we have seen from Figure (5.12) and Table (5.2), ETRAN18G and ANISN-CSDM are in good agreement at the surface. The relatively large difference at the surface, which appears in Figure (5.14), occurs because the normalization peak predicted by ETRAN18G is higher than that predicted by ANISN-CSDM. The excellent agreement between the ANISN-CSDM normalized results and the measured values

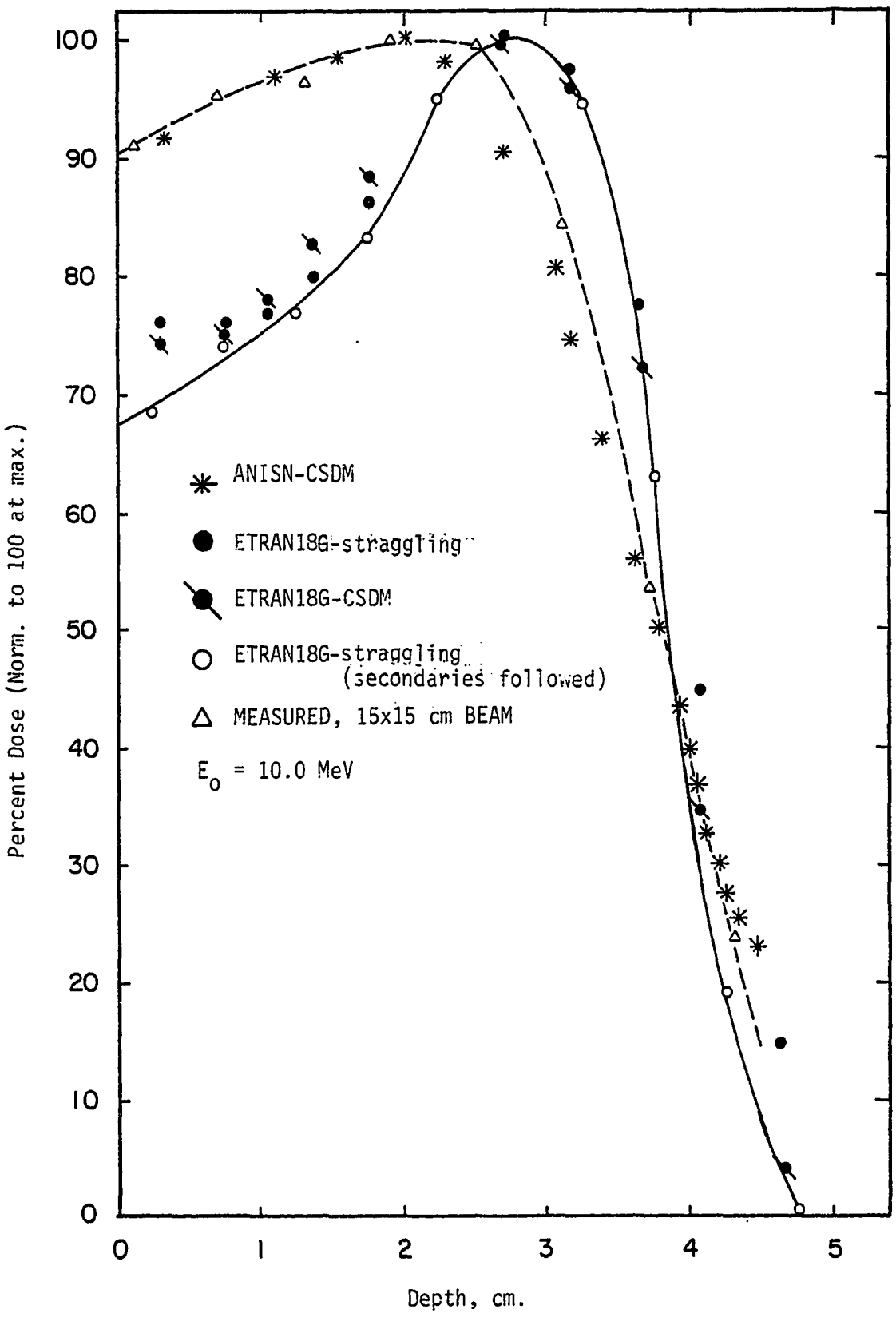

Figure (5.13): Normalized energy deposition in H_2O.

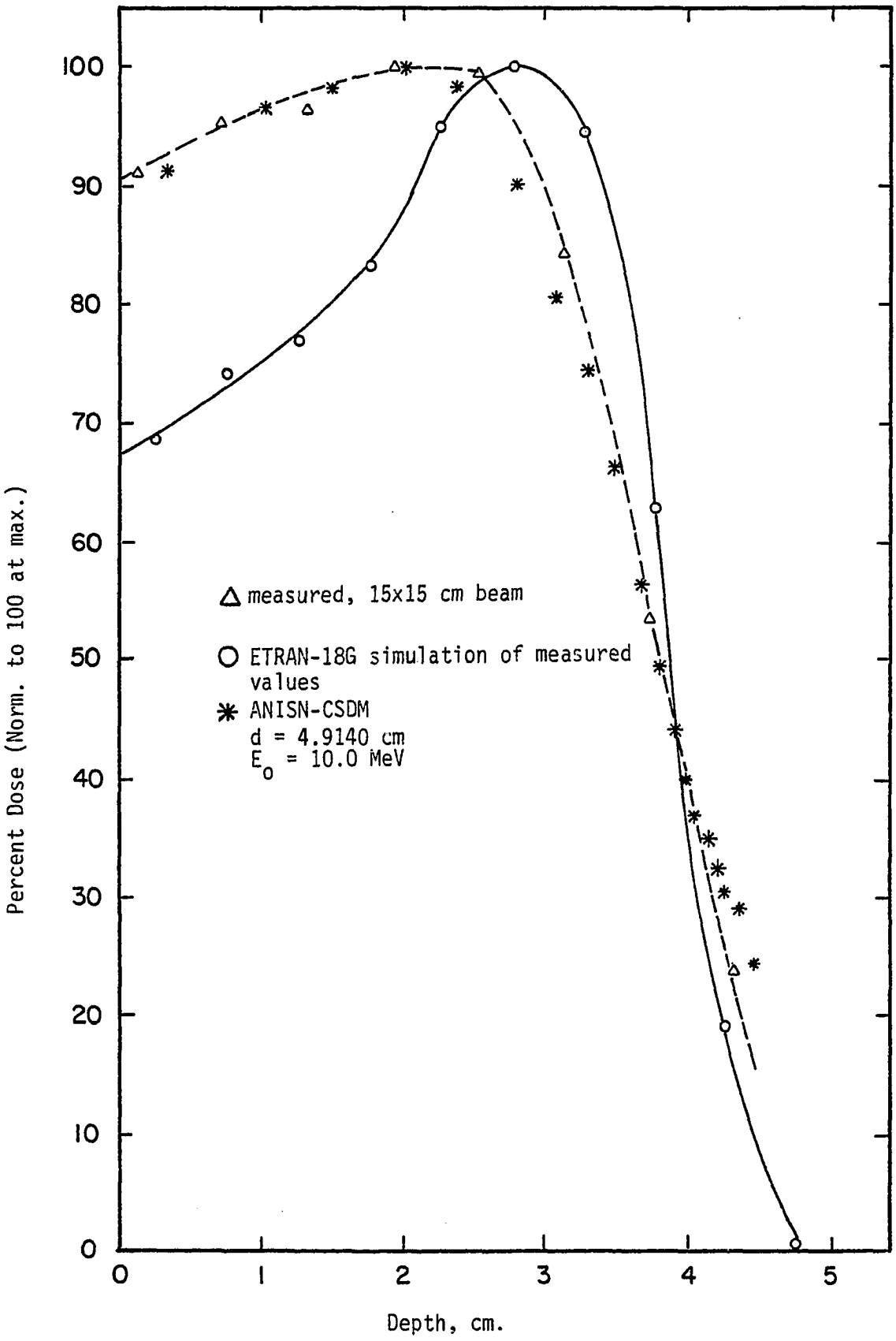

Figure (5.14): Normalized energy deposition in H_2O.

indicate that the ANISN-CSDM results are probably more accurate than those predicted by ETRAN18G.

Further analysis of the water transport results given in Figure (5.12) indicates that the ANISN-CSDM predicts slightly more energy deposition at the high energy edge of the energy deposition distribution compared to all ETRAN18G calculational models. This difference between the ANISN-CSDM and ETRAN18G (Monte Carlo method) becomes more significant in Figure (5.14) where the normalized energy deposition (percent dose) has been plotted over the full range of the incident particle. From Figure (5.14) it may be observed that the ANISN-CSDM result is in excellent agreement with the experimental data (59). In addition to the previous discussion, this good agreement between the experimental data and the ANISN-CSDM could also result from the fact that inelastic collisions are relatively accurately incorporated into the mathematical formulation of the expansion coefficients of energy transfer cross-sections. The energy loss collisions are properly redistributed in angle throughout the slowing down process of electrons. A new set of expansion coefficients has been generated for each energy group according to the average energy loss model of ANISN-CSDM. The angular effect of the inelastic collisions in ETRAN18G is approximately included in the multiple elastic scattering expansion coefficients.

In the previous paragraphs it has been observed that

the differences between energy deposition curves of ETRAN18G and ANISN-CSDM are probably caused by the energy loss-models of these electron transport schemes. This has been made clear by performing detailed transmission studies in water for slab thicknesses of 1.0 cm, 2.0 cm, 3.0 cm and 4.0 cm. The results of angular transmission studies are shown in Figures (5.15,5.16,5.17,5.18). From these figures it can be observed that the angular redistribution model of ETRAN18G-straggling is very close to ANISN-CSDM model. Then it may be concluded that the angular redistribution model of ETRAN18G is not the cause of the differences in energy deposition curves which are given in Figure (5.12).

The results of energy transmission studies in water for the same slab thicknesses are given in Figures (5.19, 5.20,5.21,5.22). From these figures it may be observed that ANISN-CSDM results show wider energy distribution of transmitted particles than ETRAN18G model. Also, the ETRAN18G model shows a sharper peak than the ANISN-CSDM model. These differences result from the fact that ETRAN18G employs a different energy loss model than ANISN-CSDM does. That is ETRAN18G has a partially deterministic energy loss model which is basically governed by the continuous slowing down model and ANISN-CSDM has a probabilistic energy loss model. These energy loss models were discussed in detail in the previous paragraphs. It is apparent that the probabilistic energy loss model is closer to reality than the ETRAN18G

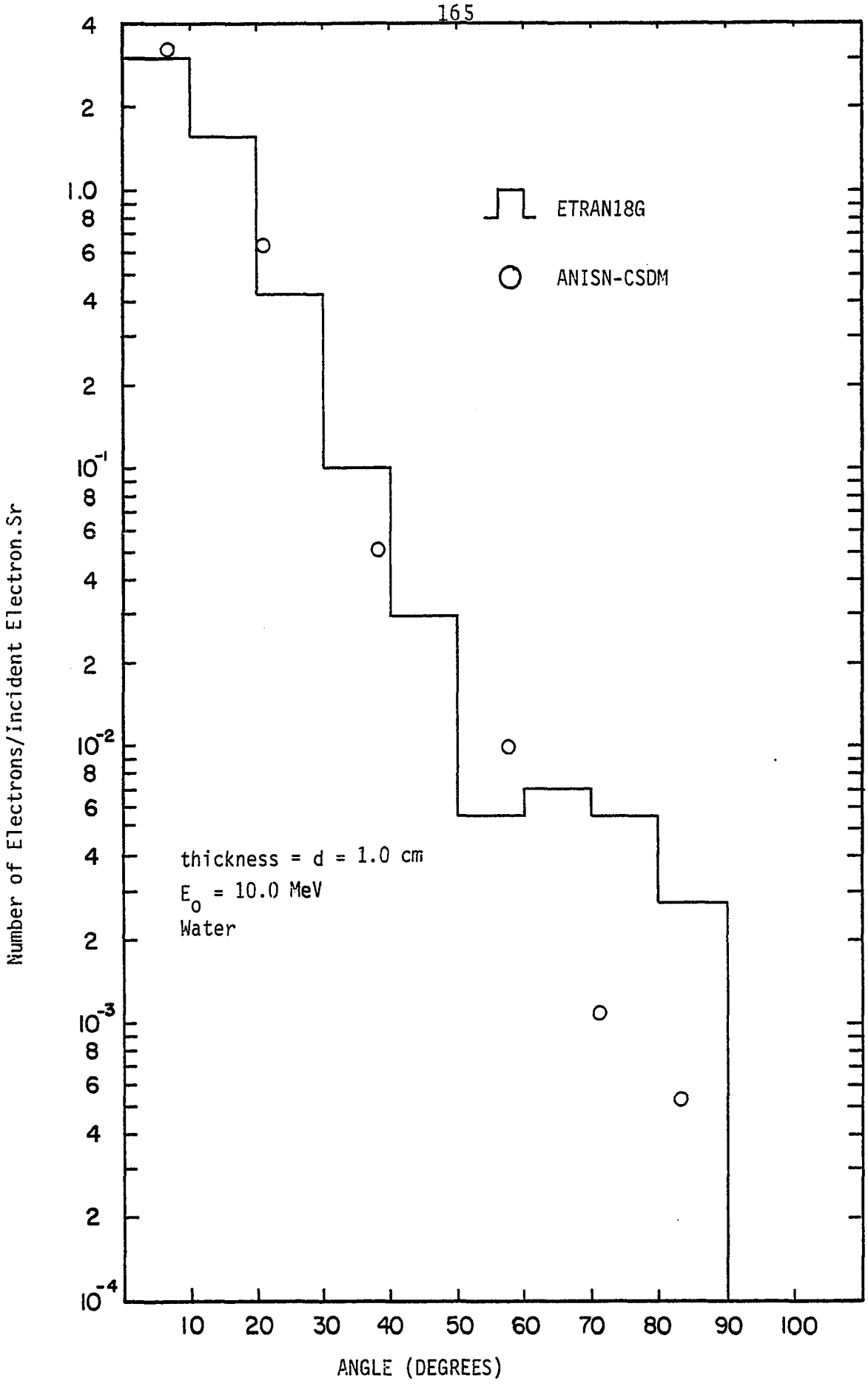

Figure (5.15): Angular distribution of transmitted electrons in H_2O(1.0 cm).

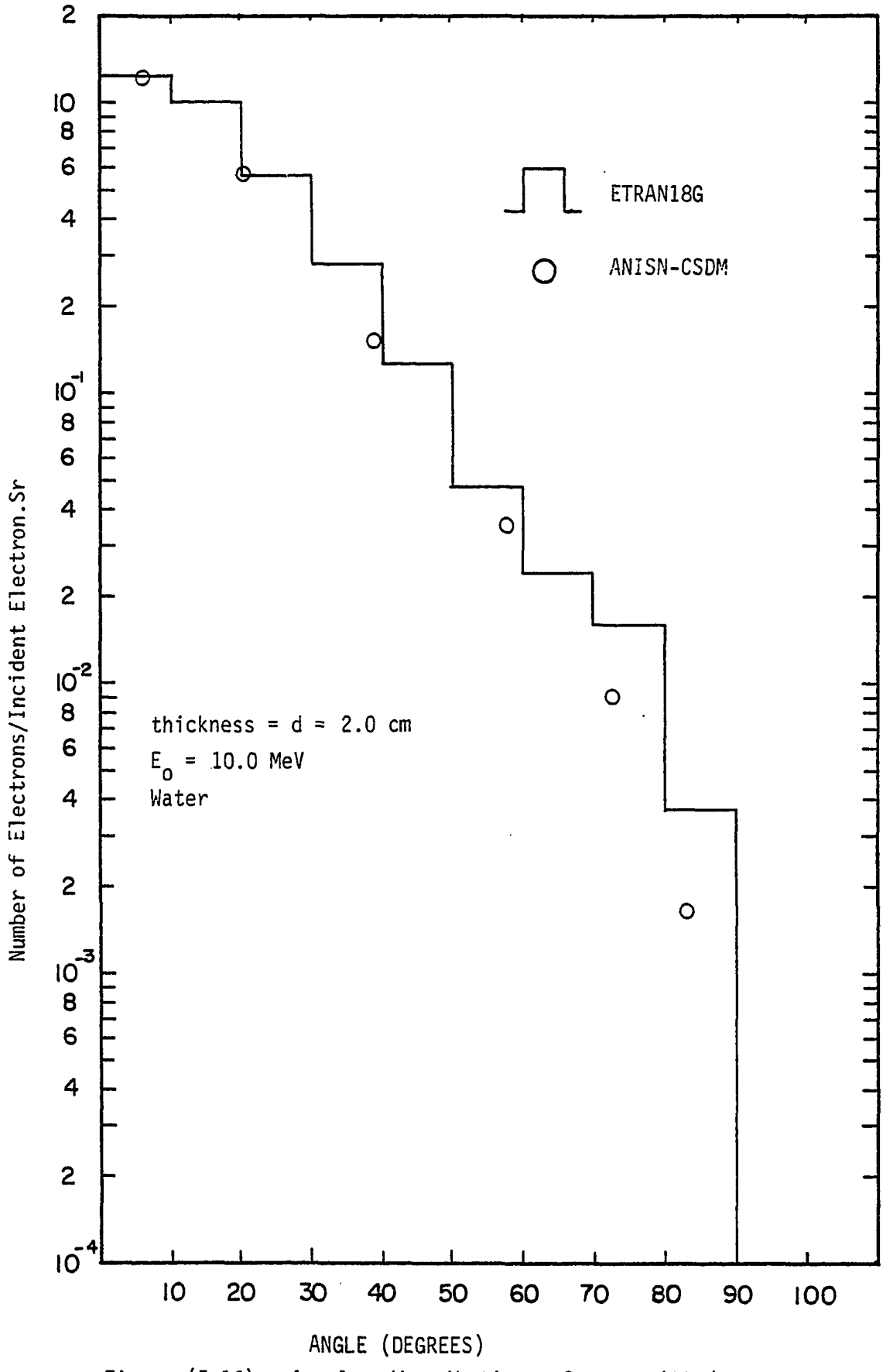

Figure (5.16): Angular distributions of transmitted electrons in H_2O(2.0 cm).

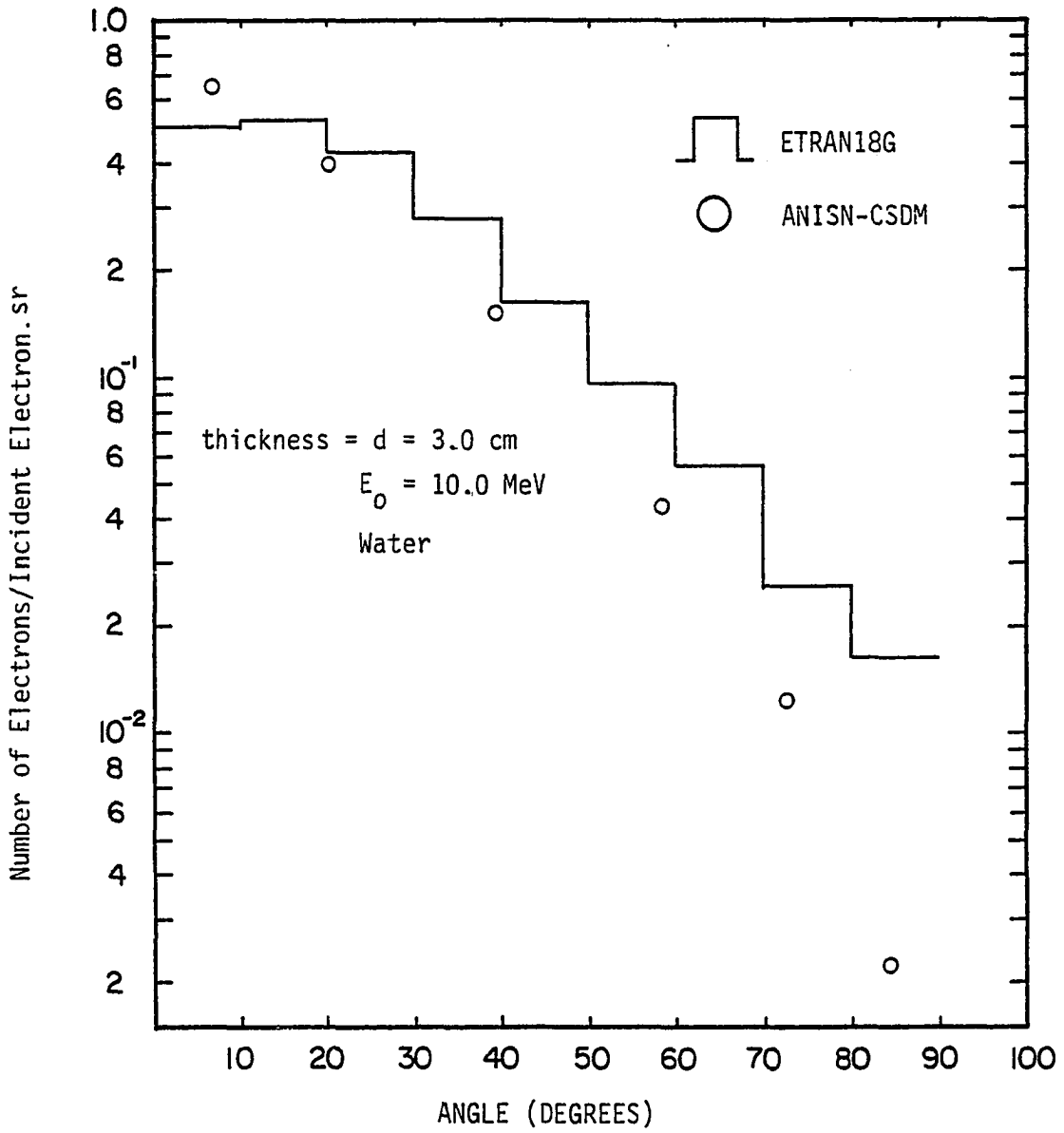

Figure (5.17): Angular distributions of transmitted electrons in H_2O(3.0 cm).

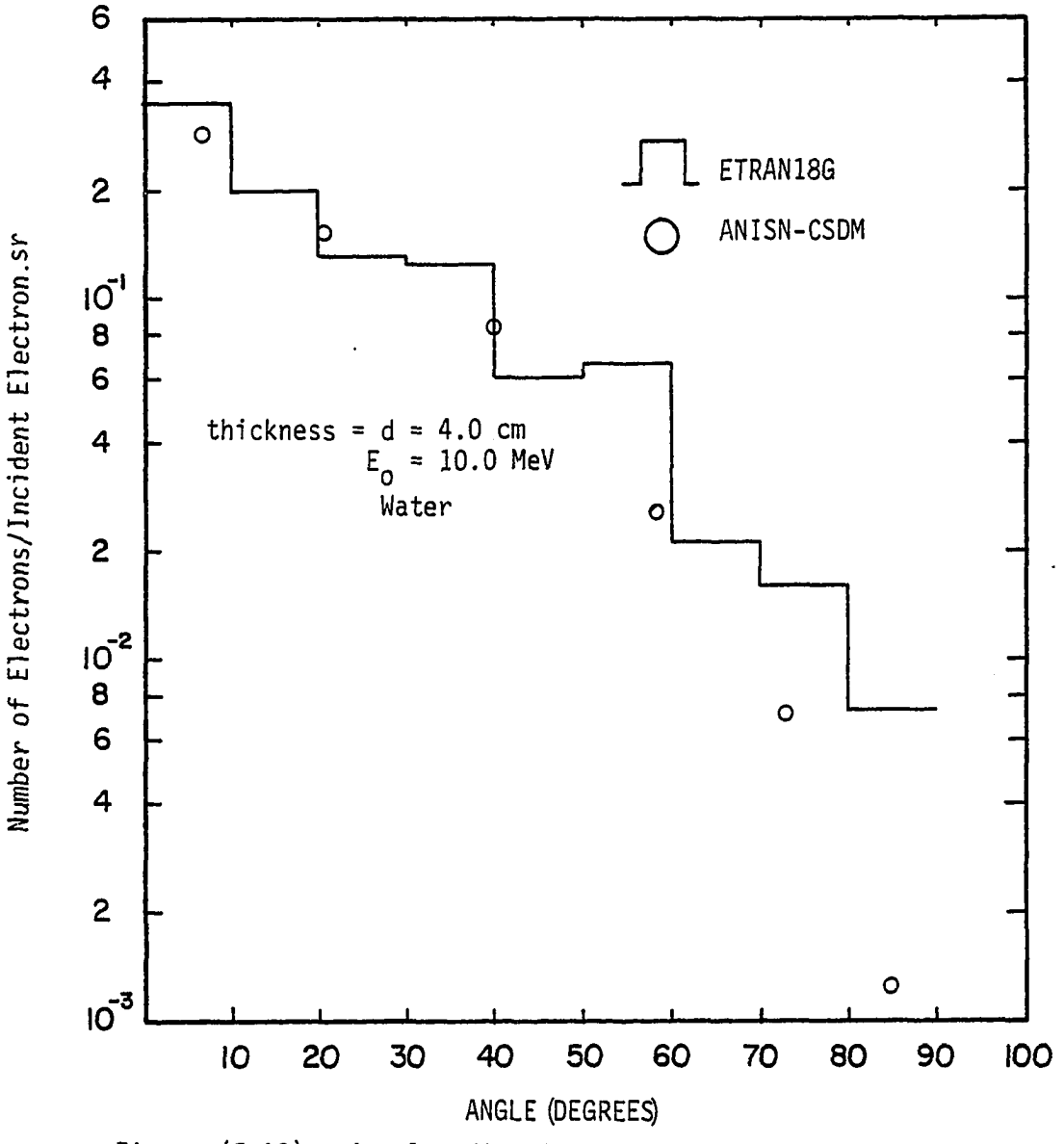

Figure (5.18): Angular distribution of transmitted electrons in H_2O (4.0 cm).

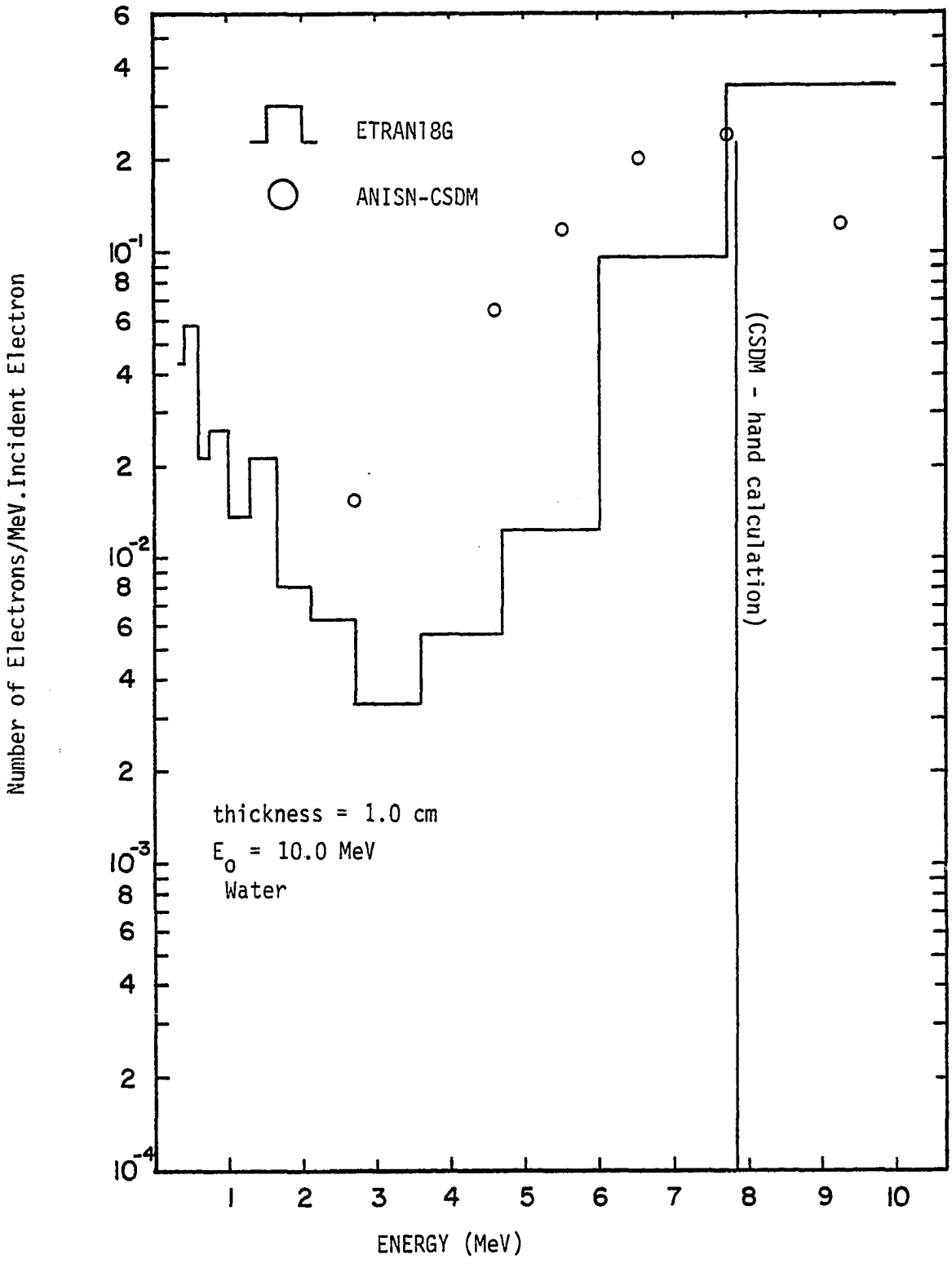

Figure (5.19): Energy distribution of transmitted electrons in H_2O (1.0 cm).

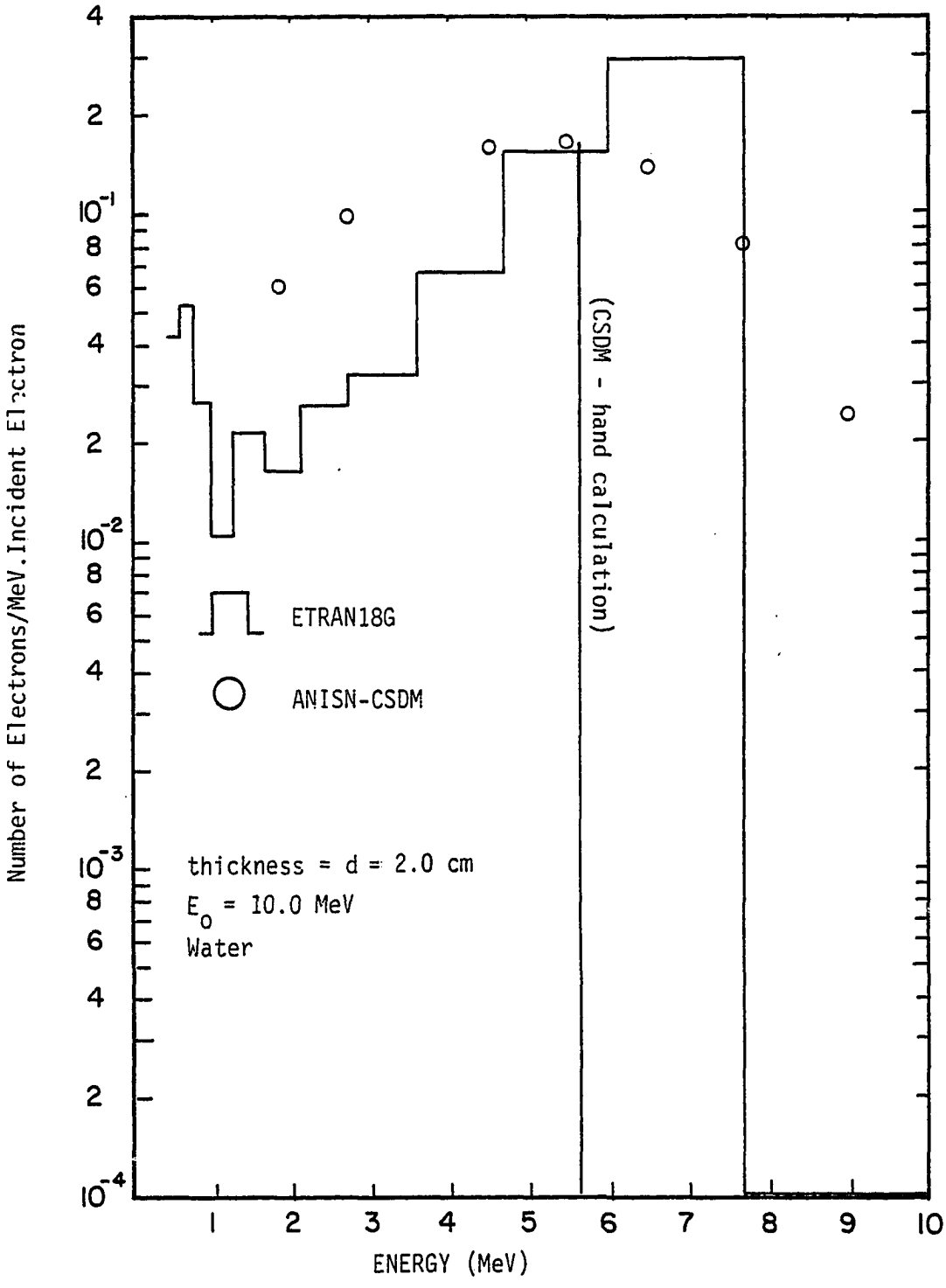

Figure (5.20): Energy distribution of transmitted electrons in H_2O (2.0 cm).

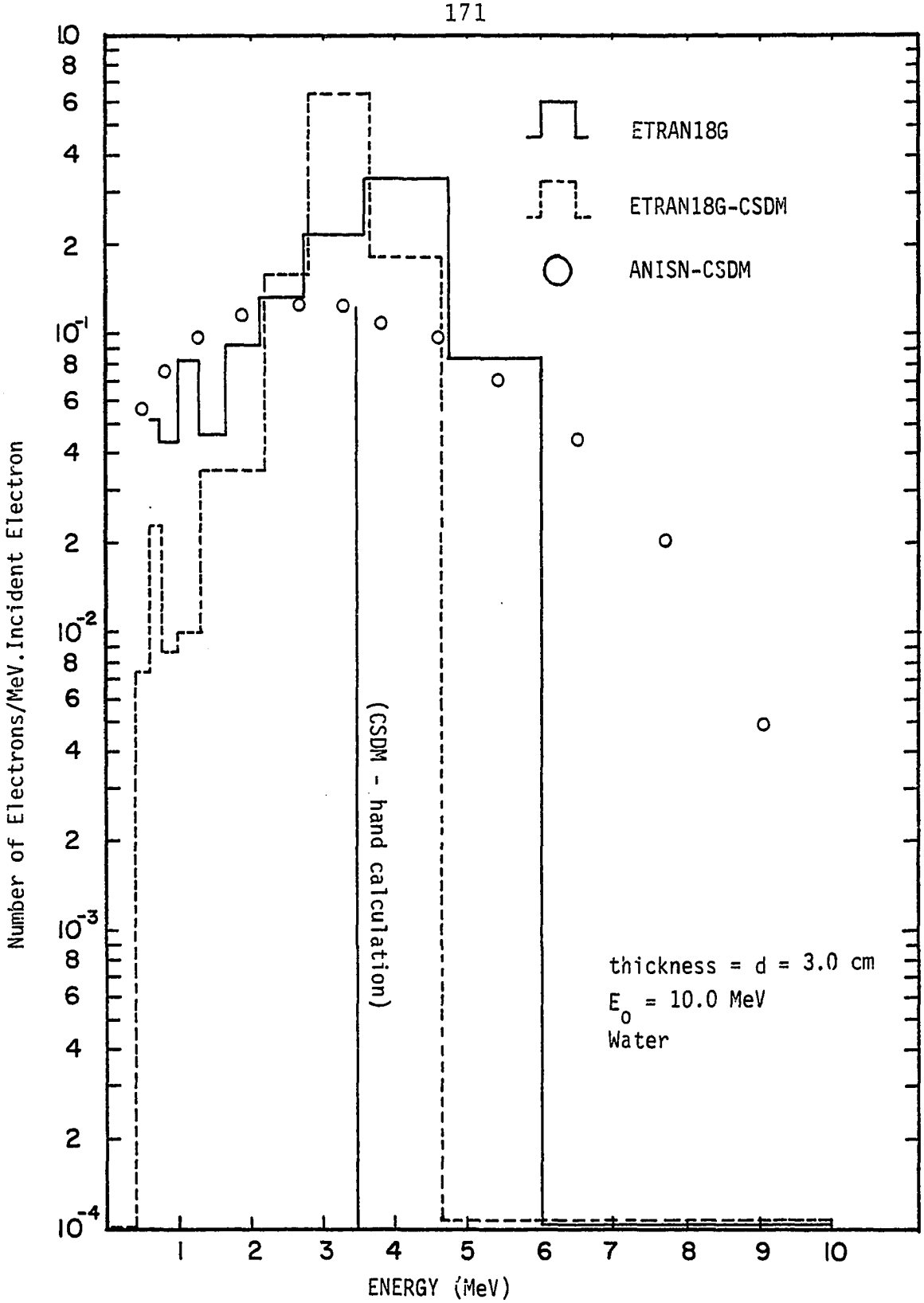

Figure (5.21): Energy distribution of transmitted electrons in H_2O (3.0 cm).

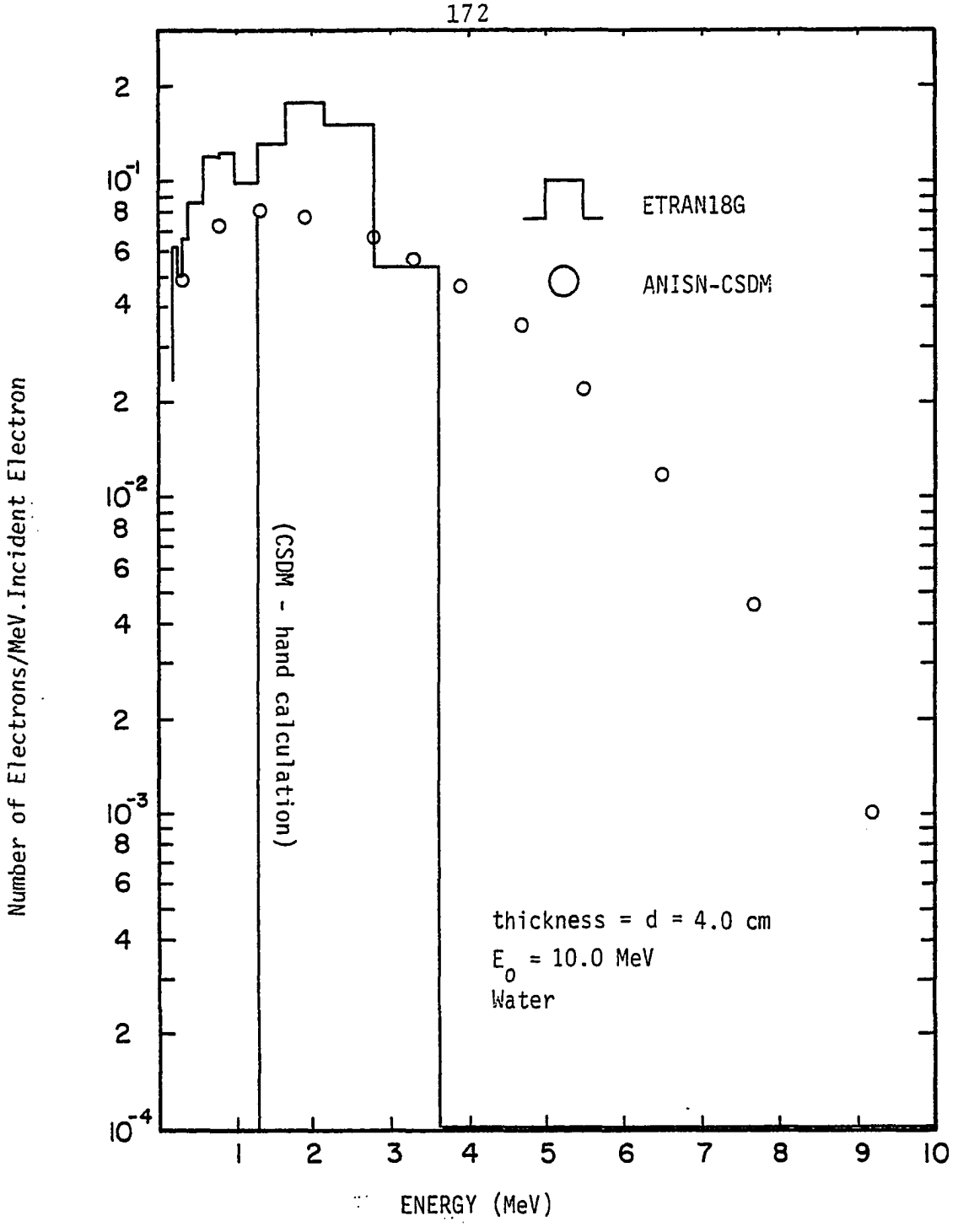

Figure (5.22): Energy distribution of transmitted electrons in H_2O (4.0 cm).

continuous slowing down model of energy loss and the energy deposition differences result from this difference in models.

The energy distribution result of transmitted particles by ETRAN18G-CSDM is also given in Figure (5.21). From this figure it may be seen that ETRAN18G-CSDM result shows a narrower energy distribution at a lower energy than ETRAN18G-straggling model. This could come from the fact that ETRAN18G-CSDM has a completely deterministic energy loss model, but ETRAN-straggling has a partially deterministic energy loss model. That is, ETRAN18G-CSDM uses an energy loss model so that energy-loss fluctuations are disregarded, and the energy loss by collisions is predicted by the stopping power expression. ETRAN18G-straggling model computes some of the energy losses, by sampling from a distribution, but the deterministic part of the calculation requires a minimum energy loss.

The further analysis of Figure (5.21) indicates that the energies of front (high energy) edges of calculational models decrease in the order of ANISN-CSDM, ETRAN18G-straggling, ETRAN18G-CSDM and CSDM-hand calculations. That is, ANISN-CSDM has the highest front edge energy and CSDM-hand calculations has the lowest. The two ETRAN18G results fall in between these two upper and lower front edge energies where ETRAN18G-straggling has higher front edge energy than ETRAN18G-CSDM. This difference between the front edge

energies could be explained as follows: The CSDM-hand calculations represent a transport case in which the energy loss is determined directly from the knowledge of stopping power at initial energy and the depth, 3.0 cm. In ETRAN18G-CSDM corrections are applied to account for varying path lengths in reaching a depth of 3 cm while producing the energy loss predicted by stopping power. This can be called angle straggling and results in a smaller minimum energy loss, as represented by the front edge for this case. In the ETRAN18G-straggling case, the particle loses its energy in two parts. In the first part, the energy loss is due to CSDM of energy loss, and the second part is due to a probabilistic energy loss mechanism. It seems that the energy loss due to CSDM constitutes the major energy loss in the energy range considered. Here, angle straggling also occurs. In ANISN-CSDM the energy loss of a primary particle is entirely determined by a probabilistic process. In Figure (5.21) the width of the distribution is somewhat a measure of the fraction of energy loss which is determined probabilistically. In ANISN-CSDM the energy loss is totally determined based on probabilistic interactions, and therefore the energy distribution is wider than other reported results. The next wider energy distribution is predicted by ETRAN18G-straggling because only a fraction of energy loss is determined by sampling (probabilistic). ETRAN18G-CSDM does not include any energy straggling, relating energy loss directly to path

length. A distribution results, however, because scattering produces different path lengths (angle straggling). The CSDM-hand calculation result does not show a distribution because it does not include either angle or energy straggling. The CSDM-hand calculation result is indicated by a solid line whose height is about the height of ANISN-CSDM. It is shown so just for convenience. In fact, the solid line has an infinite height. The CSDM-hand calculation results are given in Figures (5.19,5.20,5.22) in solid lines also. Each of these solid lines has the same interpretation. That is, it represents the energy distribution of a primary particle at the designated depths without any angle deflection or energy variation attached to the primary particle. These solid lines may also be called "stopping power model-hand calculations."

The analysis of Figure (5.21) indicates that a greater degree of probabilistic energy losses in ETRAN18G could result in a wider energy distribution of transmitted particles and would produce results more nearly matching experiments and in substantial agreement with ANISN-CSDM.

b. 1.0 MeV Electrons Normally Incident on an Aluminum Slab

The total and normalized energy depositions in an aluminum slab of thickness 0.32 gm/cm^2 as a function of depth are given in Figures (5.23 and (5.24) respectively. The results are produced by ANISN-CSDM and the ETRAN18G-straggling calculational models. The purpose of this ANISN-CSDM

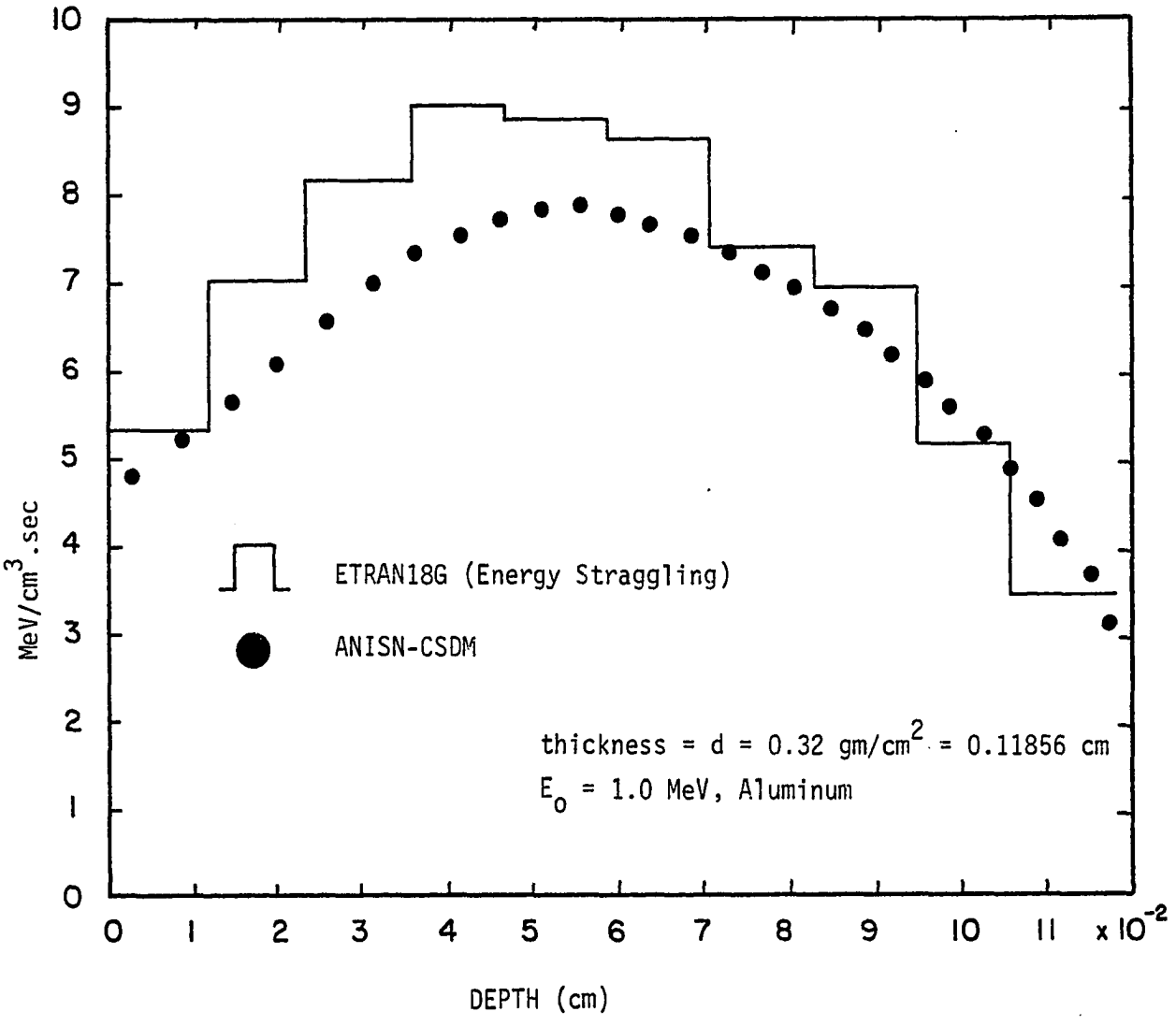

Figure (5.23): Unnormalized energy deposition in Al.

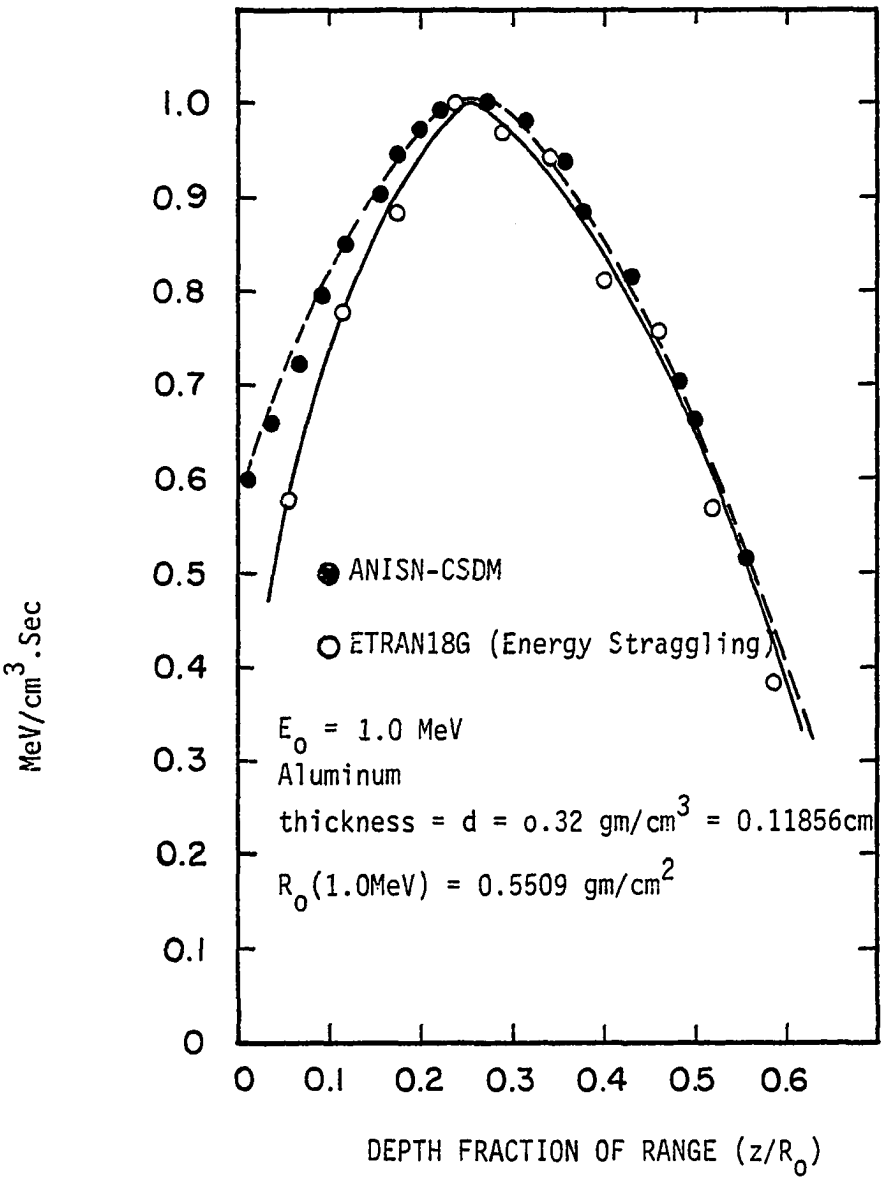

Figure (5.24): Normalized energy deposition in Al.

result is to justify the accuracy of the method in a low Z transport medium with relatively low energy electrons and to observe if there is a similarity between normalized energy deposition curves of water and aluminum and as a companion to the aluminum transmission results. The ANISN-CSDM transport result is compared with the best ETRAN18G model. From Figures (5.23,5.24) it may be seen that the transport results are in reasonable agreement. As in water, the ETRAN18G-straggling model shows a slightly higher energy deposition peak compared to the ANISN-CSDM result. As discussed in the previous subsection, this happens because of the energy loss model of ETRAN18G-straggling. In this energy loss model of ETRAN18G, the primary particle loses some finite energy per step deterministically, but ANISN-CSDM has a completely probabilistic energy loss model. Near the peak of the total energy deposition curve, Figure (5.23), ANISN-CSDM predicts slightly less energy deposition compared to the ETRAN18G result. This may occur because the continuous slowing down part of the energy loss mechanisms in ETRAN18G-straggling predicts again require energy losses, distorting the energy spectrum as slowing-down proceeds. In general, the small differences between ANISN-CSDM and ETRAN18G energy deposition curves are not significant compared to the differences for water, where the incident energy was much greater (10.0 MeV rather than 1.0 MeV). The greater differences which occur with gold for 1.0 MeV electrons must therefore be

related to the greater Z.

The ANISN-CSDM electron transport model has been tested in three different transport mediums. These test calculations include low energy and relatively high incident energy electrons and high Z and low Z mediums. Comparisons with experimental values have been made where available. For low energy and low Z (aluminum) results from ANISN-CSDM agree very well with ETRAN18G and experiment. For high energy and low Z (water), ANISN-CSDM agrees very well with experiment, while ETRAN18G does not. With low energy and high Z (gold), ANISN-CSDM does not agree with experiment as well as some ETRAN18G results. These comparisons will be discussed further in the following chapter.

As a final remark it may be noted that at the very high initial energies the energy loss by a primary particle does not correspond exactly to the rate of energy absorption at local points. This happens because of the following facts: (i) the energies of the secondary electrons can be high enough so that they do not necessarily dissipate their energy around the local points where they are produced. They rather dissipate their energy at a slightly greater depth in the transport medium, (ii) secondary photons (neutral particles) may be highly energetic so that they can travel large distances before they deposit their energy. Both of these phenomena may result in slightly different energy distributions in a transport medium if the energies

of the secondary particles are not negligible. The future development of the present ANISN-CSDM should be in this particular area. The critical energies where the collisional energy loss becomes equal to bremsstrhlung photon production energy loss of water, aluminum and gold are about 80 MeV, 50 MeV and 10 MeV respectively. The present calculations are much below the critical energies, and photon productions may not affect the angular redistribution of the primary particles nor the energy deposition distribution in the transport mediums.

The characteristic data for the discrete ordinates calculations which have been performed in this chapter are given in Table (5.3). From this table it may be observed that ANISN computing time increases remarkably in parallel with number of spatial intervals. Similarly ETRAN18G (straggling) computing time goes up as the slab thickness becomes larger. This is equivalent to having more spatial intervals in ANISN calculations. In the ETRAN18G calculations reported in this work, 1000 initial electrons (histories) were used. This was generally sufficient so that statistical differences were smaller than other observed differences and could be excluded from the comparisons.

TABLE (5.3)

Characteristic data for the Discrete Ordinates Calculations (ANISN)

Figure#	Order of Scat.	Order of Ang.Quad.	#Spatial intervals	#energy groups	CPU Time (minutes) ANISN	ETRAN18G
Figure (5.4)	96	48	9	85	9.	2.31
Figure (5.5)	96	48	19	85	20.	4.06
Figure (5.6)	96	48	29	85	30.	5.10
Figure (5.11(a))	39	48	7	61	4.16	6.42
Figure (5.12)	73	48	33	30	13.06	8.54
Figure (5.15) Figure (5.19)	73	48	3	30	3.23	3.16
Figure (5.16) Figure (5.20)	73	48	5	30	3.48	4.28
Figure (5.17) Figure (5.21)	73	48	8	30	8.55	5.57
Figure (5.18) Figure (2.22)	73	48	14	30	12.11	7.56

CHAPTER VI

DISCUSSION OF THE RESULTS

The computer code ANISN is a one-dimensional S_N transport theory code with general anisotropic scattering. It can be used to produce transport results (fluxes and reaction rates) in the analysis of the nuclear systems. In this work the standard ANISN computer code, intended for use with neutrons and gamma rays, has been used to produce electron transport results for different transport mediums. The types of problems which have been solved are: the scalar flux solutions in thin aluminum slabs, transmission through relatively thick aluminum and gold slabs, and energy deposition in thick aluminum and in water slabs whose thickness is greater than the range of the incident particle. No discrete ordinates method (DOM) results have been previously reported for electron transport problems in which the slab thickness is comparable to the range of the incident particle.

The electron transport problem represents a numerically difficult case. The scattering cross-sections are very large. With large ingroup scattering cross-sections convergence of the iterated solution becomes very difficult and fine spatial mesh is needed. Since the scattering is highly forward

peaked, it requires many terms to accurately represent the angular behavior of cross-sections and fine angular mesh to represent the transport behavior. As a result of this, deep penetration radiation transport problems require extremely large computer time and storage compared to that required for other transport problems. For practical engineering calculations, one must remove some of these difficulties in order to reduce the problem size to a manageable level and also produce good transport results. The extended transport corrected cross-section concept was introduced in Chapter (IV) to reduce the expansion order of highly forward peaked elastic scattering cross-sections. The use of a single average inelastic scatter per spatial interval reduces the order of inelastic scattering while increasing the energy group width and spatial width. It is still necessary to use fine meshes in the angular variable in order to represent the highly forward scattering nature of the electron interactions. It might be possible to use asymmetrical quadrature sets in the S_N calculation of highly forward peaked transport cases. The details of this formulation may be found in the literature (58). In this study a standard symmetrical S_{48} Gaussian angular quadrature set has been used. A unit shell source which is incident normally on the slab face at $x = 0$ is also represented in this set, and was input into the discrete direction nearest the axis.

The ANISN-CSDM (ANISN-Continuous Slowing Down Model) of electron transport which has been developed in this work is a "one collision model" in terms of both the elastic scattering and inelastic scattering. The choice of the spatial interval size is similar to that of the condensed random walk concept as used in the ETRAN codes. In general, the spatial interval size in ANISN-CSDM is chosen to be equal to the effective elastic or inelastic mean-free-path of the primary particle. Since the mean-free-paths implied by the model are greater than in other DOM models (smaller cross-sections), larger spatial intervals can be used. There exists a one-to-one relationship between the average energy losses and the corresponding spatial displacements in the process of slowing-down the primary particle in the transport medium. Thus proper spatial interval widths may be chosen through the η value in a way that the overall core storage requirement of the problem may be reduced to a manageable size. It has been found that such a concept is very useful for high-energy electron transport such as in the comparison calculations made for water. Thus, the ANISN-CSDM is capable of producing very good electron transport results for high initial electron energies with relatively large energy and spatial intervals. Comparison of these results in water with experimental results have shown that ANISN-CSDM produces results which are closer to measured energy deposition

distributions than those produced by the best ETRAN18G model. As it was discussed in the previous chapter, the difference between results of ANISN-CSDM and ETRAN18G occurs because each transport technique uses different energy loss models. The ANISN-CSDM employs a probabilistic energy loss model which results in wider energy distribution at any depth in a transport medium. The ETRAN18G models employ partially deterministic energy loss models. Therefore it results in narrower energy distribution than ANISN-CSDM at any depth. In ETRAN18G the probability of passing a spatial interval without losing energy is zero. This comes from its partially deterministic energy loss models. This is a significant distinction between the two electron transport techniques. In general, ANISN-CSDM and the ETRAN18G results differ in the predicted energy deposition distributions in water at relatively high initial energies. The ANISN-CSDM results probably agree better with measured energy deposition because the energy loss model is closer to reality than the ETRAN18G energy loss model. The comparison of absolute energy deposition in water by the two methods is given in Figure (5.12). The peak value of the energy deposition in the ETRAN18G models is higher than the peak value predicted by ANISN-CSDM. Therefore, the normalized energy deposition curves, Figure (5.14), show a significant difference at the incident surface. However, such a difference is not noticeable in the total corrected energy deposition curves as given in Figure (5.12).

In addition, the normalized ANISN-CSDM results, as given in Figure (5.14), agree very well with the experimental results of Anderson (59). The ETRAN18G results, since normalized to the large predicted peak, do not agree as well. Note that the high energy (10.0 MeV) electron transport in water represents a transport problem in which the energy deposition distribution as a function of the penetration depth is being investigated.

The transmission studies (with 1.0 MeV electrons) in aluminum slabs of various thicknesses with identical initial boundary conditions have shown good agreement with the experimental results. One may note that in the transmission studies the basic desired transport result is the energy distribution of the emerged primary particle at the right boundary of the slabs whose thicknesses are chosen to be less than the range of the incident particle. In transport results which have been produced in this study, a variable η has been employed. The value of η ranges from $46 \times I$ to $6 \times I$ in the transmission studies of the aluminum slabs for all different thicknesses. The ANISN-CSDM also employs a variable energy group width. It uses a variable η value which decreases in magnitude as the primary particle slows down to low energies where energy group widths also decrease. The energy group size and the magnitude of η decrease similarly as transport proceeds to lower energies. The η is a

critical parameter in the sense that efficient deep radiation transport results may be produced by choosing its magnitude appropriately. The accuracy of the results may also be improved by small η values. The magnitude of the η determines the total number of spatial intervals in the ANISN-CSDM for electron transport. It has also been observed that the transport results which have been produced by the ANISN-CSDM do not strongly depend on the spatial interval size. The ANISN general guideline suggests that one collision of each type per spatial interval be used for the ANISN-CSDM; but the total number of spatial intervals can be reduced approximately by a factor two and still produce nearly the same transport results. The reduction of the total number of spatial intervals means that there will be more than one collision of each type per spatial interval because the spatial interval sizes become larger, while the slab thickness remains the same. The manageability of the electron transport problem size should always be kept in mind, especially for deep penetration radiation transport problems. For codes which do not use a multiple scattering approximation, too many spatial intervals may be required to get detailed transport results. The ANISN-CSDM like ETRAN18G models, can alleviate this difficulty. For example, the $d = 0.32$ gm/cm^2 aluminum transport case requires 52 spatial intervals. Essentially the same electron transport results

have been produced by 29 spatial intervals. Corresponding calculation which was performed by Bartine et al. uses over a hundred of spatial intervals. It is preferable to produce electron transport results with the normal guidelines of the problem if possible. Complete expansion of the cross-sections should be included in the standard calculations. One can still produce acceptable transport results after reducing the expansion order of the in-group scattering cross-sections, using the extended transport correction. This reduces the computing time significantly. This idea has been successfully tested in the 10.0 MeV electron transport calculations in water. The electron transport results before and after application of the reduction of expansion order of in-group scattering cross-section remain the same. The same idea was also applied successfully to one-group electron transport calculations to simulate some selected results of Morel (8).

A parametric study of η in gold indicates that the transport results which are produced by the ANISN-CSDM are not strongly dependent of the magnitude of η. This observation confirms the validity of the mathematical model which has been used to produce the energy-loss cross-sections and angular expansion coefficients. This occurs because the cross-sections are corrected for the energy losses less than η which had been excluded from the average energy loss calculation of ANISN-CSDM. The result of energy distribution of

the transmitted particles in gold has indicated that ANISN-CSDM relatively overestimates the peak value of the distribution. It is not clear why this occurs; but some related observations and comments may indicate possible causes. ANISN-CSDM and ETRAN18G are in general agreement with experimental leakage from thin aluminum slabs. Inelastic angular distributions are the same for aluminum and gold, but elastic distributions are less forward for gold. As a result, gold leakage for the same relative slab thickness should be less than aluminum leakage. This is seen by the experimental result and by the results of both codes. ANISN-CSDM, however, predicts somewhat greater leakage from the gold slab than does ETRAN18G, and more than is seen from experiment.

In the test calculations of gold, it has been observed that reasonably good transport results could be obtained by using wider inelastic distributions in place of the inelastic distributions implied by the present model, ANISN-CSDM. That is, inputting wider distribution of the inelastic expansion coefficients to cross-section matrices could reduce the magnitude of the peak of transmitted particles.

Another contributing factor might be the approximation by which small angle inelastic scatters are excluded. These would also result in small energy deposition. This deposition is not excluded, however, since the total energy loss in small energy transfer collisions (less than η) is included in the overall inelastic cross-sections. That is, the

macroscopic inelastic cross-sections are represented by using the total correct stopping power (the sum of total collisional and radiative stopping powers) as given by equation (3.23). The energy loss actually occurring in small angle scatters is thus represented by a few larger angle scatters. The remaining small angle scatters do not occur, allowing continuing forward motion. The combined increase of a few large-angle scatters and reduction in small-angle scatters may produce a more forward transport approximation. This may presumably result in more leakage in thin slabs, as given in Figures (5.11(a), 5.11(b)).

A further angle approximation is the use of angular distributions of scattered electrons, each with the same energy loss. This can be considered as a separation of variables. That is, the same energy loss (an average model energy loss takes the primary particle from the energy group g to g+1) is assumed for all possible inelastic collisions whether the angle change is small (associated with small energy transfer collisions) or large (associated with large energy transfer collisions). This insufficient angle-energy correlation in ANISN-CSDM may be improved by using the Group Skipping Model of electron transport (which was discussed in Chapter (IV)), because in this model angle-energy correlation is represented more accurately than in either the ANISN-CSDM or the ETRAN18G models.

In addition, in thin slabs a primary particle in this

model may not make sufficient elastic or inelastic collisions so that they could reduce the peak of the transmitted particles at the right boundary of the slab. It appears that in a thin gold slab transport results are biased in favor of more forward collisions, thereby overestimating the leakage of particles.

While the ANISN-CSDM may be improved to give better results with high Z materials, the remainder of the simulation calculations using ANISN-CSDM have been observed to agree very well with the available experimental results. Therefore, it seems that the ANISN-CSDM average energy loss model adequately represents the physical reality for some important cases.

The ANISN-CSDM model of electron transport includes a deflection operator for the small energy transfer collisions, because the energy loss of small energy transfer collisions is represented by the model energy transfer collision in each energy group. That is, the small energy transfer collisions are replaced by the large energy transfer collisions. From the results of parametric study of η in gold, it may be observed that attaching a deflection operator to the small energy transfer collisions of Bartine et al. would further broaden the distribution of scattered particles and would probably decrease the magnitude of the peak instead of increasing it. It seems that the deflection operator which was suggested by Ligou (9) for small energy transfer

collisions (discussed in Chapter (II)) may not improve the magnitude of the peak in the Bartine et al. work, but rather reduce the leakage, making it further from the experimental result.

In summary, the ideas of the ANISN-CSDM basic data are analogous to the Monte Carlo calculational data. The ANISN-CSDM cross-section matrices are basically more consistent in terms of the energy conservation according to the squashed collision energy loss model. The ETRAN18G angular treatment is treated entirely through the continuous slowing down model interactions by a Legendre expansion of the elastic scatters. This is then corrected to include the effect of inelastic scatters. The ANISN-CSDM electron transport model appears to conform more closely to reality because it treats elastic and inelastic angular effects separately. The angular transmission studies indicate that there has not been any significant difference in the angular information (except gold) which has been produced by both of these electron transport schemes as a result of the difference in approximation methods. However, it was noted that the ANISN-CSDM has a probabilistic energy loss model, and the ETRAN18G has a partially deterministic energy loss model through continuous slowing down. This difference in the energy loss models can be observed from the results of the energy transmission studies in water slabs at relatively high initial energies.

In general, the results of ANISN-CSDM simulation

calculations have indicated that the ANISN-CSDM may be used as an alternate tool to other available electron transport codes in producing good electron transport results at relatively high electron energies.

CHAPTER VII

CONCLUSIONS AND RECOMMENDATIONS

In this study a Continuous Slowing Down Model of electron transport, ANISN-CSDM, has been developed for use in the one-dimensional discrete ordinates computer code ANISN. This model could be applied to transport of other charged particles, provided that the required average properties of the model and the correct stopping power could be evaluated in order to formulate the associated elastic and inelastic cross-sections. The accuracy and the generality of ANISN-CSDM have been demonstrated by comparing the calculations with the available experimental results and the Monte Carlo calculational models. The ANISN-CSDM transport results which have been produced for comparisons were performed under three separate groups of calculations as discussed in the following paragraphs.

The first part of the calculations has been performed to demonstrate the validity of the multiple elastic scattering approximation. This included tests of the extended transport corrected cross-section concept. The results were given in Figures (5.2,5.3). From these figures it may be observed that there exists an excellent agreement between ANISN-CSDM

results and the results which were reported by Morel (8).

The second part of the calculations has been performed to demonstrate the accuracy of the method by simulating the corresponding experimental results and the results of the Monte Carlo calculational models. In this part, the energy and angular transmission studies have been performed in aluminum and gold slabs because the corresponding experimental and calculational results are available for comparisons. As given in Figures (5.4,5.5,5.6,5.7,5.8,5.9), the transmission studies in aluminum include three separate simulation cases, each of which represents a different material thickness. The energy distributions of the transmitted particles at the right boundary of the slabs are produced to compare with the experimental results and the Monte Carlo calculational models. It has been observed that the ANISN-CSDM results are in good agreement with the experimental and the Monte Carlo results. Similar calculations have been performed in gold, in addition to a parametric study of the selection of η. The parametric study of η confirms the user-oriented feature of the ANISN-CSDM electron transport model. That is, the produced electron transport results are somewhat independent of the choice of η. The ANISN-CSDM results are in good agreement with the experimental and the ETRAN18G-straggling results along the high and low energy edges of the distribution. The ANISN-CSDM predicts a slightly greater peak value than the experimental

and ETRAN18G-straggling results. This difference, as discussed in the previous chapter, may come from insufficient angle-energy correlation in ANISN-CSDM. That is, actual energy losses of small energy transfre collisions are represented by a few larger angle scatters.

The third part of the calculations has been performed for energy deposition distribution calculations to confirm the accuracy and the utility of the method at relatively low and high electron energies. This part includes the production of the energy deposition distribution in water because of the fact that experimental results are available in connection with the medical physics applications. No discrete ordinates method result has been yet reported for the calculation of the energy deposition in slabs whose thickness is in the range of the primary particle. From Figure (5.14) it may be seen that the ANISN-CSDM result is in excellent agreement with the experimental result. It has been observed that the ETRAN18G models predict slightly greater energy depositions than ANISN-CSDM. This difference, as discussed in the previous chapter, may result from the different energy loss models which have been employed by both of the electron transport schemes. In addition to the water results, energy deposition in aluminum ($d = 0.32\ gm/cm^2$) has also been produced. The total and normalized energy deposition distributions in aluminum are given in Figures (5.23,5.24) for electrons at

1.0 MeV. From Figure (5.23) it may be seen that the ANISN-CSDM predicts a slightly greater normalized energy deposition as compared to the Monte Carlo model. This observation is similar to the water result which was given in Figure (5.14). From Figures (5.23,5.24) it may be observed that there exists a reasonable agreement between ANISN-CSDM and the ETRAN18G results.

In summary, the ANISN-CSDM of the electron transport model has been developed into an economical and accurate tool for the radiation transport analysis problems. The two major developments in this study may be outlined as: (1) the application of the condensed random walk concept of ETRAN family of computer codes into the discrete ordinates method; (2) and the representation of the inelastic cross-sections by the collisional average energy loss model. It was stated that there are one elastic and one inelastic model collision per spatial interval in the ANISN-CSDM model of electron transport. The single elastic collision is allowed by the application of the condensed random walk concept into the discrete ordinates method which in turn allows relatively large spatial intervals with multiple scattering. This multiple scattering approximation replaces the detailed small interval calculations of Bartine et al. This approximation permits more efficient approximate calculations and makes the deep penetration radiation transport

analysis possible within computer storage and time limitations. The single inelastic scatter is allowed by defining an average inelastic energy loss and equating this to an energy group width, thereby specifying a mechanism for continuous slowing down. By excluding small energy-loss collisions from the specification of group width, sufficiently large energy groups result so that an economical computer calculation is possible.

The basis for the development of the ANISN-CSDM electron transport model is not the ANISN computer code, but the ANISN cross-section format. The ANISN computer code has been used to test the electron-continuous slowing down model (ANISN-CSDM) cross-sections. The input format for ANISN has been accepted by other discrete ordinates and Monte Carlo computer codes. Therefore, the cross-section data which has been generated by the developed model can be used in several computer codes. As a result, electron transport calculations need no longer be limited to large special purpose codes, but can use many codes routinely used in nuclear engineering. The ANISN-CSDM model is largely specified in the Cross-Section Processing Code (CRXPC) which has been designed in this study to produce the standard ANISN data in the Group Independent Tape (GIT) format. This Group Independent cross-section tape is required for a transport computation which involves fine grid size in energy, angle, spatial variables;

and the high expansion order of cross-sections. The standardization of the data handling is one of the significant features of the ANISN-CSDM.

The ANISN-CSDM of electron transport does not follow the secondary particles. Energy deposition beyond the range of the primary particle may not be calculated accurately by ANISN-CSDM. Future work in the ANISN-CSDM should include the following of the produced secondary electrons and photons. This ANISN-CSDM may be developed into a more accurate radiation transport analysis tool if the photon productions are treated separately. It is also possible to investigate the applicability of ANISN-CSDM to charged particles other than electrons and positrons. It may be observed that ANISN-CSDM, as it is, may be applied to the photon transport radiation analysis. The ANISN-CSDM calculations have shown that accurate transport results can be produced for relatively low computing times. The problem size may always be reduced to a manageable level by a proper choice of the energy group structure which is determined by the value of η (upper bound of small energy transfer collisions). In the transmission studies the slab thicknesses are relatively small. Such a transport problem overall computer core storage requirement is usually not large. Therefore, one may employ fine energy group structure in the transmission studies. For deep radiation penetration transport cases the slab thicknesses are

usually large. In this case detailed transport calculations may not be possible. Then it is possible to use coarse energy group structure. The accuracy of ANISN-CSDM may be improved by smaller n values in the low energy transport cases. Because this results in larger computing time and storage, however this may not be an optimum engineering solution of the problem.

BIBLIOGRAPHY

1. "ETRAN Manual: Monte Carlo System for electron and photon transport through extended media, CCC-107, ORNL.

2. Halbleib, J. A. Sr. and W. H. Vendevender, "TIGER, a one-dimensional, multilayer electron/photon Monte Carlo transport code," Nuc. Sci. Engr. 57, 94 (1975).

3. Halbleib, J. A. Sr. and W. H. Vandevender, "CYLTRAN, a cylindrical geometry, multimaterial electron/photon Monte Carlo transport code," Nuc. Sci. Engr. 61, 288 (1976).

4. Halbleib, J. A. Sr., "SPHERE, a spherical-geometry, multimaterial electron/photon Monte Carlo transport code," Nuc. Sci. Engr. 66, 269 (1978).

5. Halbleib, J. A. Sr., "ACCEPT: A three-dimensional electron/photon Monte Carlo transport code using combinatorial geometry," SAND79-0415, Sandia Laboratories (1979).

6. Bartine, D. E., et al., "Low-energy electron transport by the method of discrete ordinates." ORNL-TM-3438, August 1971.

7. Hoffman, T. J., "Sputtering calculations with the discrete-ordinates method," Sci. and Engr. (68), 204-211, 1978.

8. Morel, J. E., "On the validity of the extended transport cross-section correction for low-energy electron transport," Nuc. Sci. and Engr. (71), 64-71, 1979.

9. Ligou, J., "Discrete and continuous interaction in charged particle transport theory," Nuc. Sci. and Engr. (70), May 1979.

10. Dupuy, C. H. S., Radiation Damage Processes in Materials, NATO Advanced Study Institute Series, E-8, 1975.

11. Olander, D. R., Fundamental Aspects of Nuc. Reactor Fuel Elements, ERDA Tech. Info. Center, Oak Ridge, TN, 1976.

12. "ANISN-ORNL multigroup one-dimensional discrete ordinates transport code with anisotropic scattering manual."

13. Greenspan, E. and D. Shvarts, Nuc. Fusion (16), 2, 1976.

14. Haldy, P. A. and J. Ligou, Nuc. Fusion (17), 6, 1977.

15. Kammash, T., Fusion Reactor Physics (Principles & Technology), Ann Arbor Science Publishers, Inc., 1976.

16. Zerby, C. D. and F. L. Keller, "Electron transport theory, calculations, and experiments," Nuc. Sci. and Engr. (27), 190-218, 1967.

17. Smith, A., J. Janek and R. Adler, Electron Conduction in Solids, 1967.

18. Knoll, G. F., Radiation Detection Methods, 1979, John Wiley & Sons, New York.

19. Seltzer, S. M. and M. J. Berger, "Monte Carlo studies of electron and photon transport at energies up to 1000 MeV," NBSIR 78-July 1978.

20. Berger, M. J. and S. M. Seltzer, NASA SP-3012, 1964.

21. Secre, E., Experimental Nuclear Physics, Vol. 1, 166-357, John Wiley & Sons, Inc. 1952.

22. Evans, R. D., The Atomic Nucleus, 1955, McGraw-Hill Book Co.

23. Goudsmit, S. and J. L. Saunderson, "Multiple scattering of electrons (I and II) Phys. Rev. (57), (58), 1940.

24. Landau, L., Journ. of Phys. USSR (8), 201-205, 1944.

25. Rasetti, F., Elements of Nuclear Physics.

26. Bethe, H. A., Z. Physik (5) 550, 1950.

27. Bethe, H. A., Z. Physik (76), 293, 1938.

28. Bethe, H. A., Handbuck der Physik, Julius Springer, Berlin, (24), 273, 1933.

29. Rohrlich, F. and B. C. Carlson, "Positron-electron differences in energy loss and multiple scattering," Phys. Rev. (93), 38-44, 1954.

30. Uehling, Edwin A., "Penetration of heavy charged particles in matter," Annual Rev. of Nuc. Sci., Vol. 4, 1954.

31. Hofstadter, Robert, "Nuclear and nucleon scattering of high-energy electrons," Ann. Rev. of Nuc. Sci., Vol. 7, 1957.

32. Barber, W. C., "Inelastic electron scattering," Annual Rev. of Nuc. Sci., Vol. 12, 1962.

33. Fano, U., "Penetrations of protons, alpha particles and mesons," Ann. Rev. of Nuc. Sci., Vol. 13, 1963.

34. Northcliffe, Lee C., "Passage of heavy ions through matter," Annual Rev. of Nuc. Sci., Vol. 13, 1963.

35. Cordaro, M. C. and M. S. Zuckers, "A method for solving time-dependent electron transport problems," Nuc. Sci. and Engr. (45), 107-116, 1971.

36. Spencer, L. V., "Theory of electron penetration," Phys. Rev. (98) 1597-1615, 1955.

37. Gupta, S. K. and M. A. Parasad, "Electron transport in one-dimensional finite systems," Nuc. Sci. and Engr. (70), 1979.

38. Berger, M. J., "Monte Carlo calculation of the penetration and diffusion of fast charged particles," from Methods in Computational Physics, Vol. 1, Academic Press, 1963.

39. Scheider, D. O. and D. V. Cormack, "Monte Carlo calculations of electron energy loss," Rad. Res. (11) 418-429, 1959.

40. Spencer, L. V. and F. H. Attix' "A theory of cavity ionization," Rad. Res. (3) 239-254, 1955.

41. Perkins, J. F., "Monte Carlo calculation of transport of fast electrons," Phys. Rev. (126), 1781, 1962.

42. McGarrigle, K. S. and B. W. Mar, "Computer codes for the evaluation of space radiation hazards, D2-90418, The Boeing Co., 1963.

43. Henry, A. F., Nuc. Reactor Analysis, MIT Press, 1975.

44. Duderstadt, J. J. and W. R. Martin, Transport Theory, John Wiley & Sons, New York, 1979.

45. Carlson, B., "Solution of transport equation by S_N approximation," LA-1891, 1955.

46. Bell, G. I. and S. Glasstone, Nuclear Reactor Theory, Van Nostrand Reinhold Co., 1970.

47. Lewis, H. W., "Multiple scattering in an infinite medium," Phys. Rev. (78), 526-529.

48. Von Neumann, J. and S. Ulam, "Random ergolic theorems," Bull. Amer. Math. Soc. Abstract 51-9-165, 51, 660, 1945.

49. Metropolis, N. and S. Ulam, "The Monte Carlo method," J. Am. Stat. Assoc. 44, 335 341, 1949.

50. Wick, G. C., "Uber ebene diffusions probleme, Z. Phys. (121), 702, 1943.

51. Chandrasekhar, S., Astrophysics J. (100), 76, 1944.

52. Chandrasekhar, S., Rad. Trans., Oxford, 1950.

53. Carlson, B. C., Proc. Symp. in Appl. Math., Vol. (11), 1961.

54. Lee, C. E., "The discrete S_N approximation to transport theory," LA 2595, 1962.

55. Duderstadt, J. J., Nuclear Reactor Analysis, John Wiley and Sons, Inc., 1975.

56. Bethe, H. A., Physical Review, Vol. 89, No. 6, 1953.

57. Rester, D. H. and J. H. Derrickson, "Electron transmission for Al, Sn, and Au targets at electron bombarding energies of 1.0 and 2.5 MeV," Journ. of Appl. Phys., Vol. 42, No. 2, 1971.

58. Cerbone, R. J. and K. D. Lathrop, "S_N calculation of highly forward peaked neutron angular fluxes using asymmetrical quadrature sets, Gulf General Atomic, Inc., 1968.

59. Anderson, D., The University of Oklahoma Health Sciences Center, Oklahoma City, Oklahoma.

60. Price, William J., Nuclear Radiation Detection (2d Ed.), 1964.

61. Miller, Dudley G., Radioactivity and Radiation Detection, 1972.

62. Lathrop, K. D. and B. G. Carlson, "Discrete ordinates angular quadrature of the neutron transport equation," LA-3186, Feb. 1965.

63. Computing Methods in Reactor Physics, edited by H. Greenspan, C. N. Kelber, D. Okrent, Gordon and Breach Science Publishers, N.Y.

64. Nahum, Alan E., Calculations of electron flux spectra in water irradiated with megavoltage electron and photon beams with applications to dosimetry, a Thesis, The University of Edinburg, July 1975.

65. Berger, M. J., S. M. Seltzer S. E. Chappell, J. C. Humphreys and J. W. Motz, Nucl. Instr. and Meth., 69, 181, 1969.

66. Kreyszig, Advanced Engineering Mathematics (3d Ed.), John Wiley & Sons, Inc., 1972.

67. Carrier, George and Carl E. Pearson, Partial Differential Equations, Academic Press, 1976.

68. Hildebrand, Francis B., Methods of Applied Mathematics, (2d Ed.), Prentice-Hall, Inc., 1965.

69. Bell, G. I., G. E. Hansen and H. A. Sandmeier, "Multiple treatments of anisotropic scattering in S_N multigroup transport calculations, Nuc. Sci. and Engr. 28, 376-383, 1967.

70. Engle, W. W. Jr. and F. R. Mynatt (UCC-OR) "A comparison at two methods of inner iteration convergence acceleration in discrete ordinates codes," American Nuclear Society Transactions, Vol. 11, 1968.

71. Conte, S. D. and Carl de Boor, Elementary Numerical Analysis: An Algorithmic Approach, 2d Ed., McGraw-Hill Book Company, 1972.

72. Cress, P., P. Dirksen and J. W. Graham, FORTRAN VI with WATFOR and WATFIV, Prentice-Hall, Inc., 1968.

73. Trubey, D. K. and Betty F. Moskewitz, "A review of the discrete ordinates S_n method for radiation transport calculations," ORNL-RSIC-19, March 1968.

74. Wilson, R. R., "The range and straggling of high energy electrons," Phys. Rev. 84, No. 1, 1951.

75. Mar, B. W., "An electron shielding analysis for space vehicles," Nuc. Sc. & Engr. 24, 193-199, 1966.

76. Fano, U., "Inelastic collisions and the Moliere theory of multiple scattering, Phys. Rev. 93, No. 1, 1954.

77. Hebbard, D. F. and P. R. Wilson, "The effect of multiple scattering on electron energy loss distributions," Australian J. Phys. 8, (90-97).

78. Kessaris, N. D., "Penetration of high-energy electron beams in water, Phys. Rev. 45, No. 1.

79. Kessaris, N. D., "Spectra of high-energy electron beams in water," Radiation Research, 43, 281-287, 1970.

80. Chen, J. J. L. and S. D. Warshaw, "The energy loss of electrons passing through water," Phys. Rev. 84, No. 2, 1951.

81. Wilson, J. W., "Methods of shield analysis for protection against electrons in space," Nuclear Technology, 35, 1977.

82. Van de Putte, D. W., "Computation of the Goudsmit-Saunderson distribution in electron transport," Nuclear Instruments & Methods 115, 1975, 117-120, North-Holland Publishing Co.

83. Carter, L. L. and E. D. Cashwell, "Particle-transport simulation with the Monte Carlo method, ERDA Critical Review Series, TI D-26607, 1975.

84. Lamarsh, John R., Introduction to Nuclear Engineering, Addison-Wesley Publishing Co., 1975.

APPENDIX I

THE DIFFERENTIAL MØLLER CROSS-SECTION FOR INELASTIC ELECTRON-ELECTRON COLLISIONS

For a given initial energy $E_0 = 1.0$ MeV, the Figure (I.1) which will be given below shows the variation of the total Møller inelastic differential scattering cross-section as a function of the final energy of the scattered particle, W. The expression which has been used to produce the figure is as follows:

$$\frac{d\sigma_{inel}(E_0,W)}{dW} = 2\pi r_0^2 \times \left(\frac{\rho \times N_A}{M} \times Z\right) \times \frac{(T+1)^2}{T^2(T+2)} \times$$

$$\left\{ \frac{1}{\left(\frac{W}{E_0}\right)^2} - \frac{2K-1}{K^2} \frac{1}{\frac{W}{E_0}\left(1-\frac{W}{E_0}\right)} + \frac{1}{\left(1-\frac{W}{E_0}\right)^2} + \left(\frac{K-1}{K}\right)^2 \right\}$$

This has dimensions of 1/MeV cm. It is the energy part of the double differential microscopic inelastic electron-electron scattering cross-section which was given by equation (2.13) in Chapter (II).

$$\frac{d^2\sigma(E_0 \to W, \vec{\Omega}' \to \Omega)}{dW d\Omega} = \frac{d\sigma_{inel}(E_0,W)}{dW} \; \frac{\delta(\vec{\Omega}' \cdot \vec{\Omega} - f(E_0,W))}{2\pi}$$

where

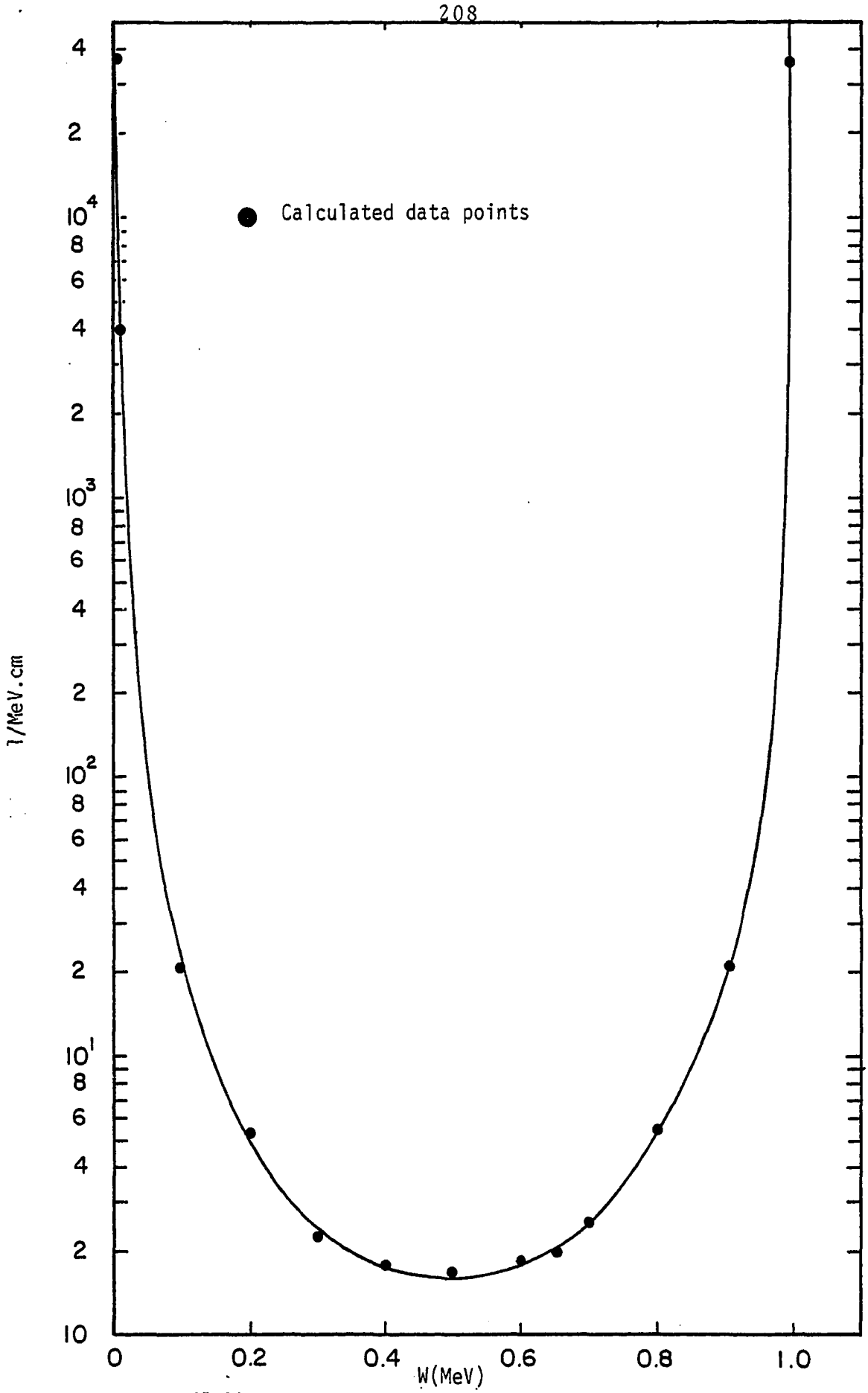

Figure (I.1): Differential Møller total energy transfer cross-section.

$$f(E_0,W) = \cos\theta_\ell \qquad \text{if } W < E_0/2;$$

$$f(E_0,W) = \cos\theta_h \qquad \text{if } W \geq E_0/2.$$

$$\cos\theta_h = \left[\frac{W(E_0 + 2mc^2)}{E_0(W + 2mc^2)} \right]^{1/2}$$

$$\cos\theta_\ell = \left[\frac{(E_0 - W)(E_0 + 2mc^2)}{E_0(E_0 - W + 2mc^2)} \right]^{1/2}$$

where $\cos\theta_\ell$ and $\cos\theta_h$ satisfy the following condition:

$$\cos\theta_h \geq \cos\theta_\ell \geq 0.$$

The double differential scattering cross-section characterizes the scattering from an incident energy E_0, direction $\vec{\Omega}$, to a final energy W in dW, and angle $\vec{\Omega}'$ in $d\Omega$. The $\vec{\Omega}$ and $\vec{\Omega}'$ represent the initial and the final directions of primary particle. In general, $\vec{\Omega}$ denotes a unit vector which is defined as follows

$$\vec{\Omega} = \frac{\vec{v}}{|\vec{v}|} .$$

It may be observed that the differential energy transfer cross-section,

$$\frac{d\sigma_{inel}(E_0 W)}{dW} ,$$

has one simple pole at $W = E_0$, and two poles of second order at $W = E_0$ and $W = 0$. The energy transfer differential cross-section is symmetric in W and $E_0 - W$. Thus by replacing W with $E_0 - W$, one can produce the original differential energy

transfer cross-section. This means that the interactions of the primary electrons and the secondary electrons are governed by the same differential cross-section. This symmetry property of the electron differential energy transfer cross-section may be seen in Figure (I.1) at E_0 = 1.0 MeV.

APPENDIX II

A SUMMARY OF THE NUMERICAL SOLUTION OF THE NEUTRON TRANSPORT EQUATION

In the following paragraphs a general structure of the S_N difference equations will be constructed. The S_N method which was first introduced by Carlson is a special case of the DOM. The characteristic of this scheme is that the directional particle flux varies linearly between the interpolation points in μ-r space, Figure (II.1). Let us assume a stationary transport equation in a spherical geometry. The energy group index may be dropped for simplicity. Then the associated transport equation may be given as follows with an isotropic source term:

$$\mu \frac{\partial \phi(r,\mu)}{\partial r} + \frac{1}{r}(1-\mu^2) \frac{\partial \phi(r,\mu)}{\partial \mu} + \Sigma_t \phi(r,\mu) = S(r)$$

The anisotropic source, the shell source, can also be considered as well as an isotropic source. In the above equation r and μ represent radial angular variables; i.e., μ is the cosine of the angle between the particle direction and the radius vector. Now consider the domain of $\mu \varepsilon [-1,+1]$ and break it into a set of intervals as produced below:

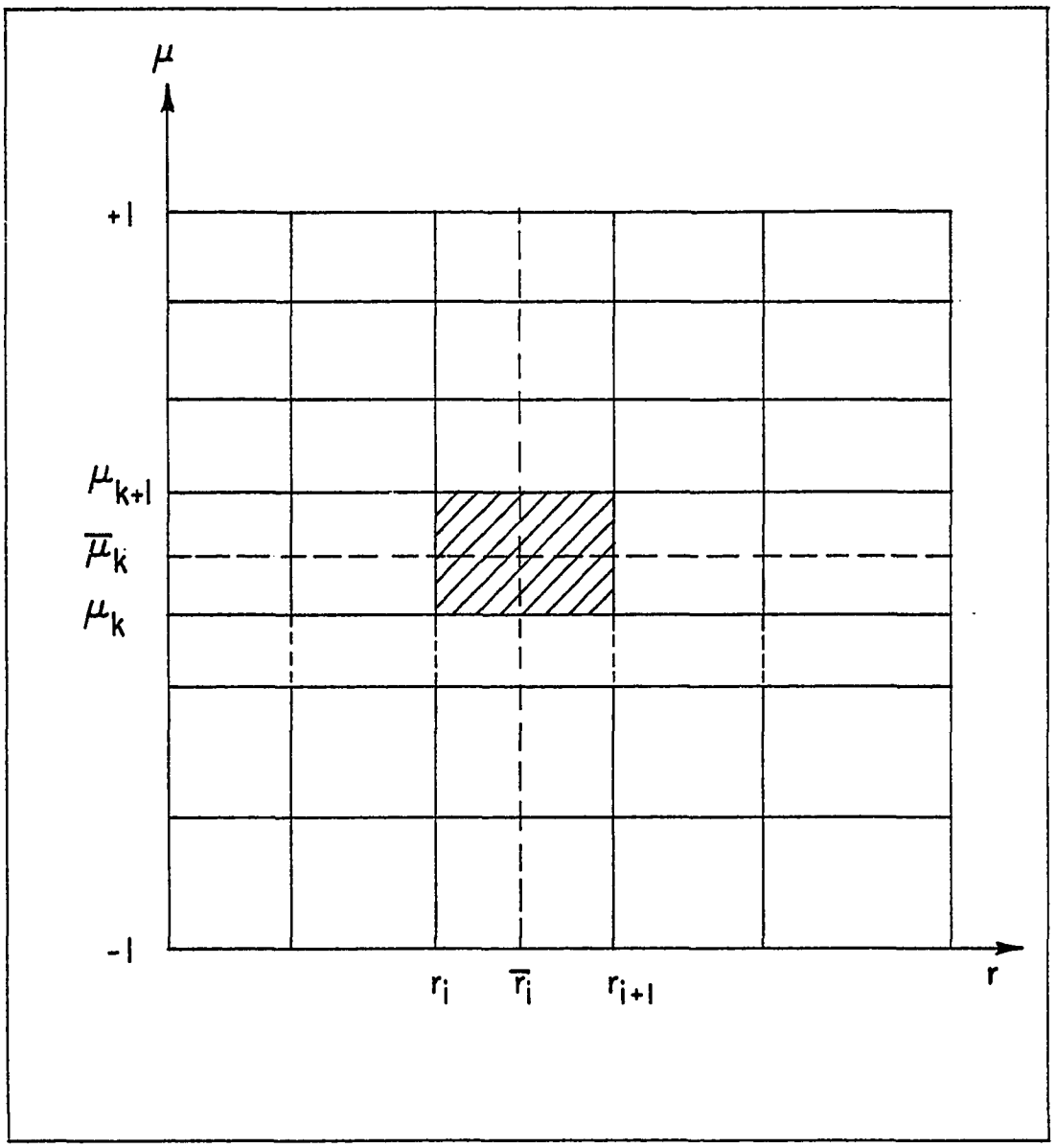

Figure (II.1) A mesh in μ-r space for S_N calculations.

$$\mu_k = -1 + \frac{2k}{N} \qquad , \; k = 0,1,0,\ldots,N$$

where an even number of equal μ-intervals are considered. One may observe that N is the total number of segments and $\mu_0 = -1$, $\mu_N = +1$. Denote these are a set of μ values by $\{\mu_k\}$. One may also express the interval midpoints of established μ_k-segments as

$$\bar{\mu}_k = -1 + \frac{2k-1}{N} \qquad , \; k = 1,2,3,\ldots,N$$

The $\bar{\mu}_k$'s may be treated as the "discrete directions" of the S_N method. They possess equal weights 1/N such that when the average angular flux in a cell has been determined one may obtain the $\bar{\phi}_i$ by the expressions (i's are index for spatial variable)

$$\frac{1}{N} \sum_m \bar{\phi}_{ik} \qquad , \; \bar{\phi}_{ik} = \text{average angular flux in a cell in } \mu\text{-r space.}$$

Similarly radial variable can be treated discretely to define a set of r values, $\{r_i\}$. Then one can construct a cell in r-μ space as shown on Figure (II.1). The set $\{r_i\}$ does include real physical boundaries of the problem and the size of $\Delta r_i = r_i - r_{i-1}$ depends on the type of problem and resolution desired. Define the following particle fluxes:

$$\phi_i \equiv \phi(r_i,\bar{\mu}_k) \equiv \text{the flux at } r_i \text{ for a given discrete direction } \bar{\mu}_k$$

$$\phi_k \equiv \phi(\bar{r}_i,\mu_k) \equiv \text{the flux at } \mu_k \text{ for a given } \bar{r}_i$$

where $\bar{\mu}_k$ defined earlier and

$$\bar{r}_i = 0.5 \times (r_i - r_{i-1}).$$

Let $\Delta(i) = r_i - r_{i-1}$

$$\Delta(k) = \mu_k - \mu_{k-1}$$

$$s(i) = \frac{\Delta(i)}{r_i^*}$$

with

$$r_i^* = \frac{2(r_i^3 - r_{i-1}^3)}{3(r_i^2 - r_{i-1})}$$

also define

$$\gamma_k = \frac{1-\mu^2}{\Delta(k)}$$

$$\phi_k = 2\,\bar{\phi}_{ik} - \phi_{k-1}$$

$$\bar{\phi}_{ik} = 0.5 \times (\phi_i + \phi_{i-1})$$

It is assumed in the above expressions that the flux, $\phi(\mu,r)$, varying linearly in the cell A_{ik} of μ-r space for all independent variables. Such a linear variation of the angular flux in between the discrete points is a characteristic of the S_N scheme of the solution of transport equation.

The finite difference form of the steady state transport equation may be constructed by using the diamond differencing. The details of the derivation may be found in the literature (38,44,45,53,54,63). In the diamond-central difference approximation the flux is defined at the midpoint of the cell.

The difference equation form of transport equation may be given as follows:

$$\bar{\mu}_k \, (\phi_i - \phi_{i-1}) + \gamma_k s(i) \, (\phi_i + \phi_{i-1} - \phi_{k-1}) - \gamma_k \, s(i) \phi_{k-1}$$

$$+ 0.5 \times \Sigma_{t_i} \, \Delta(i) \, (\phi_i + \phi_{i-1}) = \Delta(i) \, S_i$$

where Σ_{t_i} and S_i are the midpoint values of Σ_t, S are the midpoint values of Σ_t, S in the cell A_{ik} in μ-r space. The last expression can be cast into the following form by re-arranging terms in order to solve ϕ_i's.

$$(\bar{\mu}_k + \gamma_k \, s(i) + \frac{\Sigma_{t_i} \, \Delta(i)}{2}) \phi_i + (-\bar{\mu}_k + \gamma_k \, s(i) + \frac{\Sigma_{t_i} \Delta(i)}{2}) \phi_{i-1}$$

$$= \Delta(i) \, S_i + 2\gamma_k \, s(i) \, \phi_{k-1}$$

For given S_i and the boundary conditions the flux ϕ_i can be determined. One may observe that for m = 0:

$\bar{\mu}_0 = -1, \quad \gamma_0 = 0$ are the starting values.

Assuming that ϕ_0 is known, then one can evaluate ϕ_1, etc. The determination of ϕ_i recursively for spatial indexes i, one needs to solve the final expression for

(i) ϕ_{i-1} if $\mu_k < 0$

(ii) ϕ_i if $\mu_k < 0$.

The constructed form of discrete S_N equation may not give satisfactory results if $\Sigma_{t_i} \Delta(i)$ product becomes large (it may occur for certain energy groups in some regions of reactor core). The position dependent flux, ϕ_i, would change

algebraic sign. It does not represent a physical flux. Such difficulties could be removed by using step functions in difference equation formulation of transport equation instead of a linear variation assumption of angular flux between angle and spatial variables.

Enough consideration ought to be given to how to construct the mesh cells. The desired solution may be produced by a proper selection of space, angle and energy mesh sizes. For cases which involve deep radiation transport problems one should not use a coarse mesh in independent variables. Fine mesh structure is required for such cases. The improvement of the produced transport results depends on the established mesh structure. The computing tools available may also put a limit on the problem size which requires a finite amount of locations in the computer core. The accuracy desired and computing tools available are somewhat interrelated to each other.

APPENDIX III

SOME PROPERTIES OF THE LEGENDRE POLYNOMIALS AND SPHERICAL HARMONICS

(1) The Legendre Polynomials (22,43,44,46,66,67,68)

The Legendre polynomials may be taken as a class of solutions of the ordinary differential equation, Legendre equation. They may be defined by the following expressions:

$$P_n(x) = \frac{1}{2^n}\ \frac{1}{n!}\ \frac{d^n}{dx^n}(x^2-1)^n \quad , \qquad n=1,2,3,\ldots$$

with

$$P_0(x) = 1,\ P_1(x) = x,\ P_2(x) = \frac{1}{2}(3x^2-1),$$

$$P_3(x) = \frac{1}{2}(5x^3-3x),\ldots$$

The orthogonality condition that $P_n(x)$'s satisfy is

$$\int_{-1}^{+1} P_{\ell'}(x)\ P_{\ell}(x)\ dx = \frac{2\delta_{\ell\ell'}}{2\ell+1} \qquad -1 < x < +1 \quad ,$$

where

$$\delta_{\ell\ell'} = \begin{cases} 1 & \text{if } \ell = \ell' \\ 0 & \text{otherwise} \end{cases}$$

The Legendre polynomials satisfy various recursion relations typified by

$$(2\ell + 1)x\ P_\ell(x) = (\ell+1)\ P_{\ell+1}(x) + \ell\ P_{\ell-1}\ (x)$$

$$(x^2-1)\ \frac{dP_\ell}{dx} = \ell(x\ P_\ell - P_{\ell-1})$$

$$\ell\ P_\ell(x) = x\ P_\ell'\ (x) - P_{\ell-1}'\ (x)$$

$$(2\ell+1)\ P_\ell(x) = P_{\ell+1}'\ (x) - P_{\ell-1}'\ (x).$$

They form a complete set of orthogonal functions for the expansion of a function say, $\sigma(x)$, defined on the interval $-1 \leq x \leq +1$, where $\sigma(x)$ should be real and square integrable. Then one may write

$$\sigma(x) \cong \sum_{\ell=0}^{LMAX} \sigma_\ell P_\ell(x)$$

where

$$\sigma_\ell = \frac{2\ell+1}{2} \int_{-1}^{+1} \sigma(x) P_\ell(x)\, dx$$

(2) The Associated Legendre Function:

It is $P_\ell^m(x)$, defined as follows:

$$P_\ell^m(x) = (-1)^m\ (1-x^2)^{\frac{m}{2}}\ \ \frac{d^m P_\ell(x)}{dx^m}$$

provided $m = 1,2,3,\ldots,$

One may observe that $P_\ell^0(x) = P_\ell(x)$.

For negative integral values of m such that $|m| \leq \ell$ one may obtain

$$P_\ell^{-m}(x) = (-1)^m\ \frac{(\ell-m)!}{(\ell+m)!}\ P_\ell^m(x)$$

The associated Legendre polynomials also obey the appropriate orthogonality conditions.

(3) The Spherical Harmonics:

They are a complete set of functions in the angular variables ($\mu = \cos\theta$) and ψ that specify the direction of the unit vector $\vec{\Omega}$ relative to a system of cartesian coordinates. The spherical harmonics in their normalized form are given as follows:

$$Y_\ell^m(\vec{\Omega}) = Y_\ell^m(\mu,\psi) = \left\{\frac{2\ell+1}{4\pi} \times \frac{(\ell-m)!}{(\ell+m)!}\right\}^{1/2} P_\ell^m(\cos\theta)e^{im\psi}$$

They are orthonormal functions and satisfy the following property:

$$\int_{4\pi} d\vec{\Omega}\, Y_\ell^m(\vec{\Omega})\, Y_{\ell'}^{*m'}(\vec{\Omega}') = \int_{-1}^{+1}\int_{0}^{2\pi} Y_\ell^m(\theta,\psi)\, Y_{\ell'}^{*m'}(\theta,\psi)\, d\mu\, d\psi = \delta_{\ell\ell'}\,\delta_{mm'}.$$

A function $g(\theta,\psi)$ can be expanded in terms of spherical harmonics as

$$g(\theta,\psi) = \sum_{\ell=0}^{LMAX}\sum_{m=-\ell}^{+\ell} g_{\ell m} Y_{\ell m}(\theta,\psi)$$

where

$$g_{\ell m} = \int_0^{2\pi}\int_{-1}^{+1} g(\theta,\psi)\, Y_{\ell m}^*(\theta,\psi)\, d(\cos\theta)\, d\psi.$$

The addition theorems of spherical harmonics and Legendre polynomials may be given as follows:

$$P_\ell(\mu_0) = \frac{4\pi}{2\ell+1}\sum_{m=-\ell}^{\ell} Y_{\ell m}^*(\theta',\psi')\, Y_{\ell m}(\theta,\psi)$$

$$P_\ell(\mu_0) = P(\mu)P_\ell(\mu') + 2\sum_{m=1}^{\ell}\frac{(\ell-m)!}{(\ell+m)!} P_\ell^m(\mu)\, P_\ell^m(\mu')\cos m(\psi-\psi')$$

The further detailed properties of the Legendre polynomials and spherical harmonics may be found in the literature.